Effective SU(2) theory for the pseudogap state

X. Montiel,[1,2] T. Kloss,[1,3] and C. Pépin[1]
[1]*IPhT, L'Orme des Merisiers, CEA-Saclay, 91191 Gif-sur-Yvette, France*
[2]*Department of Physics, Royal Holloway, University of London, Egham, Surrey TW20 0EX, United Kingdom*
[3]*INAC-PHELIQS, Université Grenoble Alpes and CEA, 38000 Grenoble, France*
(Received 21 November 2016; revised manuscript received 8 February 2017; published 13 March 2017)

This paper exposes in a detailed manner the recent findings about the SU(2) scenario for the underdoped phase of the cuprate superconductors. The SU(2) symmetry is formulated as a rotation between the d-wave superconducting (SC) phase and a d-wave charge order. We define the operators responsible for the SU(2) rotations and we derive the nonlinear σ model associated with it. In this framework, we demonstrate that SU(2) fluctuations are massless in finite portions of the Brillouin zone corresponding to the antinodal regions $(0,\pi)$ and $(\pi,0)$. We argue that the presence of SU(2) fluctuations in the antinodal region leads to the opening of Fermi arcs around the Fermi surface and to the formation of the pseudogap. Moreover, we show that SU(2) fluctuations lead, in turn, to the emergence of a finite momentum SC order—or pair density wave (PDW)—and more importantly to a new kind of excitonic particle-hole pairs liquid, the resonant excitonic state (RES), which is made of patches of preformed particle-hole pairs with multiple momenta. When the RES liquid becomes critical, we demonstrate that electronic scattering through the critical modes leads to anomalous transport properties. This new finding can account for the strange metal (SM) phase at finite temperature, on the right-hand side of the SC dome, shedding light on another notoriously mysterious part of the phase diagram of the cuprates.

DOI: 10.1103/PhysRevB.95.104510

I. INTRODUCTION

When doping a Mott insulator, the system becomes a superconductor at high temperature. This phenomenon remains one of the most enduring mysteries of materials science. The origin of the pseudogap (PG) phase [1,2], which shows a loss of electronic density of states at finite temperatures above the superconducting (SC) state, in the underdoped regime, has generated some intense debate in the past thirty years, and still remains an open issue [3–12]. The mystery of the PG phase is maybe better seen within the angle-resolved photoemission (ARPES) measurements, in which we observe a continuous evolution from small hole pockets at low oxygen doping $x < 0.05$, to Fermi arcs at intermediate doping (or underdoped region) $0.08 < x < 0.19$, to finally the opening of a larger Fermi surface in the overdoped region $0.20 < x$. The notion of Fermi "arcs" instead of closed Fermi surface of electrons has a groundbreaking character because it breaks the Luttinger theorem relating the counting of the conduction electrons with the "volume" of the Fermi surface [13–18]. The theories of the PG can be divided into two major lines of thought. In the first line of thought, the emphasis is given to the proximity to the Mott insulator at zero doping ($x = 0$), and argue that the considerable strength of the Coulomb interactions for these systems produce strong correlations between the electrons, from the scale of 1 eV down to the lowest energy scales [5]. Exotic states are created, the most notoriously famous of them being the resonating valence bond (RVB) state proposed in the early days, just after the discovery of the YBCO [19–22]. This approach has also lead to many numerical advances including the celebrated dynamical mean-field theory (DMFT) [23–27], designed to capture the proximity to the Mott transition, as well as field theory treatment including gauge field [28–36], with U(1), or SU(2) symmetries [5,20,21]. The second type of theories assumes the existence of a singularity in the phase diagram, for example, with the presence of a quantum critical point (QCP)—also called a zero temperature phase transition, where the quantum fluctuations dominate the thermal ones [37–49]. While the correlations between electrons are not very strong at the UV scale, they drastically grow when the temperature is reduced, leading to a strong coupling in the vicinity of the QCP.

The importance of phase fluctuations for small hole concentration when approaching the Mott transition was outlined in a seminal study of the underdoped regime of cuprates [50]. The main argument is simply that when the electron density gets locked at the brink of localization, the phase fluctuates within the phase-density duality relation. Three types of fluctuations were identified: the quantum phase fluctuations arising from the Heisenberg uncertainty principle, the classical—thermal—phase fluctuations, and the fluctuations of the amplitude of the order parameter promoted by some extra degree of freedom. This line of approach was explored in details in the "preformed pairs" scenario, where Cooper pairs are forming at a temperature $T > T_c$, with the phase coherence setting precisely at T_c [51–56], as well as in scenarios involving phase separation in real space with, for example, the formation of stripes [57–65]. It has to be noticed that a scenario has already attributed the opening of the PG to fluctuating charge order [49]. In this scenario, the Cooper pairing enables the opening of the PG in the antinodal region, allowing the formation of the Fermi arcs in the nodal part of the Fermi surface.

Despite very intense and focused experimental search, preformed pairs were not observed at the PG energy scale T^*, and phase fluctuations were found only in a window of 15 K above T_c [66–69]. A question then naturally arises: where is the enormous amount of classical phase fluctuations that should be present in the underdoped regime?

In this paper, we argue that a new type of pairing fluctuations has to be considered in the underdoped region, governed by

an emergent SU(2) symmetry which rotates the superconducting state towards the charge sector [70–76]. Within the SU(2) paradigm, pairing fluctuations do not only involve the phase of the U(1) superconducting order parameter, but also "pairing" fluctuations towards the charge sector as well as charge phase fluctuations. For example, these operators can rotate a pair density wave (PDW)—or finite momentum superconducting order, into a charge density wave (CDW) state with the same wave vector, as was recently reported [77], but it can also rotate a standard d-wave superconducting state into a new kind of excitonic state. Support for the concept of an underlying SU(2) symmetry in the background of the underdoped region comes from the recent findings of CDW in the phase diagram of the cuprates, and subsequent theoretical investigations over this findings [78–92]. This started around a decade ago with a first observation of modulations inside vortices in Bi2212 [93,94]. Subsequent studies with Fermi surface reconstruction showed that this feature was generic [95,96], also verified in Bi-2201 [97,98], and that the charge patterns corresponded to two axial wave vectors $(0, Q_y)$ and $(Q_x, 0)$, incommensurate with the lattice periodicity, and which magnitude of the wave vectors growing with oxygen doping. Quantum oscillations in YBCO [99,100], NMR [101–103], and [104] x-ray studies, hard [105,106] and soft [107–110], provided a new understanding in the nature of the charge ordering, as a reasonably long-ranged excitation ($\sim 20\, a_0$, where a_0 is the elementary cell parameter of the square lattice) stabilized to a true long-range order upon a magnetic field larger than 17 T [104,111].

May be the strongest suggestion that d-wave charge order and SC are mysteriously related by a symmetry, comes from the phase diagram showing the response of charge ordering as a function of temperature and magnetic field, in the underdoped region [99,101,104,111–113]. Similar energy scales are observed for both orders, with a sharp (and flat) transition at $H_0 = 17$ T, very suggestive of a "spin-flop"-type transition between the two states.

Bulk probe spectroscopies also hint towards the presence of a collective mode in the underdoped phase of the cuprates. It has been argued that the A_{1g} mode in Raman scattering [114–119] can be associated with the presence of SU(2) symmetry [120,121]. Likewise a theory [11,122–125] for the PG state shall address the long standing observation by inelastic neutron scattering (INS) of a finite energy resonance around the AF wave vector (π, π) in both the SC and PG states of those compounds [126–132].

The formation of the PG state is accompanied by $\mathbf{Q} = \mathbf{0}$ orders as observed by INS techniques [133,134] and transport measurements [135]. These orders have been interpreted as loop currents [133,134] or nematicity [135], which have led to recent theoretical developments [136–143].

Typically, the constraint in the nonlinear σ model associated with SU(2) fluctuations, creates a strong coupling between the two channels, which in turn generates phase separation [144,145]. We succinctly describe this situation in the second part of this paper, with the creation of patches or droplets, of excitonic particle-hole pairs. The statistics of such objects is analogous to the phase separation of polarons in an electronic medium [146], and is also related to the emergence of skyrmions in the pseudospin space, which come out of the nonlinear σ model. The detailed link between these approaches is deferred to a future work.

In this paper, the SU(2) symmetry emerges from short-range AF correlations, which is a more realistic starting point for the phase diagram of the cuprates than our previous study [72] where the proximity to an AF QCP was assumed. Although a few of the essential ideas developed in this paper have already been introduced elsewhere [147] like the idea of particle-hole "droplet," or excitonic patches, the detailed calculations behind these ideas have never been presented so far. The description of the nonlinear σ model is given for the first time, directly starting from a realistic short-range AF correlation and a realistic electronic dispersion rather than from a more idealistic eight-hot-spot model close to an AF QCP. It is shown that the coupling between the nonlinear σ model and the underlying fermions restricts the SU(2) fluctuations to the antinodal region of the BZ, which is a crucial new feature of the theory. The rotation of the charge ordering wave vectors from the diagonal to the axes is explained for the first time. The symmetries of the emerging orders, CDW and PDW, are clarified. Moreover, the study of the strange metal, and the implications of our proposal for the PG to anomalous transport properties in this region of the phase diagram are given here for the first time.

The paper is organized as follows. In Sec. II, we introduce the pseudospin operators relevant to our study, and the triplet representation on which they apply, which rotates the d-wave SC state to a d-wave CDW. In Sec. III, we give a mean-field decoupling of a Hamiltonian pertaining to the solution of cuprate superconductors, which retains mainly short-range AF interactions. The decoupling in the charge and SC channels gives a degeneracy (at the hot spots) between the two channels, for a wide range of doping. It defines the temperature scale below which on can get SU(2) fluctuations. In Sec. IV, we start our study of the fluctuations between the two states, introduce the effective Lagrangian with its symmetric part and symmetry breaking part. In Sec. V, we use the SU(2) symmetric part of the Lagrangian to perform the integration over the fermionic degrees of freedom, leading to the standard expression for the nonlinear σ model. In Sec. VI, we focus on the symmetry breaking term, and show that massless SU(2) fluctuations occur only on specific loci of the Brillouin zone, that we call SU(2) lines. Everywhere else in the Brillouin zone the fluctuations are heavily massive. In Sec. VII, we start to study the effect of the SU(2) fluctuations on the charge and SC channels. We show that SU(2) pairing fluctuations induce a nematic response and, importantly, tilt the charge ordering modulation wave vector from the diagonal (Q_0, Q_0) to the axes $(Q_0, 0)$ and $(0, Q_0)$. In Sec. VIII, we discuss the possibility that SU(2) fluctuations lead to the emergence of preformed excitonic (particle-hole) pairs owing many $2\mathbf{p}_F$ wave vectors, whereas similar study in the SC channels leads to the emergence of a small pair density wave contribution with the same wave vectors $(Q_0, 0)$ and $(0, Q_0)$ as in the CDW channel. Finally, in Sec. X, we depict a global phase diagram for the physics of the underdoped region of the cuprates using heuristic arguments from the SU(2) theory. We also study the strange metal regime at optimal doping and show that our pictures provides very anomalous transport exponents, with in particular a resistivity going like $\rho \sim T/\ln T$ in three spatial dimensions.

II. THE SU(2) SYMMETRY

The paradigm of emerging symmetry is not new [148] and possibly one of its most famous proponents is the SO(5) theory for cuprate superconductors [149–154] where it was proposed that the d-wave SC state can be rotated into the AF sector. Thermal fluctuations between the two states, described by the nonlinear σ model were shown to become massively dominant in the underdoped region of the phase diagram and it was suggested that they were responsible for the formation of the pseudogap.

The present study is based on the assumption that an underlying SU(2) symmetry governs the phase diagram in the underdoped region of the cuprates. In contrast to SO(5) symmetry described above, the SU(2) symmetry we talk about here connects the SC and CDW sectors. This concept of pseudospin symmetry is not new and can be traced back to the Yang and Zhang for Hubbard model at half-filling [155,156]. A set of pseudospin operators were introduced, which rotate the d-wave SC state into a d-wave modulated charge order. The pseudospin idea was later used in the context of the d-density wave (DDW) [157] and nematic states [158], using as well the SU(2) pseudospin operators in order to rotate the d-wave SC state towards one of those two. Recently, the ubiquitous presence of charge excitations in the underdoped region, and the stabilization of long-range CDW in high magnetic fields ($B > 17$ T) lead to the revival of the idea of emerging SU(2) symmetry, and the pseudospin operators in this case rotate the d-SC state towards the charge sector.

In this section, we give the mathematical definitions of the pseudospin operators of the SU(2) symmetry and describe explicitly the $l = 1$ minimal representation. We rapidly review previous work on the eight-hot-spot model, generalization to the more realistic model including short-range AF correlations are given in Sec. III.

A. The "eight-hot-spot" model

The SU(2) symmetry rotating the d-wave superconductor to the charge channel was first derived in the context of the eight hot-spots model [70,72], where the Fermi surface is reduced to eight points related two by two by the wave vector $\mathbf{Q} = (\pi,\pi)$ as depicted in Fig. 1. In this model, electrons interact through critical bosonic modes following the Lagrangian $L = L_\psi + L_\phi$:

$$L_\psi = \psi^\dagger(\partial_\tau + \varepsilon_\mathbf{k} + \lambda\phi\cdot\sigma)\psi, \tag{1}$$

$$L_\phi = \phi\frac{D^{-1}}{2}\phi + \frac{g}{2}\phi^4, \tag{2}$$

where ψ is the electron field with dispersion $\varepsilon_\mathbf{k}$ around each hot spot, coupled to the spin fluctuation field ϕ evolving through the spin-wave propagator of a typical Ornstein-Zernike form:

$$D^{-1} = \frac{\omega^2}{v_s^2} + (\mathbf{q}-\mathbf{Q})^2 + m_a. \tag{3}$$

m_a is the mass which characterizes the distance to the quantum critical point (QCP). σ is the Pauli spin in Eq. (1). When the Fermi dispersion $\xi_\mathbf{k}$ is linearized around each hot spot, one obtains a composite order as a precursor of antiferromagnetism. The composite order parameter can be viewed as a non-Abelian superconductor

$$\hat{b} = b\hat{u}, \quad \text{with } u = \begin{pmatrix} \chi & \Delta \\ -\Delta^* & \chi^* \end{pmatrix}, \quad \text{and } |\chi|^2 + |\Delta|^2 = 1. \tag{4}$$

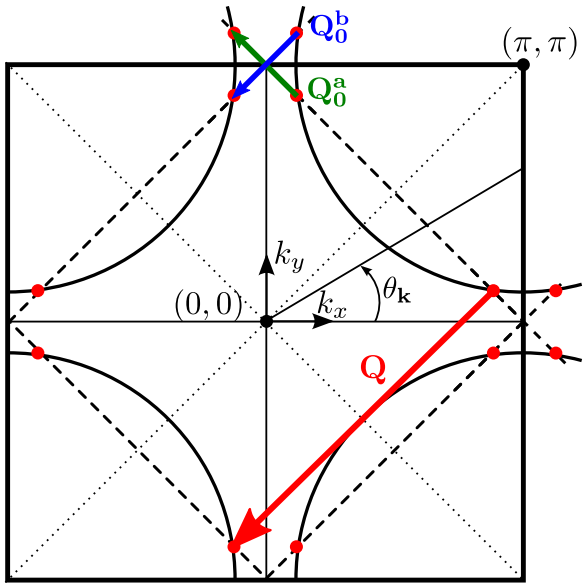

FIG. 1. Schematic representation of a hole-doped cuprate Fermi surface in the first BZ. The "hot spots" (red points) are the point of the FS close to the critical AFM modes and connected by the vector $\mathbf{Q} = (\pi,\pi)$. Two different ordering vectors $\mathbf{Q}_0^a$ and $\mathbf{Q}_0^b$ (green and blue), coupling hot spots between two opposed FS in the antinodal region are shown. The angle $\theta_\mathbf{k}$ localizes the points in the first BZ.

Instead of having a U(1) phase as it is the case superconductors, the operator $\hat{b}$ has now an SU(2) phase rotating between the d-wave SC channel $\Delta = \frac{1}{\sqrt{2}}\sum_\mathbf{k} d_\mathbf{k}\psi_{\mathbf{k}\downarrow}\psi_{-\mathbf{k}\uparrow}$, with $d_\mathbf{k} = 2\cos(2\theta_\mathbf{k})$ and the d-wave Peierls channel $\chi = \frac{1}{2}\sum_{\mathbf{k},\sigma} d_\mathbf{k}\psi^\dagger_{\mathbf{k}+\mathbf{Q}_0\sigma}\psi_{\mathbf{k},\sigma}$ also called quadrupolar order [72]. Within this simplified model, $\mathbf{k}$ is defined in a small region around each hot spot and the definition of the charge wave vector $\mathbf{Q}_0 = (\pm\mathbf{Q}_a,\pm\mathbf{Q}_\mathbf{b})$ depends on the of the hot spot in $\mathbf{k}$ space (see Fig. 1). $\mathbf{Q}_0$ is the a $\mathbf{k}$-dependent, diagonal wave vector, which relates, using an umklapp wave vector, the two hot spots opposite to each other across the Fermi surface. Note that the choice of $\mathbf{Q}_a$ or $\mathbf{Q}_b$ is tight to the precise each hot spot. The precursing order $\hat{b}$ thus possesses an exact SU(2) symmetry, which relates the SC channel to the charge channel, and importantly, it is driven by AF fluctuations which dominate in the vicinity of the QCP.

B. Operators

In this paper, we study a generalization of the SU(2) symmetry of the eight-hot-spot model in the case of a real compound, with a generic dispersion not reduced to the eight hot spots, including the curvature. The first step in this direction is to introduce the notion of involution, implicitly present in the $\mathbf{k}$ dependence of the $\mathbf{Q}_0$ modulation vector in Sec. II A.

An involution is a mapping which sends $\mathbf{k} \to \bar{\mathbf{k}}$, such that for each $\mathbf{k}$ vector, we have

$$\bar{\bar{\mathbf{k}}} = \mathbf{k} \text{ and } \overline{(-\mathbf{k})} = -(\bar{\mathbf{k}}). \tag{5}$$

Such a mapping was already present in the definition of the $\mathbf{k}$-dependent wave vector in Sec. II A. It is important for the generalization to the entire BZ, because it ensures that the SU(2) algebra defined below is self-constrained, and does not produce harmonics with each product of two operators. Concrete examples of the involution that we use in this study, are given in the next paragraph and are depicted in Figs. 2(a)–2(c).

We now move to the definition of the pseudospin operators associated with the SU(2) symmetry. The pseudospin operators η^+, $\eta^- = (\eta^+)^\dagger$ and η^z are defined as

$$\eta^+ = \sum_{\mathbf{k}} \psi^\dagger_{\mathbf{k}\uparrow} \psi^\dagger_{\bar{\mathbf{k}}\downarrow}, \tag{6a}$$

$$\eta_z = \frac{1}{2} \sum_{\mathbf{k}} (\psi^\dagger_{\mathbf{k}\uparrow} \psi_{\mathbf{k}\uparrow} + \psi^\dagger_{\bar{\mathbf{k}}\downarrow} \psi_{\bar{\mathbf{k}}\downarrow} - 1). \tag{6b}$$

The operators in Eq. (6) form and SU(2) algebra and are thus called pseudospin operators. They can act on various representations, but in the present scenario for the underdoped region, the representation chosen is a $l = 1$ triplet involving two conjugated SC operators (Δ_{-1} and Δ_1) and a d-wave charge sector operator Δ_0, which are defined as

$$\Delta_{-1} = \frac{1}{\sqrt{2}} \sum_{\mathbf{k}} \bar{d}_{\mathbf{k}} \psi_{\mathbf{k}\downarrow} \psi_{-\mathbf{k}\uparrow}, \tag{7a}$$

$$\Delta_0 = \frac{1}{2} \sum_{\mathbf{k},\sigma} \bar{d}_{\mathbf{k}} \psi^\dagger_{\bar{\mathbf{k}}\sigma} \psi_{-\mathbf{k},\sigma}, \tag{7b}$$

$$\Delta_1 = -\frac{1}{\sqrt{2}} \sum_{\mathbf{k}} \bar{d}_{\mathbf{k}} \psi^\dagger_{\mathbf{k}\uparrow} \psi^\dagger_{-\mathbf{k}\downarrow}. \tag{7c}$$

The form factor is given by $\bar{d}_{\mathbf{k}} = (d_{\mathbf{k}} + d_{\bar{\mathbf{k}}})/2$, with $d_{\mathbf{k}} = 2\cos(2\theta_{\mathbf{k}})$, and $\theta_{\mathbf{k}}$ the angle spanning the BZ. The standard SU(2) relations

$$[\eta^\pm, \Delta_m] = \sqrt{l(l+1) - m(m \pm 1)}\, \Delta_{m\pm 1} \tag{8}$$

$$\text{and} \quad [\eta_z, \Delta_m] = m \Delta_m \tag{9}$$

are valid here.

C. The involutions

1. Definitions

For the physics of underdoped cuprates, we consider and compare three types of involutions depicted below:

$$\text{(A)} \qquad \bar{\mathbf{k}} = -\mathbf{k} + 2\mathbf{k}_F, \tag{10}$$

where $\mathbf{k}_F$ is the Fermi wave vector parallel to $\mathbf{k}$. This form connects each wave vector in the BZ with a "$2\mathbf{k}_F$" partner close to the opposite side of the Fermi surface $\psi_{\mathbf{k}} \to \psi^\dagger_{\mathbf{k}-2\mathbf{k}_F}$ [see Fig. 2(a)]. The pseudospin SU(2) symmetry is exactly realized in the eight-hot-spot spin-fermion model, where the electronic density is linearized around the hot spots [70,72]. In this case, there are only four "$2\mathbf{k}_F$" wave vectors denoted by

$$\text{(B)} \qquad \bar{\mathbf{k}} = -\mathbf{k} + \mathbf{Q_0}, \quad \text{with } \mathbf{Q}_0 = (\pm\mathbf{Q}_a, \pm\mathbf{Q_b}), \tag{11}$$

which are aligned with the diagonal of the BZ. For a generic Fermi surface, multiple $2\mathbf{k}_F$ wave vectors can be chosen, as depicted in Fig. 2(a), or alternatively we can keep the four wave vectors defined for eight-hot-spot model and generalize their action on the whole BZ as shown in Fig. 2(b).

An important point to stress out is that the two forms of possible involutions Eq. (10) and Eq. (11) are degenerate in the eight-hot-spot model, since at the hot spots, the "$2\mathbf{k}_F$" wave vectors reduce to the four wave vectors of Eq. (11). In the case of a full Fermi surface, the two generalizations give very different physics that we will describe in the following paragraph. Before, let us introduce a third kind of involution which corresponds to a the particle-hole transformation $\psi_{\mathbf{k}} \to \psi^\dagger_{\mathbf{k}}$ and for which we have

$$\text{(C)} \qquad \bar{\mathbf{k}} = \mathbf{k}. \tag{12}$$

Case C is presented in Fig. 2(c). This case corresponds to an ordering vector of $-2\mathbf{k}$.

2. Physical interpretation

The three kinds of involutions rotate a superconducting doublet Δ_{-1}, Δ_1, Eqs. (7), into an alternative channel in the charge sector Δ_0, Eq. (7b). The forms of Δ_0 vary explicitly, however, in three cases:

$$\text{(A)} \qquad \Delta_0 = \frac{1}{2} \sum_{\mathbf{k},\sigma} \bar{d}_{\mathbf{k}} \psi^\dagger_{\mathbf{k}-2\mathbf{k}_F\sigma} \psi_{\mathbf{k},\sigma}, \tag{13a}$$

$$\text{(B)} \qquad \Delta_0 = \frac{1}{2} \sum_{\mathbf{k},\sigma} \bar{d}_{\mathbf{k}} \psi^\dagger_{\mathbf{k}-\mathbf{Q}_0\sigma} \psi_{\mathbf{k},\sigma}, \tag{13b}$$

$$\text{(C)} \qquad \Delta_0 = \frac{1}{2} \sum_{\mathbf{k},\sigma} \bar{d}_{\mathbf{k}} \psi^\dagger_{-\mathbf{k}\sigma} \psi_{\mathbf{k},\sigma}. \tag{13c}$$

The charge order parameters A, B, and C couple very differently with the conduction electrons, represented in Fig. 2 and differently than SC order parameter represented in Fig. 3.

In the case of the "Peierls" or "$2\mathbf{k}_F$" coupling, the electronic dispersion is translated by "$2\mathbf{k}_F$" around each point of the Fermi surface, which leads to an obvious band crossing and opening of a gap. The same is valid for (B), where the electronic dispersion is translated by the wave vector $\pm\mathbf{Q}_{a,b}$ around the zone edge, leading to band crossing and the opening of a gap. The situation C, however, is drastically different since without an inversion symmetry point we have $\xi_{\mathbf{k}} = \xi_{-\mathbf{k}}$ and the transformation does not lead to the opening of a gap.

For comparison, let us mention the SC parts Δ_{-1}, Δ_1, for which the opening of the gap is ensured by the charge conjugation leading to a reversing of the electron energy

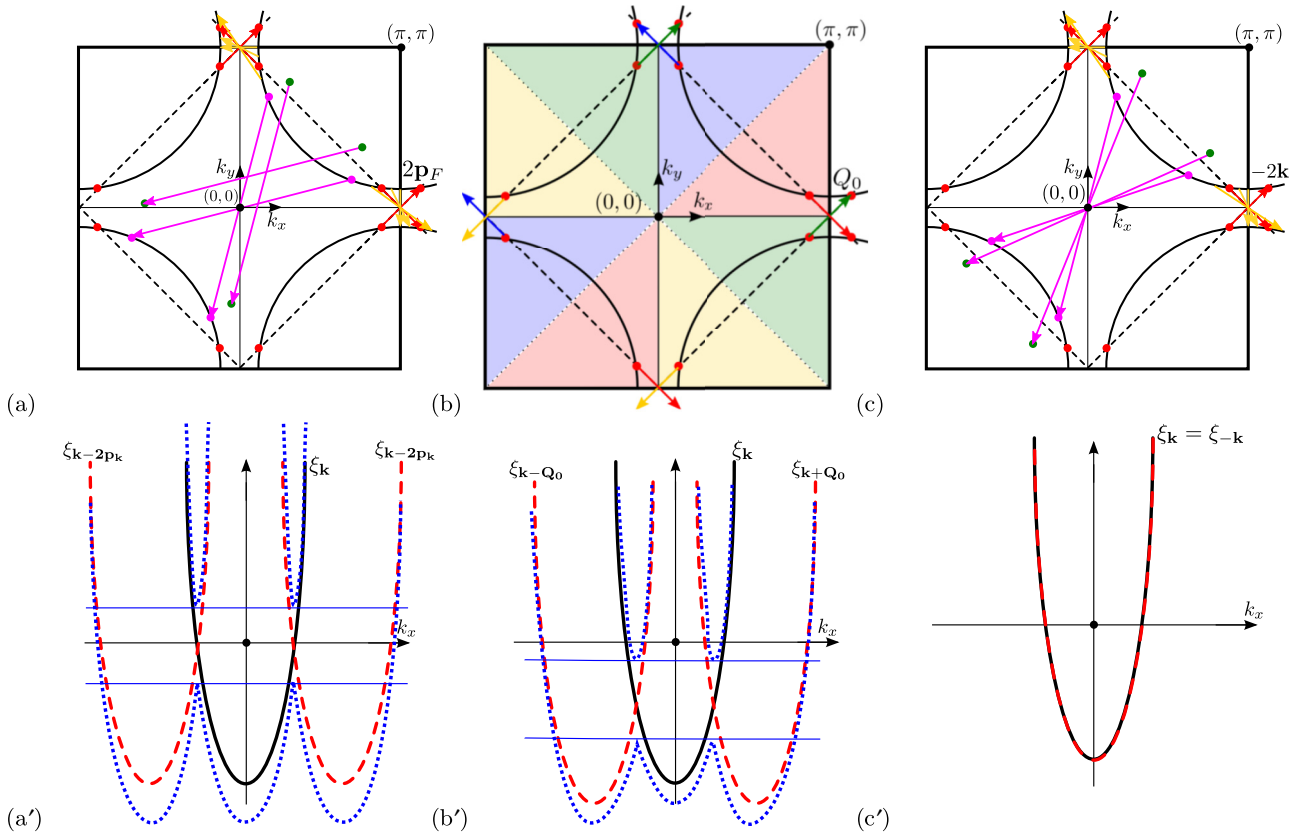

FIG. 2. We represent in the first BZ of the different involution scenario: (a) $\overline{\mathbf{k}} = -\mathbf{k} + 2\mathbf{k}_F$, (b) $\overline{\mathbf{k}} = -\mathbf{k} + \mathbf{Q_0}$ with $\mathbf{Q}_0 = (\pm\mathbf{Q}_a, \pm\mathbf{Q_b})$, and (c) $\overline{\mathbf{k}} = \mathbf{k}$. We represent the bare (solid line), shifted (dashed line) and hybridized (dotted line) electronic band dispersion along the $(\pi,0)$ to (π,π) direction in (a′) $\overline{\mathbf{k}} = -\mathbf{k} + 2\mathbf{k}_F$, (b′) $\mathbf{Q}_0 = (\pm\mathbf{Q}_a, \pm\mathbf{Q_b})$, and (c′) $\overline{\mathbf{k}} = \mathbf{k}$ scenarios. As drawn in the figures (a′) and (b′), the opening of the gap opens at the crossing of the original and shifted spectra. In (a′), the opening of the gap occurs at the Fermi surface while it is the case at only one point for an incommensurate ordering vector. For example, in the scenario (b′), this opening occurs below the Fermi surface. In absence of symmetry breaking, it is not able to open a gap between two identical electronic band as presented in (c′).

$\xi_{\mathbf{k}} \to -\xi_{-\mathbf{k}}$ with a band crossing locked at the Fermi level. The picture is also drastically different in real space, and the easiest way to see it is to Fourier transform the ladder operator η^+ Eq. (11) in the three cases:

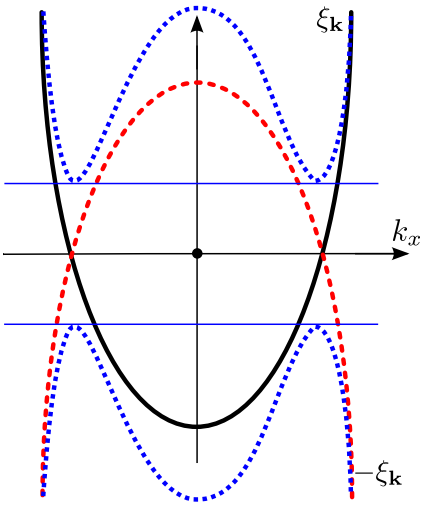

FIG. 3. Representation of the electronic spectrum for a superconducting scenario. The superconducting state provides a hybridization between an electronic and a hole spectrum. The gap opens at the Fermi surface and does not depend on the curvature.

$$\text{(A)} \quad \eta^+ = \sum_{\mathbf{k}} \psi^\dagger_{\mathbf{k}\uparrow} \psi^\dagger_{-\mathbf{k}+2\mathbf{k}_F\downarrow}, \tag{14a}$$

$$\text{(B)} \quad \eta^+ = \sum_{\mathbf{k}} \psi^\dagger_{\mathbf{k}\uparrow} \psi^\dagger_{-\mathbf{k}+\mathbf{Q}_0\downarrow}, \tag{14b}$$

$$\text{(C)} \quad \eta^+ = \sum_{\mathbf{k}} \psi^\dagger_{\mathbf{k}\uparrow} \psi^\dagger_{\mathbf{k}\downarrow}. \tag{14c}$$

In the three cases, (14) correspond to a finite wave vector pairing—also called Fulde-Ferrell-Larkin-Ovshinnikov (FFLO) pairing, at wave vectors $2\mathbf{k}_F$ in case A, $\mathbf{Q}_0$ in case B, and $2\mathbf{k}$ in case C. This leads to a rewriting of the ladder operators as

$$\text{(A)} \quad \eta^+ = \sum_{\mathbf{k}} \sum_{i,j} e^{i2\mathbf{k}_F\cdot(r_i+r_j)/2} e^{i\tilde{\mathbf{k}}_a\cdot(r_i-r_j)} \psi^\dagger_{i\uparrow} \psi^\dagger_{j\downarrow}, \tag{15a}$$

$$\text{(B)} \quad \eta^+ = \sum_{\mathbf{k}} \sum_{i,j} e^{i\mathbf{Q}_0\cdot(r_i+r_j)/2} e^{i\tilde{\mathbf{k}}_b\cdot(r_i-r_j)} \psi^\dagger_{i\uparrow} \psi^\dagger_{j\downarrow}, \tag{15b}$$

$$\text{(C)} \quad \eta^+ = \sum_{\mathbf{k}} \sum_{i,j} e^{i2\mathbf{k}\cdot(r_i+r_j)/2} \psi^\dagger_{i\uparrow} \psi^\dagger_{j\downarrow}. \tag{15c}$$

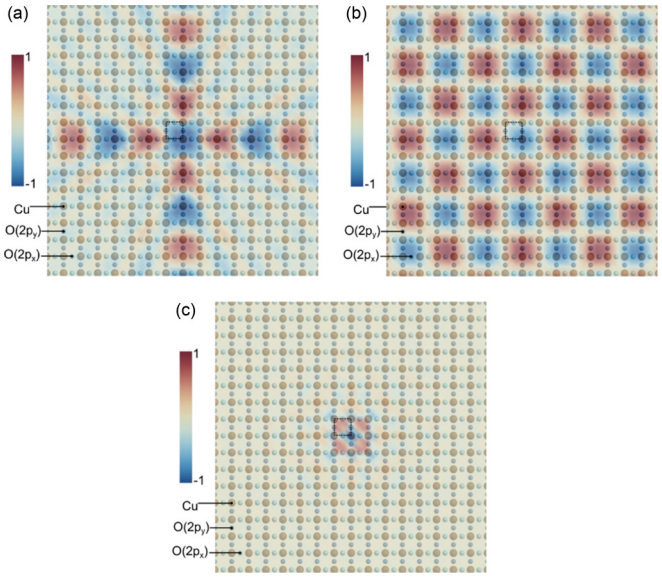

FIG. 4. Charge density in the real space in the different involution scenarios: (a) $\bar{\mathbf{k}} = -\mathbf{k} + 2\mathbf{k}_F$, (b) $\mathbf{Q}_0 = (\pm\mathbf{Q}_a, \pm\mathbf{Q}_b)$, and (c) $\bar{\mathbf{k}} = \mathbf{k}$.

In case A, $2\mathbf{k}_F$ depends on $\mathbf{k}$ while $\tilde{\mathbf{k}}_a = \mathbf{k} - \mathbf{k}_F$ is small close to the Fermi energy. In this case, the summation over $\mathbf{k}$ leads to a localization of the center of mass of the pair $r_i + r_j = 0$. The same holds in case C where the summation over $\mathbf{k}$ does not affect the variable $r_i - r_j$. Case B, however, is the opposite, since $\mathbf{Q}_0$ is a finite wave vector independent of $\mathbf{k}$, while $\tilde{\mathbf{k}}_b = \mathbf{k} - \mathbf{Q}_0/2$ is $\mathbf{k}$-dependent and locates the relative position of the pair to the be small $r_i - r_j = 0$. Case B is similar to a standard, zero momentum superconductor, for which we would have $\eta^+ = \sum_{\mathbf{k}} \psi^\dagger_{\mathbf{k}\uparrow}\psi^\dagger_{-\mathbf{k}\downarrow}$, leading to $\eta^+ = \sum_{\mathbf{k}}\sum_{i,j} e^{i\mathbf{k}\cdot(r_i - r_j)}\psi^\dagger_{\mathbf{i}\uparrow}\psi^\dagger_{j\downarrow}$, for which the $\mathbf{k}$ summation located $r_i - r_j = 0$.

Real-space pictures illustrating the three situations are given in Fig. 4. We note the cross-structure in (a) showing the singularity of the origin, which comes from the multiple wave vectors, leading to a typical checkerboard structure in (b), which corresponds to and order with the superposition of the two axial wave vectors $(0, \mathbf{Q_0})$ and $(\mathbf{Q_0}, 0)$. Case (c), which never leads to the opening of a gap, shows a very small typical length scale.

The real-space picture associated with the physics of the objects depicted in Fig. 4(a) has been described in Ref. [147], and will be addressed again in Secs. VIII and X. Noticeably, the structure depicted in Fig. 4(a) has two energy scales, one associated with the relative distance between electrons and holes in the pair, and the other one associated to the position and extension around the center of mass $(r_i + r_j)/2$. The summation over the multiple $2\mathbf{p}_F$ wave vectors produces a localization of the center of mass at the origin, which is typically associated with the formation of a local object, with a specific modulation pattern. The study of the physics of such objects, or patches, goes beyond the scope of this paper, but it is interesting to see that already at the level of the symmetries, one sees a profound difference in real space between patches of particle-hole pairs [Fig. 4(a)] and uniform checkerboard phase [Fig. 4(b)].

The same game can be played with the charge states given in Eqs. (13):

$$\text{(A)}\quad \Delta_0 = \frac{1}{2}\sum_{\mathbf{k},\sigma}\sum_{i,j} e^{i2\mathbf{k}_F\cdot(r_i+r_j)/2} e^{i\tilde{\mathbf{k}}_a\cdot(r_i-r_j)}\overline{d}_{\mathbf{k}}\psi^\dagger_{i\sigma}\psi_{j\sigma}, \tag{16a}$$

$$\text{(B)}\quad \Delta_0 = \frac{1}{2}\sum_{\mathbf{k},\sigma}\sum_{i,j} e^{i\mathbf{Q}_0\cdot(r_i+r_j)/2} e^{i\tilde{\mathbf{k}}_b\cdot(r_i-r_j)}\overline{d}_{\mathbf{k}}\psi^\dagger_{i\sigma}\psi_{j\sigma}, \tag{16b}$$

$$\text{(C)}\quad \Delta_0 = \frac{1}{2}\sum_{\mathbf{k},\sigma}\sum_{i,j} e^{i2\mathbf{k}\cdot(r_i+r_j)/2}\overline{d}_{\mathbf{k}}\psi^\dagger_{i\sigma}\psi_{j\sigma}. \tag{16c}$$

Note the similarity of Eqs. (15) and (16), which lead to the same real-space interpretations.

III. THE SU(2) ENVELOP

A. The starting model with short-range AF interactions

There are a few models which are well-known to give rise to d-wave superconductivity. The repulsive Hubbard-model can be mapped out onto an effective model where the superexchange between adjacent sites is described via the t-J Hamiltonian where the strong Coulomb interactions are described through a constraint of no double occupancy (see, e.g., Ref. [5] for a review):

$$H_{tJ} = \sum_{i,j,\sigma}\psi^\dagger_{i,\sigma}t_{ij}\psi_{j,\sigma} + J\sum_{\langle i,j\rangle\alpha\beta}\psi^\dagger_i\vec{\sigma}_{\alpha\beta}\psi_{i\beta}\cdot\psi^\dagger_{j\alpha'}\vec{\sigma}_{\alpha'\beta'}\psi_{j\beta'}, \tag{17}$$

where ψ is the conduction electron field, t_{ij} is the hopping matrix describing the band structure of the materials, which is typically of the order of 1 eV, $\langle i,j\rangle$ denotes the summation over nearest neighbors typical of the AF superexchange term of order 0.7 eV, and $\vec{\sigma}$ is the Pauli matrix describing the spin. The constraint of no double occupancy has to be imposed, in order to give a good treatment to the vicinity to a Mott insulator, but we neglect it for simplicity and consider that the main effects treated here come from the AF short-range interactions in Eq. (17). In momentum space, the Hamiltonian reads

$$H = \sum_{\mathbf{k}\alpha}\xi_{\mathbf{k}}\psi^\dagger_{\mathbf{k},\alpha}\psi_{\mathbf{k},\alpha} - \sum_{\substack{kk'\overline{q}\\ \sigma\sigma'}} J_{\overline{\mathbf{q}}}\psi^\dagger_{\sigma,\mathbf{k}+\overline{\mathbf{q}}}\psi_{\mathbf{k},\sigma'}\psi^\dagger_{\mathbf{k}'-\overline{\mathbf{q}}}\psi_{\mathbf{k}',\sigma}, \tag{18}$$

where $J_{\overline{\mathbf{q}}} = 2J\cos\overline{\mathbf{q}}$, with $\overline{\mathbf{q}} = \mathbf{Q} + \mathbf{q}$, and $\mathbf{Q} = (\pi,\pi)$ the AF wave vector. In contrast with Sec. II A, where the AF coupling had been taken close to a QCP where it becomes singular, we assume no such singularity here. The AF correlations are typically found to be strong and short-ranged in the cuprates, and the Hamiltonian (17) is generic enough to account for this feature. In our previous work on the eight-hot-spot model [72], the proximity to AF quantum criticality was assumed and crucial for the control of the solution. Here, although we use mean-field-like methods, the starting point is more realistic for a general theory of the PG in cuprates.

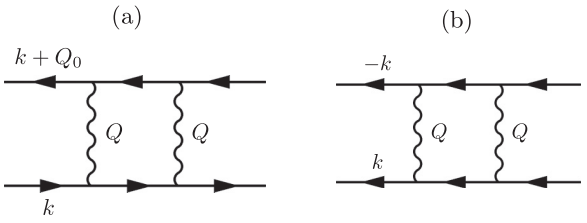

FIG. 5. Infinite ladder series corresponding to the gap equations (19) for diagram (a) and (21) for diagram (b), respectively.

B. Charge and SC decoupling

We can now decouple the second term in Eq. (18) in the charge and SC channels, which leads to two types of gap equations. (1) In the charge channel, the Hubbard-Stratonovich decoupling of Eq. (18) leads to the effective action

$$S_\chi^{\rm eff} = \int_{k,k',\bar{q}} \Bigg(J_{\bar{q}}^{-1} \chi_{k,k'} \chi_{k+\bar{q},k'+\bar{q}} + \chi_{k,k'} \sum_\sigma \psi^\dagger_{k+\bar{q},\sigma} \psi_{k'+\bar{q},\sigma} + \chi_{k+\bar{q},k'+\bar{q}} \sum_\sigma \psi^\dagger_{k,\sigma} \psi_{k',\sigma} \Bigg),$$

where $\chi_{k,k'} = \langle \sum_\sigma \psi^\dagger_{k,\sigma} \psi_{k',\sigma} \rangle$. Integrating the fermions out of the partition function and then differentiating with respect to χ leads to the gap equation, in the charge sector. Here $\mathbf{k}'-\mathbf{k} = \mathbf{Q_0}$, where $\mathbf{Q}_0$ is the incommensurate charge modulation vector [see Fig. 5(a)]:

$$\chi_{k,k'} = -\delta_{\mathbf{k}',\mathbf{k}+\mathbf{Q}_0}\, \Re T \sum_{\omega,\bar{\mathbf{q}}} J_{\bar{\mathbf{q}}} \times \frac{\chi_{k+\bar{q},k'+\bar{q}}}{(i\epsilon + i\omega - \xi_{\mathbf{k}+\bar{\mathbf{q}}})(i\epsilon' + i\omega - \xi_{\mathbf{k}'+\bar{\mathbf{q}}}) - \chi^2_{k+\bar{q},k'+\bar{q}}}. \tag{19}$$

(2) Similar action is derived in the SC channel, with

$$S_\Delta^{\rm eff} = \int_{k,k',\bar{q}} \Bigg(J_{\bar{q}}^{-1} \Delta^\dagger_{k,k'} \Delta_{k+\bar{q},k'-\bar{q}} + \Delta^\dagger_{k,k'} \sum_\sigma \sigma \psi_{k+\bar{q},\sigma} \psi_{k'-\bar{q},-\sigma} + \chi_{k+\bar{q},k'-\bar{q}} \sum_\sigma \sigma \psi^\dagger_{k,\sigma} \psi^\dagger_{k',-\sigma} \Bigg), \tag{20}$$

where $\Delta_{k,k'} = \langle \sum_\sigma \sigma \psi_{k,\sigma} \psi_{k',-\sigma} \rangle$, and $\mathbf{k}' = -\mathbf{k}$. We get the standard SC gap equation ($\Delta_k = \Delta_{k,-k}$) [see Fig. 5(b)]:

$$\Delta_k = -T \sum_{\omega,\bar{\mathbf{q}}} J_{\bar{\mathbf{q}}} \frac{\Delta_{k+\bar{q}}}{\Delta^2_{k+\bar{q}} + \xi^2_{\mathbf{k}+\bar{\mathbf{q}}} + (\epsilon+\omega)^2}. \tag{21}$$

Throughout the paper, if not stated otherwise, the calculations are made for Bi2212, with a band structure taken from Ref. [124]. Specifically, we take

$$\xi_{\mathbf{k}} = 2t_1 + t_2(\cos k_x + \cos k_y) + 2t_3 \cos k_x \cos k_y + t_4 \cos 2k_x + \cos 2k_y + t_5(\cos 2k_x \cos k_y + \cos 2k_y \cos k_x) + 2t_6 \cos 2k_x \cos 2ky - \mu, \tag{22}$$

with (in eV) $t_1 = 0.196$, $t_2 = -0.6798$, $t_3 = 0.2368$, $t_4 = -0.0794$, $t_5 = 0.0343$, and $t_6 = 0.0011$. The solution of Eqs. (19) and (21) is given in Fig. 6 for various charge

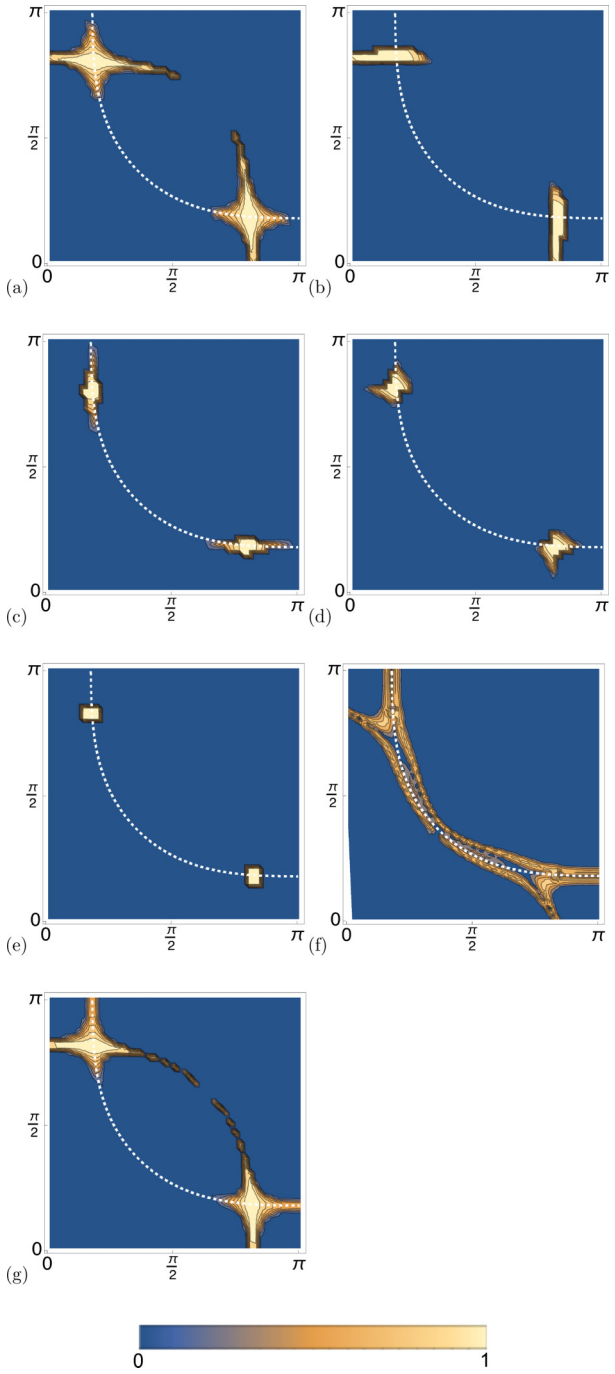

FIG. 6. (a)–(f) Solution of the gap equations $\chi_{k,k+Q_0}$ from Eq. (19) and (f) the superconducting order parameter Δ_k from (21). Vanishing solutions are color-coded in blue while nonvanishing points are depicted in yellow. We took various modulation wave vectors $\mathbf{Q}_0$ with (a) the diagonal wave vector $\mathbf{Q}_0 = (Q_\mathbf{0}, Q_\mathbf{0})$ linking two hot spots, (b) the axial wave vector $\mathbf{Q}_0 = (Q_\mathbf{0}, 0)$, (c) $\mathbf{Q}_0 = (0, Q_\mathbf{0})$, which are observed experimentally, (d) the AF wave vector $\mathbf{Q}_0 = (\pi,\pi)$, (e) the null wave vector $\mathbf{Q}_0 = (0,0)$, and (f) the $2\mathbf{p}_F$-wave vector corresponding to the involution described in Eq. (10). The solution of the SC gap equation is given in (g). The calculations are made on the band structure of Bi2212 form Ref. [124] (see details in the text for the band parameters). The calculations are made within the approximation $J_{\bar{\mathbf{q}}} = J\delta(\bar{\mathbf{q}})$, with $J = 0.35$, which restricts the q integration at the vector (π,π). The energy units, if not stated otherwise, are in eV.

modulation vectors. The main point of this preliminary study, is that all the wave vectors have an equivalent response at the hot spot, which is also the same as the SC response. In other words, all the orders considered above are quasidegenerate at the hot spots. The difference between the gap solution of various wave vectors lies in its extension in $\mathbf{k}$ space, which is more pronounced for the SC, the $2\mathbf{p}_F$ and the diagonal $\mathbf{Q}_0 = (Q_0, Q_0)$ cases. The only modulation wave vectors which give a nonzero answer are the ones relating two hot spots, or surrounding the hot spots in the case of the SC and $2\mathbf{p}_F$ orders. An important point is that d-wave symmetry is required to satisfied Eqs. (19) and (21). A simple way to see this is to notice that the gap equations relate the two antinodal zones $\mathbf{k} \to \mathbf{k} + \mathbf{Q}$, with $\mathbf{Q} = (\pi,\pi)$ the AF wave vector. Solutions with $\Delta_{\mathbf{k}} = -\Delta_{\mathbf{k}+\mathbf{Q}}$ are thus stabilized.

The case of strong coupling is treated in Appendix A, where we see that, as the coupling increased, the shape of the SC and CDW changes. The SC solution is now gapping out the entire Fermi surface whereas the CDW solutions are confined within the antinodal regions. The development of the SU(2) fluctuations requires the mean-field decoupling to give sensibly equal values of the order parameters in the two sectors. This is true at the hot spots, as seen in the next Sec. III C, but it is not valid anymore far away from the hot spot. A simple way to quantize this effect is to define the cutoff energy scale below which SU(2) fluctuations are present, as the mean of the gaps in the two sectors,

$$\Delta^2_{\mathrm{SU(2)}} = \sqrt{\chi^2 \Delta^2}, \tag{23}$$

so that $\Delta_{\mathrm{SU(2)}}$ naturally vanishes away from the hot spots.

C. Cutoff energy scale

The starting point of our reflexion is to notice that a simple model with short-range AF correlations, which is minimal to describe the underdoped regime of cuprate superconductors, has a few quasidegenerate solutions at the hot spot, including the d-wave SC and d-wave charge orders. Our assumption, starting from now, is that this simple model gives a good insight, and hints that an SU(2) symmetry is present in the phase diagram of those compounds, which relates the d-wave SC state to the d-wave charge sector. The SU(2) symmetry is broken at low temperature, but then fluctuations will exist up to a temperature scale which defines the SU(2) dome. In Fig. 7, the solutions at the hot spots of the d-wave SC and d-wave CDW are given for various wave vectors, as a functions of the decreasing AF coupling constant J present in Eqs. (19) and (21). J slowly decreases from $J = J_0 = 1$ at half-filling ($p = 0$, where p is the hole doping), to $J \simeq 0$ at larger hole doping. Assuming a scaling relation of the type $p \sim (J_0 - J)^{\alpha}$, we get a form of the PG dome very close to the one experimentally observed in cuprates. For a wide region of hole doping, the SC solution at the hot spot is degenerate with the CDW one. When $J \sim 0$, the CDW solution is lost whereas the SC solution survives. The phase diagrams of Fig. 7 mimic the situation in the underdoped regime of the cuprates as a function of hole doping. The region where the two solutions are degenerate is interpreted in our framework as the SU(2) envelope, below which SU(2) fluctuations are present. They will be described in the next section.

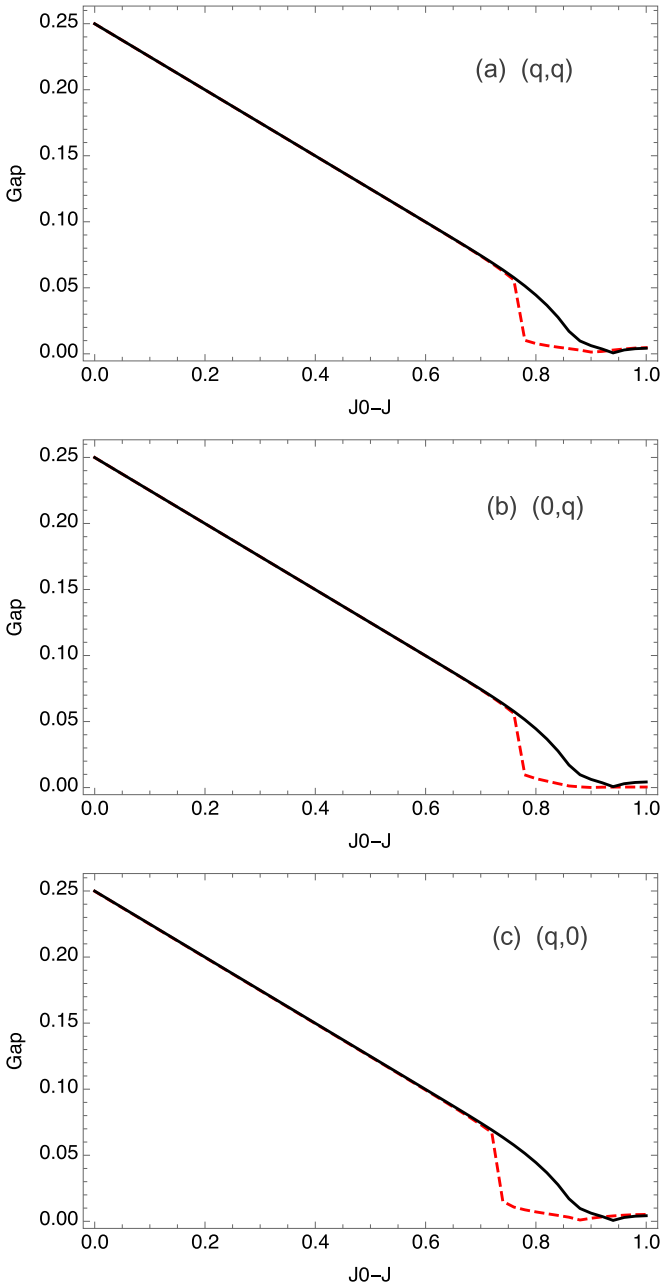

FIG. 7. Comparison of the d-wave charge $\chi_{k,k+Q_0}$ solution of Eq. (19) (dashed red) and d-wave SC Δ_k solution of Eq. (21) (black line) taken at the hot spot. We compare various modulation wave vectors for $\chi_{k,k+Q_0}$ with (a) the diagonal wave vector $\mathbf{Q}_0 = (Q_0, Q_0)$ linking two hot spots, (b) the axial wave vector $\mathbf{Q}_0 = (0, Q_0)$, and (c)$\mathbf{Q}_0 = (Q_0, 0)$. The evolution of the SC and CDW gaps as a function of $J - J_0$ has the typical form of a dome. SC and CDW solutions at the hot spots are completely degenerate within the range of J, whereas the CDW solution is lost before the SC one when $J \sim J_0$ ($J_0 = 1$).

IV. SU(2) FLUCTUATIONS COUPLED TO FERMIONS

In the previous section, we have shown that short-range AF correlations give rise to a finite number of possible d-wave order parameters which are quasidegenerate at the hot spots. The main ideas of this paper are the following: first, this

quasidegeneracy is described by an emerging SU(2) symmetry, and second, the fluctuations associated with this symmetry are in turn lifting the degeneracy between the various modulation vectors. This section is devoted to the study of the SU(2) fluctuations.

In order to proceed with the study of the SU(2) fluctuations, we must choose one of the wave vectors associated with the charge sector. For definiteness, we start with the diagonal wave vector $\mathbf{Q_0} = (Q_0, Q_0)$, bearing in mind that it is not the one experimentally observed in the underdoped region. Our starting point is to derive the SU(2) effective model which couples to fermions. The action is comprised of three terms:

$$S_{st} = S^0_\psi + S_{\rm int} + S^0_Q. \tag{24}$$

A. Bare action S^0_ψ

S^0_ψ is the bare action for electrons, which is defined in SU(2) context as

$$S^0_\psi = -\int_{x,x'} \overline{\Psi}_x G_{0_{x,x'}}^{-1} \Psi_{x'}, \tag{25}$$

where $x = (\mathbf{r}, \tau, \sigma)$ with $\sigma \in \{\uparrow, \downarrow\}$ the spin and $\int_x \equiv \int d\mathbf{r} \int_0^\beta d\tau \sum_\sigma$ and the free inverse propagator is

$$G_{0_{x,x'}}^{-1} = \left(\partial_\tau - \hat{\xi}_{i\nabla_{\mathbf{r}}}\right)\delta^{(d)}(\mathbf{r} - \mathbf{r}')\delta(\tau - \tau')\delta_{\sigma,\sigma'}. \tag{26}$$

In momentum and imaginary frequency space, the Green functions are defined as

$$G_{k,k'}\delta_{\sigma,\sigma'} = -\langle \mathcal{T}\Psi_\sigma(k)\bar{\Psi}_{\sigma'}(k')\rangle. \tag{27}$$

The field Ψ is written in a 4×4 basis in momentum space with

$$\Psi_k = \frac{1}{\sqrt{2}}(\psi_{\mathbf{k},\sigma},\ \psi^\dagger_{-\mathbf{k}-\mathbf{Q_0},-\sigma},\ \psi_{\mathbf{k}+\mathbf{Q_0},\sigma},\ \psi^\dagger_{-\mathbf{k},-\sigma}),^T \tag{28}$$

where $()^T$ denotes the standard transposition, and

$$\overline{\Psi}_k = \frac{1}{\sqrt{2}}(\psi^\dagger_{\mathbf{k},\sigma},\ -\psi_{-\mathbf{k}-\mathbf{Q_0},-\sigma},\ \psi^\dagger_{\mathbf{k}+\mathbf{Q_0},\sigma},\ -\psi_{-\mathbf{k},-\sigma}), \tag{29}$$

where $k \equiv (i\omega_n, \mathbf{k})$ and the factor $1/\sqrt{2}$ normalizes the spin summation. Note that the conjugation in the particle-hole sector (τ) is not standard, with the "charge conjugate" defined as $\overline{\Psi} = \Psi^\dagger\tau_3$. Throughout the paper τ_α, Λ_α with $\alpha = 1,3$ stand for the Pauli matrices in each sector. In this basis, and in momentum space, the bare electron action becomes

$$S^0_\psi = -\frac{1}{\beta N}\sum_{\mathbf{k},\omega} \overline{\Psi}_k G_{0_k}^{-1}\Psi_k, \tag{30}$$

and G_0^{-1} is defined as

$$\hat{G}^{-1}_{0,k} = \left(\begin{array}{cc|cc} i\omega - \xi_{\mathbf{k}} & & & \\ & i\omega + \xi_{-\mathbf{k}-\mathbf{Q_0}} & & \\ \hline & & i\omega - \xi_{\mathbf{k}+\mathbf{Q_0}} & \\ & & & i\omega + \xi_{-\mathbf{k}} \end{array}\right)_\Lambda, \tag{31}$$

where $\mathbf{Q_0}$ is the diagonal wave vector connecting two hot spots, as defined in Eq. (6a), and $\xi_{\mathbf{k}}$ is the electronic dispersion. The 4×4 basis can be conveniently factorized as the direct product of two subspaces $\tau \otimes \Lambda$, where τ is the charge conjugation space describing the SC channel and Λ is the subspace corresponding to the translation by the vector $\mathbf{Q_0}$. In the case where the model is reduced to eight-hot-spot (see, e.g., Ref. [72]), the vector $\mathbf{Q_0}$ corresponds to the vector $2\mathbf{k}_F$ relating the diagonal hot spots in the same AN region, and we have the symmetry relations $\xi_{-\mathbf{k}} = \xi_{\mathbf{k}}$ and $\xi_{\mathbf{k}+\mathbf{Q_0}} = -\xi_{\mathbf{k}}$, the latter being valid when the dispersion is linearized around the Fermi surface and close to the hot spots. Within this approximation, we get

$$\begin{aligned}\hat{G}^{-1}_{0,hs,k} &= \left(\begin{array}{cc|cc} i\omega - \xi_{\mathbf{k}} & & & \\ & i\omega - \xi_{\mathbf{k}} & & \\ \hline & & i\omega + \xi_{\mathbf{k}} & \\ & & & i\omega + \xi_{\mathbf{k}} \end{array}\right)_\Lambda, \\ &= i\omega - \xi_{\mathbf{k}}\Lambda_3. \end{aligned} \tag{32}$$

In the form of Eq. (32), the SU(2) symmetry in $G^{-1}_{0,hs,k}$ is explicit. In all generality, it is possible to model the term breaking the SU(2) symmetry by noticing that the condition $\xi_{\mathbf{k}+\mathbf{Q_0}} = -\xi_{\mathbf{k}}$ is valid only close to the hot spot and when the dispersion is linearized around the Fermi level. If this condition is not verified, we define

$$\overline{\xi}_{\mathbf{k}} = (\xi_{\mathbf{k}} - \xi_{\mathbf{k}+\mathbf{Q_0}})/2, \tag{33}$$

$$\Delta\xi_{\mathbf{k}} = (\xi_{\mathbf{k}} + \xi_{\mathbf{k}+\mathbf{Q_0}})/2, \tag{34}$$

where $\overline{\xi}_{\mathbf{k}}$ is the symmetric dispersion and $\Delta\xi_{\mathbf{k}}$ can be understood as a curvature term. The matrix $\hat{G}_0^{-1}$ in Eq. (31) then takes the form

$$\hat{G}^{-1}_{0,k} = \begin{pmatrix} i\omega - \overline{\xi}_{\mathbf{k}} - \Delta\xi_{\mathbf{k}}\tau_3 & 0 \\ 0 & i\omega + \overline{\xi}_{\mathbf{k}} - \Delta\xi_{\mathbf{k}}\tau_3 \end{pmatrix}_\Lambda, \tag{35}$$

which we can rewrite Eq. (35) as

$$\hat{G}^{-1}_{0,k} = i\omega - \overline{\xi}_{\mathbf{k}}\Lambda_3 + \Delta\xi_{\mathbf{k}}\tau_3, \tag{36}$$

where $G^{-1}_{0,s,k} = i\omega - \overline{\xi}_{\mathbf{k}}\Lambda_3$ is SU(2)-symmetric (proportional to τ_0) and the term $\Delta\xi_{\mathbf{k}}\tau_3$ is the SU(2) symmetry-breaking term (proportional to τ_3). The separation between symmetric and symmetry breaking terms in Eqs. (35) and (36) is the crucial step, which will be useful in describing the fluctuations in Sec. V.

B. Interacting term $S_{\rm int}$

The interacting term can simply be taken as a two-body interaction

$$S^0_i = \frac{1}{4}\int_{x,x'} \gamma_{x-x'} \mathrm{Tr}[\overline{\Psi}_x\Psi_x\overline{\Psi}_{x'}\Psi_{x'}], \tag{37}$$

where Ψ is the two by four fields spinor defined in Eq. (27). The form of the propagator $\gamma_{x-x'}$ is not detailed at the moment. Using a Hubbard-Stratonovich decoupling with respect to the field $\hat{Q}_{x,x'}$, we get $S^0_i \to S_{\rm int} + S^0_Q$ from Eq. (24) with

$$S_{\rm int} = \frac{1}{2}\int_{x,x'} \mathrm{Tr}[\overline{\Psi}_x\hat{Q}_{x,x'}\Psi_{x'}], \tag{38}$$

$$S^0_Q = \frac{1}{4}\int_{x,x'} \mathrm{Tr}\left[\overline{\hat{Q}}_{x,x'}\hat{\gamma}^{-1}_{x-x'}\hat{Q}_{x',x}\right], \tag{39}$$

where the Tr runs over the matrix structure and $\hat{Q}_{x,x'} \sim \langle \overline{\Psi}_x \Psi_{x'} \rangle$ is a 4×4 matrix, which can be decomposed (within the direct product of spaces $\tau \times \Lambda$) as

$$\hat{Q}_{x,x'} = \begin{pmatrix} & \hat{q}_{x,x'} \\ \hat{q}^\dagger_{x,x'} & \end{pmatrix}_\Lambda, \tag{40}$$

with $\hat{q}_{x,x'} = Q^0_{x-x'} \hat{u}_{x,x'}$, $\hat{u}_{x,x'} = \frac{1}{N^2} \sum_{\mathbf{k},\mathbf{k}',\omega'} e^{-i\mathbf{k}\cdot r} e^{i\omega_n \tau} e^{i\mathbf{k}'\cdot r'} e^{-i\omega'_n \tau'} \hat{u}_{k,k'}$, and

$$\hat{u}_{k,k'} = \begin{pmatrix} \chi_{k,k'+Q_0} & -\sigma \Delta_{k,-k'} \\ \sigma \Delta^\dagger_{k+Q_0,-k'-Q_0} & \chi^\dagger_{-k-Q_0,-k'} \end{pmatrix}_\tau. \tag{41}$$

Mean-field effects are obtained by taking $k' = k$. Indeed, the field χ represents a particle-hole pair, suitable to describe the charge modulations ($\chi_{k,k'+Q_0} \sim \langle \psi^\dagger_{\mathbf{k},\sigma} \psi_{\mathbf{k}+Q_0,\sigma} \rangle$), while the field Δ is the SC particle-particle pairing field describing the formation of coherent pairs ($\Delta_{k,-k'} \sim \sigma \langle \psi_{\mathbf{k},-\sigma} \psi_{-\mathbf{k},\sigma} \rangle$). In this limit, the matrix $\hat{u}_{k,k'}$ in Eq. (41) writes

$$\hat{u}_k = \begin{pmatrix} \chi_{k,k+Q_0} & -\sigma \Delta_{k,-k} \\ \sigma \Delta^\dagger_{k+Q_0,-k-Q_0} & \chi^\dagger_{-k-Q_0,-k} \end{pmatrix}_\tau, \tag{42}$$

where

$$\begin{aligned} \Delta_k &\sim \sigma \langle \psi_{k,-\sigma} \psi_{-k,\sigma} \rangle, \\ \chi_k &\sim \langle \psi^\dagger_{k,\sigma} \psi_{k+Q_0,\sigma} \rangle, \\ \Delta^\dagger_{k+Q_0} &\sim \sigma \langle \psi_{k+Q_0,-\sigma} \psi_{-k-Q_0,\sigma} \rangle, \\ \chi^\dagger_{-k-Q_0} &\sim \langle \psi^\dagger_{-k-Q_0,-\sigma} \psi_{-k,-\sigma} \rangle. \end{aligned}$$

The SU(2) symmetry requires that $\Delta^\dagger_{k+Q_0,-k-Q_0} = \Delta^\dagger_{k,-k}$ and $\chi^\dagger_{-k-Q_0,-k} = \chi^\dagger_{k,k+Q_0}$, which is approximately verified in the linearized regime. The SU(2) condition then implies that $\hat{u}^\dagger \hat{u} = 1$, which in turn requires that $|\chi|^2 + |\Delta|^2 = 1$.

We now expand around the mean-field values of the parameters in order to get the small fluctuations regime. We first Fourier transform to get $\hat{Q}_{x,x'} \to \hat{Q}_{k,k'}$ and then Wigner transform it, which leads to

$$\hat{Q}_{x,x'} \to \hat{M}_{x-x',(x+x')/2}. \tag{43}$$

In the Fourier space, this writes $\hat{M}_{x-x',(x+x')/2} \to \hat{M}_{(k+k')/2,k-k'}$. We then decompose into fast and slow variables as $\hat{M} \sim \langle \overline{\Psi}_{k+q/2} \Psi_{k-q/2} \rangle$ with the fast momenta $\mathbf{k} \simeq \mathbf{k}_\mathrm{F}$ and the slow momenta $\mathbf{q} \ll \mathbf{k}_\mathrm{F}$. With the change of variables as $k \to k + q/2$ and $k' \to k - q/2$, we get $\hat{M}_{k,q}$, such as

$$S_\mathrm{int} = \frac{1}{2} \sum_{k,q,\sigma} \mathrm{Tr}[\overline{\Psi}_{k+q/2} \hat{M}_{k,q} \Psi_{k-q/2}], \tag{44}$$

where $\overline{\psi}_k$ and ψ_k are given by Eqs. (28) and (29). We have then

$$\hat{M}_{k,q} = M_k \, \hat{U}_{k,q}, \quad \text{with } \hat{U}_{k,q} = \begin{pmatrix} & \hat{u}_{k,q} \\ \hat{u}^\dagger_{k,q} & \end{pmatrix}_\Lambda, \tag{45}$$

$$\text{and } \hat{u}_{k,q} = \begin{pmatrix} \chi_{k,q} & -\sigma \Delta_{k,q} \\ \sigma \Delta^\dagger_{k+Q_0,q} & \chi^\dagger_{-k-Q_0,q} \end{pmatrix}_\tau,$$

where M_k is the magnitude of the order parameter while $\hat{u}_{k,q}$ is the SU(2) non-Abelian phase associated to it. We have

$$\begin{aligned} \Delta_{k,q} &\sim \sigma \langle \psi_{k+q/2,-\sigma} \psi_{-k+q/2,\sigma} \rangle, \\ \chi_{k,q} &\sim \langle \psi^\dagger_{k+q/2,\sigma} \psi_{k+Q_0-q/2,\sigma} \rangle, \\ \Delta^\dagger_{k+Q_0,q} &\sim \sigma \langle \psi_{k+Q_0+q/2,-\sigma} \psi_{-k-Q_0+q/2,\sigma} \rangle, \\ \chi^\dagger_{-k-Q_0,q} &\sim \langle \psi^\dagger_{-k-Q_0-q/2,-\sigma} \psi_{-k+q/2,-\sigma} \rangle. \end{aligned}$$

As mentioned above, in the linearized regime, we have $\chi^\dagger_{-k-Q_0} = \chi_k$ and $\Delta^\dagger_{k+Q_0} = -\Delta^\dagger_k$, which ensures the SU(2) condition that the determinant is equal to one, such that $|\chi|^2 + |\Delta|^2 = 1$ and also implies that $\hat{u}^\dagger_{k,q} \hat{u}_{k,q} = \hat{1}$. In this regime, we have

$$\hat{u}_{k,q} = \begin{pmatrix} \chi_{k,q} & -\sigma \Delta_{k,q} \\ \sigma \Delta^\dagger_{k,q} & \chi^\dagger_{k,q} \end{pmatrix}_\tau. \tag{46}$$

The decomposition of the interaction field $\hat{M}_{k,q}$ into an amplitude M_k and an SU(2) "phase" $\hat{u}_{k,q}$ in Eq. (45) is a second important ingredient in the study of the fluctuations in Sec. V. We will see there that the writing of the nonlinear σ model relies on the separation between a field depending only on fast variables M_k, whereas the phase will depend on slow variables only $\hat{k}_{k,q} \sim \hat{u}_q$.

C. The quadratic term S^0_Q

The quadratic term in S_{st} [Eqs. (24) and (39)] writes

$$S^0_Q = \frac{1}{4} \int_{x,x'} \mathrm{Tr}\big[\overline{\hat{Q}}_{x,x'} \hat{\gamma}^{-1}_{x-x'} \hat{Q}_{x',x}\big], \tag{47}$$

where $\hat{\gamma}^{-1}$ is a bare propagator whose form is not crucial at this stage, since it is to be renormalized by the thermal fluctuations described in Sec. V. In the case of the eight-hot-spot model [72], or of the spin fermion model with hot regions [73], this term corresponds to antiferromagnetic (AF) paramagnons mediating the formation of the SC and CDW orders, but in the minimal version of the model, which is controlled solely by the SU(2) symmetry, it is not necessary to mention the origin of the bare propagator.

V. NONLINEAR σ MODEL

We derive the fluctuations induced by the SU(2) structure presented in the two preceding sections. The generic form of the O(4) nonlinear σ model is obtained by integrating out the fermions in Eq. (24) and extracting the S_Q action, which renormalizes Eq. (47). After formally integrating out the fermions, we get

$$\begin{aligned} S_\mathrm{eff} &= \frac{1}{4} \int_{\mathbf{x},\mathbf{x}'} \hat{\gamma}^{-1}_{x-x'} \mathrm{Tr}\left[\overline{\hat{Q}}_{x,x'} \hat{Q}_{x',x} - \frac{1}{2} \ln \hat{G}^{-1}_{x,x'}\right], \\ \text{with } \hat{G}^{-1}_{x,x'} &= \partial_\tau - \hat{\xi}_{\mathbf{x}-\mathbf{x}'} + \hat{Q}_{x,x'}, \end{aligned} \tag{48}$$

where the Tr operates on the matrix structure except on the space indices and $\hat{Q}$ is the SU(2) operator obtained by the Hubbard-Stratonovich decoupling. We can now Wigner-

transform Eq. (48), which yields

$$S_{\rm eff} = \frac{1}{4}\sum_{k,q,\bar{q}} \gamma_{\bar{q}}^{-1} {\rm Tr}\hat{\bar{M}}_{k+\bar{q},q}\hat{M}_{k,q} - \frac{1}{2}\sum_{k,q} {\rm Tr}\ln \hat{G}^{-1}_{k,q}, \quad (49)$$

$$\text{with } \hat{G}^{-1}_{k,q} = \hat{G}^{-1}_{0k} - \frac{1}{2}\hat{M}_{k,q}, \quad (50)$$

with the matrix $\hat{M}$ defined in (45).

A. Separation of variables

The fluctuations associated with the nonlinear σ model are obtained by separating the fast momenta $\mathbf{k} \sim \mathbf{k}_{\rm F}$ and the slow momenta $\mathbf{q} \ll \mathbf{k}_{\rm F}$, as

$$\hat{M}_{k,q} = M_{0,k}\,\hat{U}_q, \quad \text{and} \quad \hat{U}_q = \begin{pmatrix} & \hat{u}_q \\ \hat{u}_q^\dagger & \end{pmatrix}_\Lambda, \quad (51)$$

with $M_{0,k}$ being the "fast varying" component, is a scale comparable to the SU(2) dome $\Delta_{\rm SU(2)}$ of Sec. III C. The slow varying variables are taken to act only on the SU(2) matrix $\hat{U}_q$. In the following, we first assume, using the symmetric part of the bare action in Eq. (36), that the condition of separation of variables Eq. (51) is valid everywhere and derive the effective nonlinear σ model in Secs. V B and V C. The validity of the hypothesis of separation of variables relies on the physical idea that the slow varying phases $\hat{U}_q$ can be treated as perturbations around a larger mean-field like field $M_{0,k}$. This idea will be tested in Sec. VI A, and we will discover that it is valid only in a restricted parts of the Brillouin zone (BZ).

The SU(2) condition is now given by

$$\hat{U}_q^\dagger \hat{U}_q = \hat{1}, \quad \text{or} \quad |\Delta_q|^2 + |\chi_q|^2 = 1. \quad (52)$$

Thermal fluctuations then correspond to variations of $\delta\hat{U}_q$, $M_{0,k}$ being kept as a constant:

$$\delta\hat{M}_{k,q} = M_{0,k}\,\delta\hat{U}_q. \quad (53)$$

Introducing this decoupling back into Eq. (49) we note that the first term does not contribute because of the unitarity condition (52). We henceforth expand the free energy in the second order in the Hubbard-Stratonovich fields. In real space, from Eq. (38),

$$Z = e^{-S_t}, \quad \text{with } S_t = -\tfrac{1}{2}\langle (S_{\rm int})^2\rangle_\phi, \quad (54)$$

and $F = -T\ln Z$, we get

$$F[u] = \frac{T^2}{4}\int_{x,x',x_1,x_1'} {\rm Tr}\langle \bar{\Psi}_x \hat{\bar{Q}}_{x,x'} \Psi_{x'} \bar{\Psi}_{x_1} \hat{Q}_{x_1,x_1'} \Psi_{x_1'}\rangle_\phi,$$

where the Tr runs over the 4×4 matrix and the fields are defined in Eqs. (25) and (27). Performing the Wick pairing of the fields yields with the definition of the Green functions in Eq. (27), we get

$$F[u] = \frac{T^2}{4}\int_{x,x',x_1,x_1'} {\rm Tr}\big[\hat{\bar{Q}}_{x,x'}\hat{G}_{x',x_1}\hat{Q}_{x_1,x_1'}\hat{G}_{x_1',x}\big], \quad (55)$$

which after Fourier transforming, gives

$$F[u] = \frac{T^2}{4}\sum_{\varepsilon,\varepsilon'}\sum_{\mathbf{k},\mathbf{k}',\mathbf{k_1},\mathbf{k_1'}} {\rm Tr}\big[\hat{\bar{Q}}_{k,k'}\hat{G}_{k',k_1}\hat{Q}_{k_1,k_1'}\hat{G}_{k_1',k}\big], \quad (56)$$

where the Tr runs on the spin indices, as well as on the 4×4 matrices, and $\hat{G}$ is given by

$$\hat{G}^{-1}_{k,k'} = \hat{G}^{-1}_{0,k}\delta_{k,k'} - \hat{Q}_{k,k'}, \quad (57)$$

with $\hat{G}_{0,k}$ defined in Eq. (31) and $\hat{Q}_{k,k'}$ in Eq. (40).

B. Symmetric part

We start by retaining only the SU(2)-symmetric part $\hat{G}_{0,s,k}=(i\varepsilon_n - \bar{\xi}_{\mathbf{k}}\Lambda_3)^{-1}$, leading to

$$\hat{G}^{-1}_{s,k,k'} = \hat{G}^{-1}_{0,s,k}\delta_{k,k'} - \hat{Q}_{k,k'},$$
$$= (i\varepsilon_n - \bar{\xi}_{\mathbf{k}}\Lambda_3)\delta_{k,k'} - \hat{Q}_{k,k'}. \quad (58)$$

and $\hat{G}_{0,s,k}$ given by Eq. (32). Equation (40) indicates that $\hat{Q} \sim \Lambda_1$, such that $\{\hat{Q},\Lambda_3\} = 0$ holds for arbitrary arguments x and x' (k and k', respectively) of the matrix $\hat{Q}$. Defining

$$\hat{\bar{G}}^{-1}_{s,k,k'} = (-i\varepsilon_n - \bar{\xi}_{\mathbf{k}}\Lambda_3)\delta_{k,k'} + \hat{Q}_{k,k'}, \quad (59)$$

we find

$$\hat{\bar{G}}_s^{-1}\hat{Q} = -\hat{Q}\hat{G}_s^{-1}, \quad (60)$$

which enables us to rewrite Eq. (56) as

$$F[u] = -\frac{T^2}{4}\sum_{\varepsilon,\varepsilon',\varepsilon_1,\varepsilon_1'}\sum_{\mathbf{k},\mathbf{k}',\mathbf{k_1},\mathbf{k_1'}} {\rm Tr}\big[\hat{Q}_{k,k'}\hat{G}_{s,k',k_1}\hat{\bar{G}}_{s,k_1',k}\hat{Q}_{k_1,k_1'}\big]. \quad (61)$$

Using the Wigner transformation, Eq. (61) can be recast into the form

$$F[u] = -\frac{T^2}{4}\sum_{\varepsilon,\omega,\varepsilon',\omega'}\int_{\mathbf{k},\mathbf{q},\mathbf{k}',\mathbf{q}'} {\rm Tr}[\hat{\bar{M}}_{k,q}\hat{G}_{s,k,q}\hat{\bar{G}}_{s,k',q'}\hat{M}_{k',q'}]. \quad (62)$$

Using $\delta M_{k,q}$ form Eq. (53), we get

$$F[\delta u] = -\frac{T^2}{4}\sum_{\varepsilon,\varepsilon'}\int_{\mathbf{k},\mathbf{k}'}|M_{0,k}||M_{0,k'}|$$
$$\times \sum_\omega \int d\mathbf{q}\,{\rm Tr}[\delta\hat{U}_q^\dagger\hat{G}_{s,k,q}\hat{G}_{s,k',q}\delta\hat{U}_q]. \quad (63)$$

Expanding $\hat{G}_0^{-1}$ to the second order in ω and q and noting that the terms depending only on the fact variables ε,k do not contribute, we obtain

$$F[\delta u] = \frac{T^2}{2}\sum_{\omega,\mathbf{q}} {\rm Tr}\delta\hat{u}_q^\dagger[J_0\omega^2 + J_1 q^2]\delta\hat{u}_q, \quad (64)$$

where the tr runs on the SU(2) structure and with

$$J_0 = \sum_{\varepsilon,\mathbf{k}}\frac{|M_{0,k}|^2}{|G_s^{-1}|^2}, \quad J_1 = \sum_{\varepsilon,\mathbf{k}}\frac{|M_{0,k}|^2 v_k^2}{|G_s^{-1}|^2}, \quad (65)$$

with v_k the velocity at the Fermi level. The form (63) is generic for the nonlinear σ model. J_0 and J_1 are nonvanishing only when $|M_{0,k}|$ does not vanish, which restricts the SU(2) fluctuations to be below the fluctuations dome depicted in Fig. 7.

C. Effective model

One can put Eq. (64) into a standard form [71] by introducing the four fields $n_\alpha, \alpha = 1,4$ such that $\Delta = n_1 + in_2$ and $\chi = n_3 + in_4$. The stands for action for the nonlinear σ model then writes

$$S_\sigma = -\frac{\rho_s}{T}\int d\mathbf{q}\left[\sum_{\alpha=1}^{4}\mathbf{q}^2 n_\alpha^2 - a_0\sum_{\alpha=1}^{2}n_\alpha^2 + a_0\sum_{\alpha=3}^{4}n_\alpha^2\right], \quad (66)$$

with $\rho_s = T^3\sum_{\varepsilon,\mathbf{k}}\sum_\omega |M_{0,k}|^2 v_k^2/|G^{-1}|^2$, $a_0 = a_0^{\text{disp}} + a_0^{\text{mf}}$, with $a_0^{\text{disp}} = \frac{T^3}{4\rho_s}\sum_{\varepsilon,\mathbf{k}}\sum_\omega |M_{0,k}|^2(\Delta\epsilon_k)^2/|G^{-1}|^2$, which will be treated in details in the next section. The constant term coming from the integration over ω in Eq. (64) has been neglected. A small mean-field mass term $a_0^{\text{mf}} \ll |M_{0,k}|$ has been introduced in Eq. (66), which can be generated, for example, by a magnetic field ($a_0^{\text{mf}} < 0$), which favors the CDW state, or by the increase of the chemical potential, favoring the SC ($a_0^{\text{mf}} > 0$), because of the proportionality η_z to the electron density Eq. (6b), but is not considered in this work.

VI. THE SU(2) LINE

A. Symmetry breaking term

In this section, we study the domain of validity of the hypothesis of the factorization of the fields between fast and slow variables Eq. (51). As noticed above in Eq. (35), it is possible to models in a simple way the symmetry breaking term. The term proportional to τ_3 in (35) is proportional to

$$\Delta\xi_{\mathbf{k}} = \tfrac{1}{2}\left(\xi_{\mathbf{k}+\mathbf{Q}_0} + \xi_{\mathbf{k}}\right) \quad (67)$$

brings a mass to the free propagator leading to

$$F[\delta u]_{SB} = \frac{T^2}{2}\sum_{\omega,\mathbf{q}}\sum_{\varepsilon,\mathbf{k}} J_{3,k}\,\mathrm{Tr}[\delta\hat{u}^\dagger_{k,q}\tau_3\delta\hat{u}_{k,q}\tau_3], \quad (68)$$

$$\text{where}\quad J_{3,k} = \frac{1}{4}\frac{|M_{0,k}|^2(\Delta\xi_k)^2}{|G_s^{-1}|^2}. \quad (69)$$

The effect of symmetry breaking is to produce a mass term Eq. (68), which becomes large in the nodal (π,π) region as depicted in Fig. 8. We consider that the theory ceases to be valid when the dispersion mass term $J_{3,k}$ in Eq. (69) becomes larger than one. This corresponds physically to a situation where the curvature effects from the Fermi surface in Eq. (67) become stronger than the value of the dome gap $\Delta_{\text{SU(2)}}$. In this case, the hypothesis of separation of variables ceases to be valid and the SU(2) fluctuations vanish. This can be taken into account by replacing Eq. (53) by

$$\delta\hat{M}_{k,q} = M_k\,\delta\hat{U}_q,$$
$$\text{with}\quad M_k = M_{0,k}\quad \text{if } \mathbf{k}\in C,$$
$$\text{and}\quad M_k = 0,\ \text{elsewhere}. \quad (70)$$

In the Eq. (70) above, C is the loci of the k points in the BZ where the mass $J_{3,k} \ll 1$, and thus where the theory of slowly fluctuating SU(2) phases $\hat{U}_q$ is valid. A self-consistency shall be introduced, and the coefficients of the nonlinear σ model in Eq. (65) shall be evaluated again with the fast and slow variables decoupling of Eq. (70). Alternatively, the situation can be viewed from the view point of the magnitude of the SU(2) gap $\Delta_{\text{SU(2)}} \sim M_{0,k}$ over the Fermi surface. Since the SU(2) gap requires gapping equally in the charge (CDW) and SC d-wave channels (see Fig. 7), we see from Fig. 6 that it is nonzero only in a rather wide region surrounding the AF hot spots [see Eq. (23)]. Since the evaluation of the coefficients in Eq. (65) requires summation over $|M_{0,k}|^2$, we see that the contribution of the SU(2) fluctuations is naturally restricted to the antinodal $(0,\pi)$ or $(\pi,0)$ region.

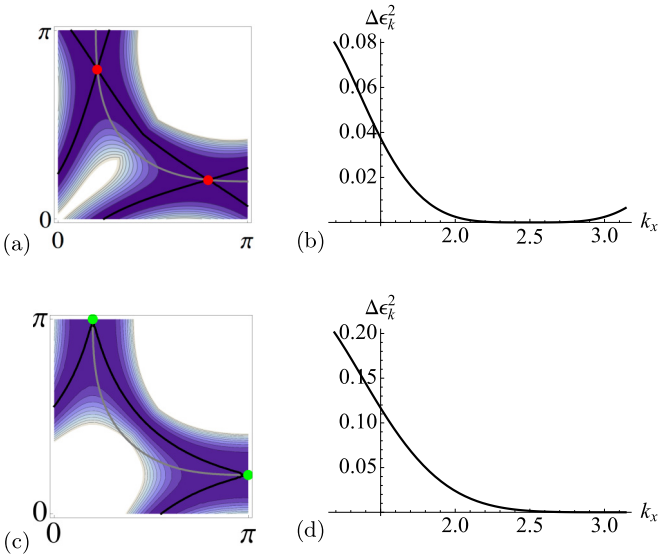

FIG. 8. (a) Visualization of $(\Delta\epsilon_{\mathbf{k}})^2$ in the positive region of the first Brillouin zone that gives rise to SU(2) symmetry breaking mass contribution. In the blue region, this contribution is small and vanishes at the two black lines as well as on the hot spots. In the nodal region, the contribution, and so the mass, is large. (b) Variation of $(\Delta\epsilon_{\mathbf{k}})^2$ as a function of k_x when we follow the Fermi surface [indicated by the grey line in (a)]. The mass $(\Delta\epsilon_{\mathbf{k}})^2$ vanishes at the hot spot and is small close to the zone edge but becomes large in the nodal region. The difference between the two upper and lower panels is the choice of the charge-ordering vectors. For (a) and (b), the charge ordering vector connects the two hot spots, whereas in (c) and (d), it connects the points at the zone edge. The dispersion is modeled in the tight-binding approximation for Bi2212, Ref. [124] (parameter set tb2).

We make the claim here that fluctuations associated with the SU(2) fields are present in the theory, but act only in restricted areas of the BZ. This produces SU(2) lines of massless fluctuations along which the electron self-energy diverges. This produces a line of zeros in the electron Green's function, in analogy with the findings of other theoretical approaches [6,151,159], Fig. 8 shows two typical cases of SU(2) lines. Figures 8(a) and 8(b) are concerned with a charge wave vector lying on the diagonal of the form $(Q_{\mathbf{0}}, Q_{\mathbf{0}})$, while Figs. 8(c) and 8(d) show the same lines of zeros of the Green's function, but for a wave vector located at the ZE. We can see in Fig. 8(b) that the minimum of the mass is located at the AF hot spots, while in Fig. 8(d), we see that it is at located at the zone edge. A more detailed study for various wave vectors, including the evolution with doping, is given in the next section.

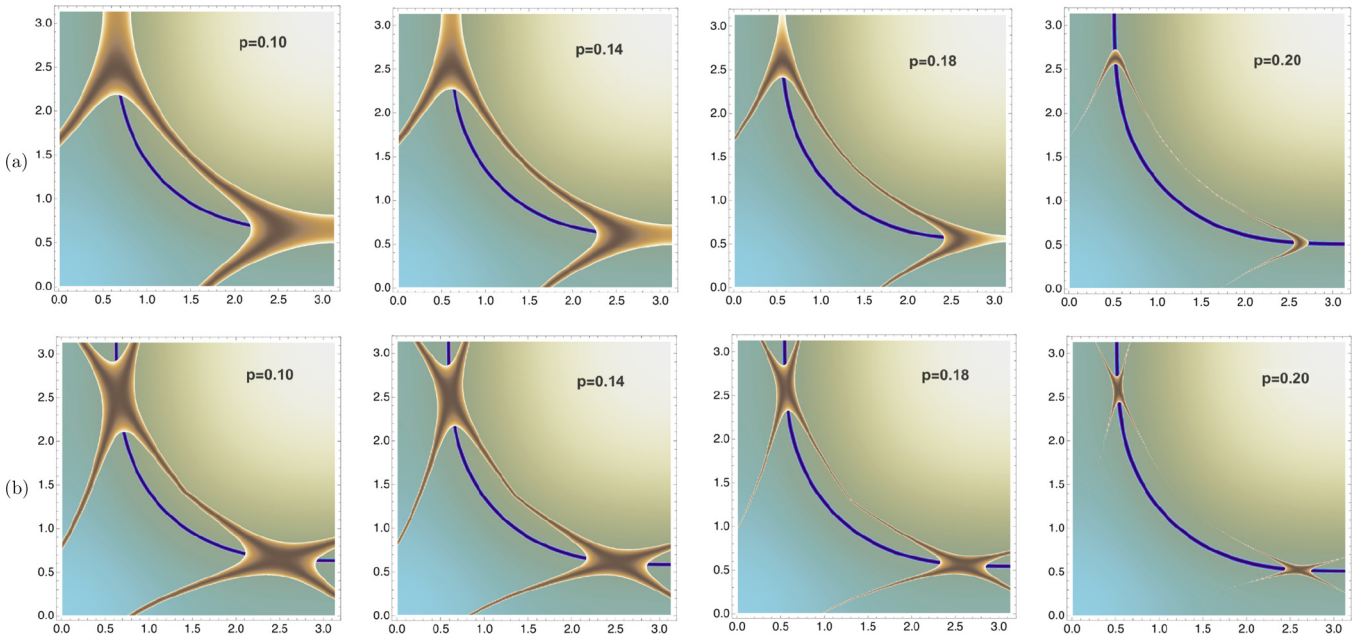

FIG. 9. Evolution of the SU(2) fluctuations as a function of the hole doping. The **k** points, which have the SU(2) mass $J_{3,k} < 1$ in Eq. (69), are represented in brown. This criterion defines the "hot regions" for which the SU(2) fluctuations are important. Note that the "hot regions" are centered around the hot spots and extend in the antinodal part of the BZ. We present two sets of curves: (a) for the axial wave vector $\mathbf{Q}_0 = (Q_{\mathbf{0}},0)$, and (b) for the diagonal wave vector $\mathbf{Q}_0 = (Q_{\mathbf{0}},Q_{\mathbf{0}})$. In Eq. (69), we approximate the factor $|M_{0,k}/G_s^{-1}|^2 \sim 1/\Delta^2_{\mathrm{SU(2)}}$, with a phenomenological form for $\Delta_{\mathrm{SU(2)}} = T^*(\frac{p_c-p}{p_c-p_0})$, with $T^* = 3\times10^{-2}$, $p_c = 0.22$, $p_0 = 0.12$, and p is the hole doping. In brown are the regions where the dispersion mass $J_{3,k} \ll 1$ in Eq. (69). Note that in both cases, the dispersion mass has a minimum at the hot spots. The electron dispersion is modeled in tight-binding approximation for Bi2212, Ref. [124] (parameter set tb2).

B. Evolution with doping

In Fig. 9, we present the evolution with doping of the hot regions for two configurations of the charge modulation wave vector. Figure 9(a) relates to the diagonal wave vector $\mathbf{Q}_0 = (Q_0,Q_0)$, while Fig. 9(b) describes the axial wave vector $\mathbf{Q}_0 = (Q_0,0)$ observed experimentally. Note that both sets of SU(2) fluctuations are massless at the hot spot. According to the simple calculation presented in Fig. 7, and assuming the relation $p \simeq J_0 - J$, we have modeled the PG by the following phenomenological variation with doping

$$\Delta_{\mathrm{SU(2)}} = T^*\left(\frac{p_c - p}{p_c - p_0}\right), \tag{71}$$

with p the hole doping, $p_0 = 0.12$ and $p_c = 0.22$.

The brown region corresponds to the loci of the points where the SU(2) mass $J_{3,k}$ in Eq. (69) is less than one, and hence where the SU(2) fluctuations are coupled to the electrons. A massless line, or SU(2) line, is visible and crosses the Fermi surface at the AF hot spots. Although the shape of the SU(2) line does not change much with doping, its width decreases until it gets located at the hot spots and then disappears. This study makes very clear the fractionalization of the Fermi surface between hot regions and cold regions. The case for a wave vector at the zone edge (ZE) is presented in Appendix B. We see that in that case, the mass minimum is located at the zone edge.

VII. ROTATION OF THE CHARGE ORDERING WAVE VECTOR AND NEMATICITY

In Sec. IV, we have decided to rotate the d-wave SC state towards a d-wave charge channel with diagonal wave vector $\mathbf{Q}_0 = (Q_{\mathbf{0}},Q_{\mathbf{0}})$. This choice was rather arbitrary, considering that all the wave vectors considered in Sec. III are quasidegenerate. We chose the diagonal wave vector simply for historical reasons, that the eight-hot-spot spin fermion model considered in our previous work possesses an exact SU(2) symmetry involving charge order with diagonal wave vectors [70,72]. In this section, we explore the effects of the SU(2) pairing fluctuations on the modulations wave vector in the charge sector. We show that the main surprising effect of these fluctuations is to lift the degeneracy between the various modulation vectors, with the uniform $\mathbf{Q}_0 = \mathbf{0}$ and axial wave vectors $\mathbf{Q}_0 = (Q_0,0)$ and $\mathbf{Q}_0 = (0,Q_0)$ becoming the leading ones. This leads to the emergence of d-wave axial charge modulations associated with a d-wave Pomeranchuk instability, or nematic order.

A. Bare polarization

We start with a simple study of the bare polarization plotted in Fig. 10(a) with the band structure of Bi2212:

$$\Pi^a_{\mathrm{bare}}(p,0) = -T\sum_k G_k G_{k+p}, \tag{72}$$

with $k = (\mathbf{k},\varepsilon)$ and $G_k^{-1} = i\varepsilon_n - \xi_{\mathbf{k}}$. Here we notice the well-known features corresponding to a maximum along the

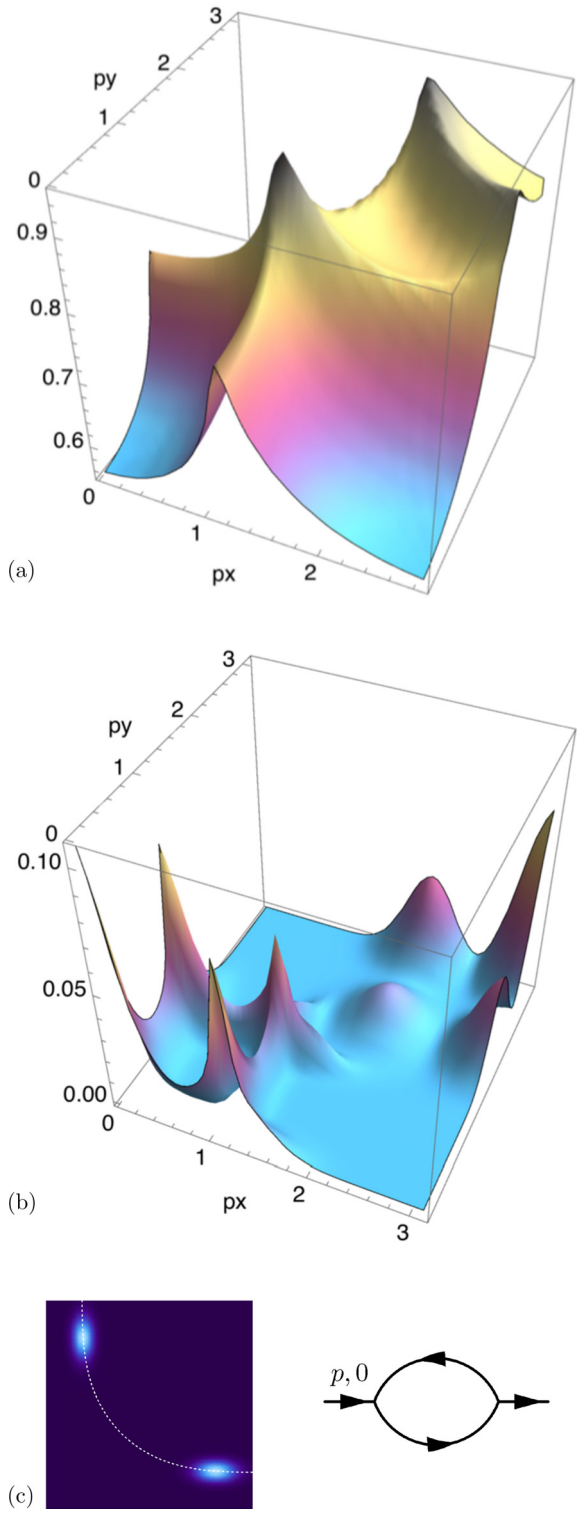

FIG. 10. Real part of the bare polarization bubble in the static limit. The electron dispersion corresponds to the usual one of Bi2212, Ref. [124]. In (a), we have depicted the bare polarization bubble, showing a maximum at the diagonal wave vector (Q_0, Q_0), as well as some features around (π,π). In (b), we show the same polarization, but restricted to the domain of validity of the SU(2) fluctuations, shown in (c). Remarkably, we observe that the intensity gets displaced, with the emergence of a peak at $\mathbf{Q} = (0,0)$, and also the predominance of the axial wave vectors $(0, Q_0)$, and $(Q_0,0)$, compared to the diagonal one.

diagonal, at the wave vector (Q_0, Q_0), as well as some structure lying close to the (π,π) region. Nothing particular is visible on the axes, apart from the line corresponding to the $2\mathbf{p}_F$ wave vectors, but overall, the value of the polarization on the axes is less important than on the diagonal. In Fig. 10(b), we give the same study of the bare polarization, but with a width of integration in $\mathbf{k}$ space restricted to the SU(2) hot regions [insert in Fig. 10(c)]:

$$\Pi^b_{\text{bare}}(p,0) = -T \sum_k M_{0,k} M_{0,k+p} G_k G_{k+p}. \quad (73)$$

The result is drastically different from the bare polarization, with the emergence of a structure at $\mathbf{Q} = (0,0)$, accompanied by a drastic increase of the pics along the axes, which precisely correspond to the wave vectors observed experimentally $(0, Q_0)$ and $(Q_0,0)$. This effect of the SU(2) regions on the pairing fluctuations is the generic feature that we describe in this section. It shows that, even if we start with a diagonal modulation vector, at rather high energy, upon the effect of the SU(2) pairing fluctuations the wave vector is tilting along the axes.

B. Vertex corrections

We provide the study of the SU(2) pairing fluctuations in Figs. 11 and 12,

$$\Pi_v(p,0) = -T \sum_{k,q} \pi^s_{k,k+p,q} G_k G_{k+p} G_{-k-q} G_{-k-p-q}, \quad (74)$$

with the four variables $k = (\mathbf{k},\varepsilon)$, $q = (\mathbf{q},\omega)$, $G_k^{-1} = i\varepsilon_n - \xi_{\mathbf{k}}$, and $G_{-k}^{-1} = -i\varepsilon_n - \xi_{-\mathbf{k}}$. The form of the SU(2) pairing propagator $\langle \Delta^\dagger_{k,q} \Delta_{k',q'} \rangle = \pi^s_{k,k',q} \delta_{\mathbf{q},\mathbf{q}'}$ has been defined in Sec. IV, Eqs. (64), (68), and (66):

$$\pi^s_{k,k',q} = M_{0,k} M_{0,k'} \frac{\pi_0}{J_0 \omega_n^2 + J_1 (\mathbf{v}\cdot\mathbf{q})^2 - a_0}. \quad (75)$$

The presence of the vertex factors $M_{0,k}$ and $M_{0,k'}$ in Eq. (75) restrict the summation over $\mathbf{k}$ to the antinodal region of the Brillouin zone. We observe that the same physical effects as the ones present in Fig. 10(b) are present in Fig. 11(a). The shape of the SU(2) hot regions does not really affect the two main observable effects, as we show in Appendix C as long as the hot regions are centered around the host spots. We observe the emergence of a peak at zero wave vector as well as the predominance of the response along the axes over the response on the diagonal. As we show in Fig. 26, the inclusion of Aslamazov-Larkin diagrams does not change the conclusion.

In Fig. 12(a), the same study is performed for hot regions centered at the zone edge. In this case, the effect is even more pronounced, with nothing left on the diagonal but a range of wave vectors that dominate around $(0, Q_0)$, and $(Q_0,0)$, with a line still visible at the wave vectors $2\mathbf{p}_F$.

C. Implications for the phase diagram of the cuprates

When comparing the bare polarization Fig. 10(a) with the effects of the SU(2) paring in Figs. 11 and 12, two main effects are noticeable. First, we observe a shift of the spectral weight from the diagonal to the axes, with the formation of CDW instabilities around the experimentally observed wave vectors $(0, Q_0)$ and $(Q_0,0)$ and second, we see the emergence of a peak

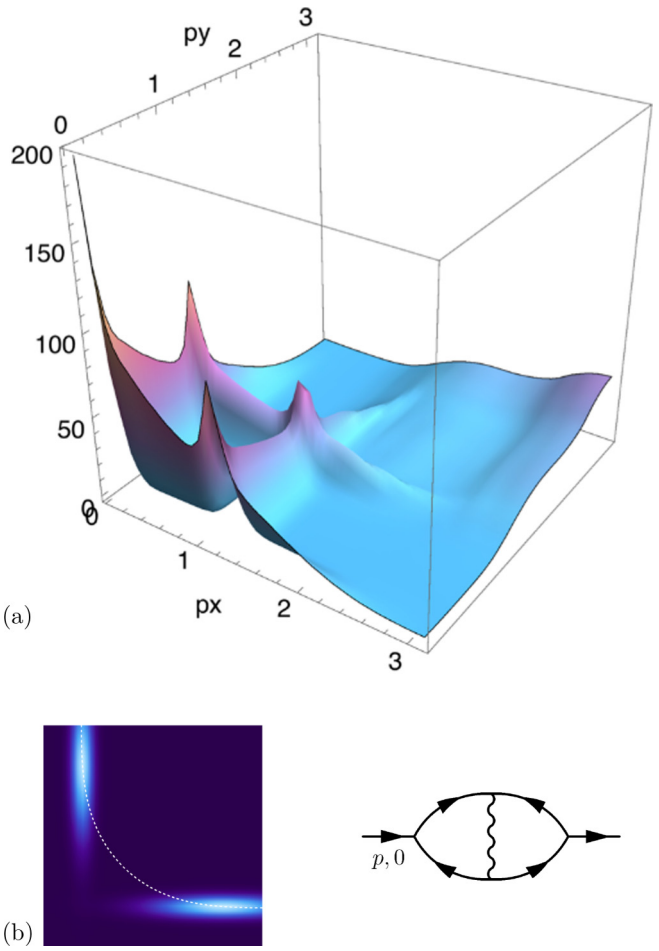

FIG. 11. (a) Real part of the polarization bubble, with one vertex correction, in the static limit. The electron dispersion corresponds to the usual one of Bi2212, Ref. [124]. The charge response is depicted in the case where the fluctuations are centered at the hot spots as shown in (b). In this case, the peak along the diagonal remains but with a lower intensity than the response along $(0, Q_0)$ and $(Q_0, 0)$.

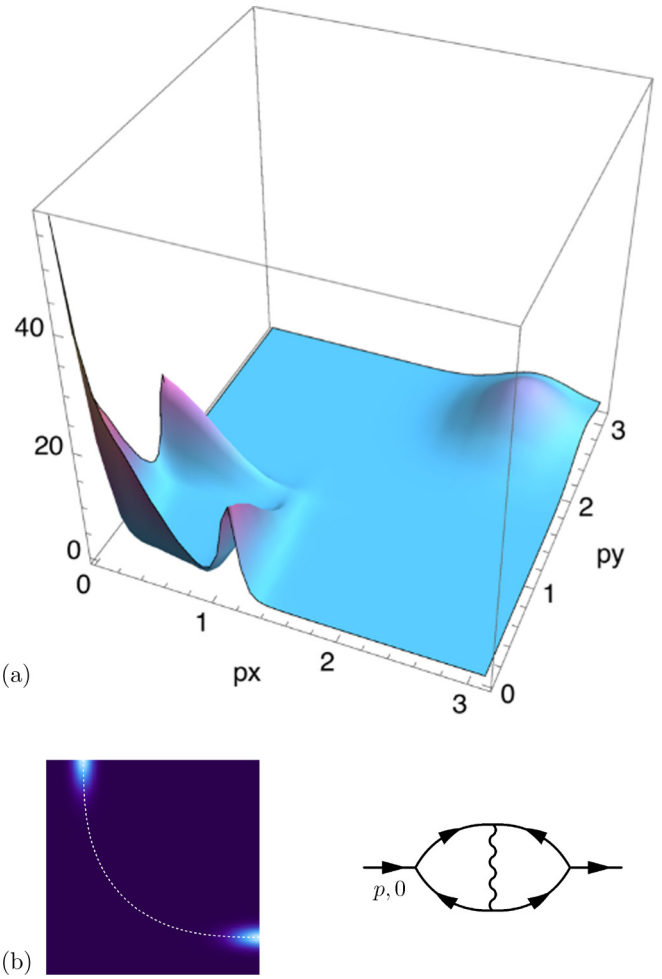

FIG. 12. Real part of the polarization bubble, with one vertex correction, in the static limit. The electron dispersion corresponds to the usual one of Bi2212, Ref. [124]. The charge response is depicted in the case where the fluctuations are centered at the zone edge, with a rather small extension. In this case, the peak along the diagonal is completely lost, while only the response along $(0, Q_0)$ and $(Q_0, 0)$ is retained.

at $\mathbf{Q} = (0,0)$. The effect of the SU(2) pairing fluctuations is thus twofold, with the peak at $\mathbf{Q} = (0,0)$ hinting at the presence of a nematic precursor around the temperature T^* [160,161], while the peaks at finite wave vectors along the axes correspond to the CDW modulations observed experimentally.

A comment with respect to the center of mass symmetry is in order. The SU(2) fluctuations considered here do not favor any specific symmetry, whether it is s (or s'), or d wave. Since those fluctuations connect gap equations around $\mathbf{q} = 0$, the gaps are stabilized around one $\mathbf{k}$ point in the Brillouin zone instead of coupling two antinodal regions as it is the case for the AF coupling. The d-wave symmetry of the $\mathbf{Q} = (0,0)$ and $(0, Q_0)$ and $(Q_0, 0)$ orders comes from the original AF correlations describes in Sec. III. The SU(2) fluctuations are lifting the degeneracy whereas the d-wave character of the charge instabilities remain. This has the important consequence that axial orders are systematically accompanied with a Pomeranchuck or nematic instability within our model.

In Appendix D, we argue that there is no vertex/self-energy cancellation in the case of a wavy fluctuations line in the Cooper channel, which leads us to consider the $\mathbf{Q} = \mathbf{0}$ peak as a real effect which accompanies the CDW modulations at finite wave vectors. In Fig. 12, when the SU(2) original wave vector has rotated around the zone edge, we observe a dispersion line around $2\mathbf{p}_F$, with a finite range of quasidegenerate wave vectors, and no well-defined peak at a preferential one. We argue in the next section, Sec. VIII, that this corresponds to the formation of excitonic pairs, which can take many wave vectors around $2\mathbf{p}_F$ in the antinodal region around the zone edge. These excitonic pairs are instrumental in the formation of the pseudogap as they will proliferate with temperature, leading to a gapping out of the antinodal region at T^*.

An important point, is that the nonlinear σ model provides a strong constraint between the charge and SC channels. This in turn gives strong mode-mode coupling. The thermodynamics of such a model typically produces some phase separation [144,145,162,163], which leads to the creation of patches of charge modulations. Whether the particle hole pairs have many wave vectors $2\mathbf{p}_F$ or condense only to one or two

wave vectors $(0, Q_0)$ and $(Q_0,0)$, depends on the degree of fluctuations in the system. A lot of SU(2) fluctuations produce the emergence of excitonic patches with multiple wave vectors, whereas when the fluctuations are frozen, the bosons condense to one wave vector. The detailed statistical study of the phase separation is left for for later work, while we give in the next section, Sec. VIII a derivation of the formation of patches of excitonic pairs with multiple wave vectors $2\mathbf{p}_F$.

VIII. PREFORMED PARTICLE-HOLE PAIRS

Nonlinear σ models are the theoretical tools for describing fluctuations from a non-Abelian group. As we saw in the previous section, Sec. VI, on the case of the SU(2) pseudospin symmetry, the corresponding nonlinear σ model is O(4). Three phases describe the fluctuations : the SC phase, the CDW phase and the phase rotating between the two modes. The goal of this section is to focus on the emergence of local modes coming from the nonlinear coupling between the two modes. These local singularities have been described as "skyrmions" or static topological defects of the theory in the past. We defer a thorough study of these for future work and focus here on a more pedestrian approach leading to similar local droplets- or patches of particle-hole pairs.

A. Particle-hole pairing formation

In this section, we study the possibility of the formation of particle hole pairs, or excitons, with strong binding energy. We will show that the excitons are bosons with a quasidegenerate line of finite momenta around $2\mathbf{p}_F$ in the antinodal region. We proceed as for the study of Cooper pairing and show that a logarithm is present in the solution of the Schrödinger equations, which is cutoff only by the curvature of the Fermi surface. Hence, for flat enough regions of the electronic dispersion, the excitonic pairing can occur.

1. Wave function

The wave function for the particle-hole pair writes

$$\psi^{\mathrm{Ch}}_{\mathbf{r},\mathbf{r}'} = \sum_{\tilde{\mathbf{k}},\mathbf{P}} e^{-i\mathbf{P}\cdot(\frac{\mathbf{r}+\mathbf{r}'}{2})} e^{i\tilde{\mathbf{k}}\cdot(\mathbf{r}-r')} \chi_{\tilde{\mathbf{k}},\mathbf{P}}, \tag{76}$$

with $\tilde{\mathbf{k}} = -\mathbf{k} + \mathbf{P}$, $\mathbf{P} = \{2\mathbf{k}_F\}$ scans the wave vectors represented in Fig. 2(a). In order to discuss the most generic solution, we first set $\chi_{\tilde{\mathbf{k}},\mathbf{P}} = cte$. The summation over $\mathbf{P}$ in Eq. (76) has an important consequence to localize the center of mass of the excitonic pair at the point zero (with this representation). The structure in $\mathbf{k}$ then gives the finite extension for the local patch as well as some possible intrinsic pattern. Note that the wave function for a Cooper pair $\Delta \sim \sigma \langle \psi_{\mathbf{k},\sigma} \psi_{-\mathbf{k},\sigma} \rangle$ with modulation vector $\mathbf{P}$ takes a very similar form:

$$\psi^{\mathrm{SC}}_{\mathbf{r},r'} = \sum_{\mathbf{k}} e^{-i\mathbf{P}\cdot(\frac{\mathbf{r}+\mathbf{r}'}{2})} e^{i\mathbf{k}\cdot(\mathbf{r}-r')} \Delta_0. \tag{77}$$

2. The Schrödinger equation

We focus now on the particle-hole instability in manner of Cooper pairing. We start from the Fermi liquid and look whether a particle-hole pair of the form given by Eq. (76) can destabilize the ground state. The equation of motion for $\psi_{\mathbf{r},\mathbf{r}'}$ writes

$$\left[-\frac{\hbar^2}{2m} \left(\partial^2_{\mathbf{r}} - \partial^2_{\mathbf{r}'} \right) + V(\mathbf{r},\mathbf{r}') \right] \psi_{\mathbf{r},\mathbf{r}'} = E \psi_{\mathbf{r},\mathbf{r}'}. \tag{78}$$

We study the potential term by taking the average over space $\langle \rangle_{\mathbf{r},\mathbf{r}'}$ of Eq. (78), which is equivalent to taking the $(\mathbf{k},\mathbf{k}') = 0$ component in momentum space:

$$\begin{aligned} \langle V_{\mathbf{r},\mathbf{r}'} \psi_{\mathbf{r},\mathbf{r}'} \rangle &= \sum_{\mathbf{k},\mathbf{k}',\mathbf{k_1},\mathbf{k}'_1} V_{\mathbf{k},\mathbf{k}'} \psi_{\mathbf{k_1},\mathbf{k}'_1} \sum_{\mathbf{r},\mathbf{r}'} e^{i(\mathbf{k}+\mathbf{k_1})\cdot\mathbf{r}} e^{-i(\mathbf{k}'+\mathbf{k}'_1)\cdot\mathbf{r}'} \\ &= \sum_{\mathbf{k},\mathbf{k}'} V_{\mathbf{k},\mathbf{k}'} \psi_{\mathbf{k},\mathbf{k}'}. \end{aligned} \tag{79}$$

Within the change of variables $\mathbf{k} \to \tilde{\mathbf{k}} - \mathbf{P}/2; \mathbf{k}' \to \tilde{\mathbf{k}}' + \mathbf{P}/2$, and $\mathbf{P} = 2\mathbf{k}_F$, we get the following equations:

$$\begin{aligned} \left(E - \frac{\hbar^2}{m} \mathbf{k}_F \cdot \tilde{\mathbf{k}} \right) \chi_{\tilde{\mathbf{k}},\mathbf{p}} &= C, \\ C &= \sum_{\tilde{\mathbf{k}}} V_{\tilde{\mathbf{k}},\tilde{\mathbf{k}}'} \chi_{\tilde{\mathbf{k}},\mathbf{P}}, \end{aligned} \tag{80}$$

where $V_{\tilde{\mathbf{k}},\tilde{\mathbf{k}}'} = \int_{\mathbf{r}} V(r) e^{i(\tilde{\mathbf{k}}-\tilde{\mathbf{k}}')\cdot\mathbf{r}}$ is an attractive potential coming from the pairing fluctuations. With ω_F the width of the fluctuation spectrum, we model

$$\begin{aligned} \bar{V} &= -\frac{V}{L^2}, \quad \text{if } 0 < \tilde{\mathbf{k}}, \tilde{\mathbf{k}}' < \frac{\omega_F}{\rho_0}, \\ &= 0 \quad \text{elsewhere.} \end{aligned} \tag{81}$$

Herein, ρ_0 is the electronic density of states at the Fermi level. Equation (10) can then easily be solved, leading to the bonding energy

$$E = -2\hbar\omega_F e^{-2/(\rho_0 V)}. \tag{82}$$

The formation of particle-hole pairs at multiple $2\mathbf{k}_F$ wave vectors is a logarithmic instability of the Fermi liquid in the presence of an attractive potential. In the standard BCS theory, the coupling between density and phase fluctuations is weak. In some specific cases, however, like the attractive Hubbard model, density and phase couple strongly and our model likewise predicts the emergence of s-wave excitonic patches. Within the SU(2) scenario for cuprates, the typical scale associated with the pairing fluctuations is strong, of order of the formation of the SU(2) dome, and can naturally be associated with the PG scale T^*.

B. Integrating the SU(2) fluctuations

In order to derive the effective action for the subleading orders, we integrate out the SU(2) fluctuations, averaging now over the effective modes $\hat{Q}$:

$$Z_{\mathrm{fin}} = e^{-S_{\mathrm{fin}}}, \quad \text{with } S_{\mathrm{fin}} = -\tfrac{1}{2} \langle (S_{\mathrm{int}})^2 \rangle_Q. \tag{83}$$

From Eq. (38), we have

$$S_{\mathrm{fin}} = -\frac{1}{8} \mathrm{Tr} \int_{x,x',x_1,x'_1} \left\langle \overline{\Psi}_x \hat{\overline{Q}}_{x,x'} \Psi_{x'} \overline{\Psi}_{x_1} \hat{Q}_{x_1,x'_1} \Psi_{x'_1} \right\rangle_Q, \tag{84}$$

where $\hat{\overline{Q}}$ and $\hat{Q}$ are defined in Eqs. (40) and (41). Using the more practical Wigner- transform defined in Eq. (51), we get

$$S_{\rm fin} = -\frac{1}{8}{\rm Tr}\sum_{k,q,k',q'}\langle\overline{\Psi}_{k+q}\hat{\overline{M}}_{k,q}\Psi_k\overline{\Psi}_{k'+q'}\hat{M}_{k',q'}\Psi_{k'}\rangle_Q. \quad (85)$$

Disentangling Eq. (85) is quite lengthy but the result produces a sum of an effective component in the SC channel (86) and another one in the charge channel (87) $S_{\rm fin} = S^a_{\rm fin} + S^b_{\rm fin}$, with

$$S^a_{\rm fin} = -\frac{1}{2}{\rm Tr}\sum_{k,q,k',q',\sigma,\sigma'}\sigma\sigma'\langle\Delta^\dagger_{k,q}\Delta_{k',q'}\rangle_Q \times \psi^\dagger_{k+q/2,\sigma}\psi^\dagger_{-k+q/2,-\sigma}\psi_{-k'+q'/2,-\sigma'}\psi_{k'+q'/2,\sigma'}, \quad (86)$$

$$S^b_{\rm fin} = -\frac{1}{2}{\rm Tr}\sum_{k,q,k',q',\sigma,\sigma'}\langle\chi^\dagger_{k,q}\chi_{k',q'}\rangle_Q \times \psi^\dagger_{k+q/2,\sigma}\psi_{k+Q_0-q/2,\sigma}\psi^\dagger_{k'+Q_0-q'/2,\sigma'}\psi_{k'+q'/2,\sigma'}. \quad (87)$$

Note that since the bosonic propagator Eq. (63) conserves the number of particles, there is no mixed term in the above equations. The forms of $\langle\Delta^\dagger_{k,q}\Delta_{k',q'}\rangle_Q$ and $\langle\chi^\dagger_{k,q}\chi_{k',q'}\rangle_Q$ are identical, up to a mass term, and are given by the nonlinear σ model, Eqs. (64) and (68),

$$\langle\Delta^\dagger_{k,q}\Delta_{k',q'}\rangle_Q = \pi^s_{k,k',q}\delta_{\mathbf{q},\mathbf{q}'}, \quad (88)$$

$$\langle\chi^\dagger_{k,q}\chi_{k',q'}\rangle_Q = \pi^c_{k,k',q}\delta_{\mathbf{q},\mathbf{q}'}, \quad (89)$$

where the form of the SU(2) propagator has been defined in Sec. IV, Eqs. (64), (68), and (66):

$$\pi^c_{k,k',q} = M_{0,k}M_{0,k'}\frac{\pi_0}{J_0\omega_n^2 + J_1(\mathbf{v}\cdot\mathbf{q})^2 + a_0}, \quad (90)$$

$$\pi^s_{k,k',q} = M_{0,k}M_{0,k'}\frac{\pi_0}{J_0\omega_n^2 + J_1(\mathbf{v}\cdot\mathbf{q})^2 - a_0}, \quad (91)$$

where a_0 is the mass term from Eq. (66),

C. Excitonic patches

One can now perform a second Hubbard-Stratonovich transformation in order to decouple $S^a_{\rm fin}[\psi]$ in Eq. (86) in the charge channel, to get $S^a_{\rm fin}[\psi] = S^a_0[\chi] + S^a_1[\psi,\chi]$, with

$$S^a_0[\chi] = -\sum_{kk'q,\sigma}\pi^{s-1}_{k,k',q}\chi_{-\sigma,q-k,q-k'}\chi_{\sigma,k,k'}, \quad (92)$$

$$S^a_1[\psi,\chi] = \sum_{kk',\sigma}[\chi_{-\sigma,-k+q,-k'+q}\psi^\dagger_{\mathbf{k},\sigma}\psi_{\mathbf{k}',\sigma} + \chi_{\sigma,k,k'}\psi^\dagger_{-\mathbf{k}+\mathbf{q},-\sigma}\psi_{-\mathbf{k}'+\mathbf{q},-\sigma}]. \quad (93)$$

A stationarity of the free energy leads to

$$\chi_{\sigma,k,k'} = \sum_q \pi^s_{k,k',q}\langle\psi^\dagger_{-\mathbf{k}+\mathbf{q},\sigma}\psi_{-\mathbf{k}'+\mathbf{q},\sigma}\rangle. \quad (94)$$

We will drop in the following the spin label of the $\chi_{k,k'}$ field, since both spin configurations are degenerate. Together with the bare fermionic action (25) one obtains the effective action

$$S^a_0[\psi] + S^a_1[\psi,\chi] = -\sum_{kk'\sigma}\overline{\tilde{\psi}}_{\mathbf{k}}\hat{G}^{-1}_{k,k'}\tilde{\psi}_{\mathbf{k}'} \quad (95)$$

with the two-component fermionic field

$$\tilde{\psi}_{\mathbf{k}} = (\psi_{\mathbf{k},-\sigma},\psi_{\mathbf{k}',\sigma})^T \quad (96)$$

and the inverse propagator

$$\hat{G}^{-1}_{k,k'} = \begin{pmatrix}(i\epsilon_n - \xi_{\mathbf{k}}) & -\chi_{-\sigma,k,k'}\\ -\chi_{\sigma,k,k'} & (i\epsilon_n + \xi_{k'})\end{pmatrix}. \quad (97)$$

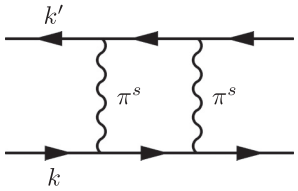

FIG. 13. Infinite ladder series corresponding to the gap equations (101).

D. Gap equation for the charge order

The gap equation to study the charge ordering of our system stems directly from the Dyson equation for the fermionic propagator:

$$\hat{G}^{-1}_{k,k'} = \hat{G}^{-1}_0 - \hat{\Sigma}_{k,k'}, \quad (98a)$$

$$\text{with} \quad \hat{G}^{-1}_0 = \begin{pmatrix}i\epsilon_n - \xi_k & \\ & i\epsilon_n - \xi_{k'}\end{pmatrix}, \quad (98b)$$

$$\text{and } \hat{\Sigma}_{k,k'} = \begin{pmatrix} & \chi_{k,k'}\\ \chi_{k,k'} & \end{pmatrix}. \quad (98c)$$

$$\hat{G}_{k,k'} = -\langle\mathcal{T}\tilde{\psi}_k\overline{\tilde{\psi}}_{k'}\rangle, \quad (99)$$

is obtained by inverting Eq. (97) and one finds

$$[\hat{G}_{k,k'}]_{12} = -\langle\psi^\dagger_{\mathbf{k},-\sigma}\psi_{\mathbf{k}',-\sigma}\rangle = -\frac{\chi_{k,k'}}{(i\epsilon_n - \xi_{\mathbf{k}})(i\epsilon'_n - \xi_{k'}) - \chi^2_{k,k'}}, \quad (100)$$

which finally yields (see Fig. 13):

$$\chi_{k,k'} = \sum_q \pi^s_{k,k',q}[\hat{G}_{q-k,q-k'}]_{12}. \quad (101)$$

The maximum solution comes from the denominator in Eq. (100), and especially from the $(\mathbf{k},\mathbf{k}')$ point close to the Fermi surface. In order to keep the solution tractable without loosing some physical effects, we neglect the frequency dependence of χ. We can then easily compute the Matsubara sum at $T = 0$. We find

$$\chi_{\mathbf{k},\mathbf{k}'} = \bar{\pi}_0\sum_{\mathbf{q}} I(\mathbf{k},\mathbf{k}',\mathbf{q}) \quad (102)$$

with

$$I(\mathbf{k},\mathbf{k}',\mathbf{q}) = \frac{\chi_{q-k,q-k'}}{2}\left[\frac{(|\omega_1|+|\omega_2|+r)\mathrm{sgn}(\omega_1\omega_2)-r}{r(|\omega_1|+|\omega_2|)(|\omega_1|+r)(|\omega_2|+r)}\right] \tag{103}$$

and

$$r = \sqrt{\bar{J}_1\xi_{\mathbf{q}}^2+\bar{a}_0}, \tag{104a}$$

$$\omega_{1/2} = (\xi_{\mathbf{q}-\mathbf{k}}+\xi_{\mathbf{q}-\mathbf{k}'})/2 \pm \sqrt{(\xi_{\mathbf{q}-\mathbf{k}}-\xi_{\mathbf{q}-\mathbf{k}'})^2/4+\chi^2_{q-k,q-k'}}, \tag{104b}$$

where $\bar{\pi}_0 = \pi_0/J_0$, $\bar{J}_1 = J_1/J_0$, and $\bar{a}_0 = a_0/J_0$.

1. Dependence of the solution on the exciton wave vectors

In a first study, we want to find all wave vectors $(\mathbf{k},\mathbf{k}')$, which give the maximum response. For this task, we solve Eq. (102) for the charge ordering parameter χ numerically for arbitrary coupling vector $\mathbf{P} = \mathbf{k}' - \mathbf{k}$. We further make the approximation $\chi_{q-k,q-k'} \approx \chi_{-k,-k'}$ on the right hand side of Eq. (102). Fixing then a reference point $\mathbf{k}$ in the first BZ, we solve the mean-field equation upon varying the coupling vector $\mathbf{P} = \mathbf{k}' - \mathbf{k}$ and look for the points $\mathbf{k}'$ where the solution is maximal. As already suspected from Eq. (102), nonzero solutions are obtained only when both points $\mathbf{k}$ and $\mathbf{k}'$ are situated close to the FS. The numerical solution in Fig. 14 shows that for all couplings $\{\mathbf{P}\}$ connecting two points of the Fermi surface, the height of nonzero χ is very similar.

2. Solution for $\mathbf{k}' - \mathbf{k} = 2\mathbf{p}_F$

In Fig. 15, we present the solution of the gap equations for a range of wave vectors connecting points around the Fermi surface in the antinodal region. Hence we called these wave vectors $2\mathbf{p}_F$. We observe that, as the coupling strength is increased, the $2\mathbf{p}_F$ wave vectors are able to gap out the entire antinodal region in the BZ. The main idea here is that the SU(2) pairing fluctuations not only rotate the original charge modulation wave vector from the diagonal to the axes, but gives space for a range of wave vectors to participate to the electron-hole pairing. As shown in Sec. VIII A, the set of $2\mathbf{p}_F$ leads to a logarithm in the direction perpendicular to the Fermi surface, and hence leads to the formation of preformed pairs. Each $2\mathbf{p}_F$ wave vector shares only a small portion of the phase space in momentum $\mathbf{k}$, around the Fermi surface, therefore the logarithmic divergence is finally cut by curvature in the direction transverse to the corresponding Fermi wave vector.

A remark about the symmetry of the charge modulations in the patch are in order here. The $2\mathbf{p}_F$ order comes from π_q^s in Eq. (101) and thus connect the ordering parameters $\chi_{k,k'}$ around the same points in the Brillouin zone. The solution of the gap equation (101) alone cannot distinguish between d-wave and s or s' order. However, as before, we have seen in Sec. III, that d-wave $2\mathbf{p}_F$ order already emerges from short-range AF correlations. The SU(2) fluctuations have thus to be seen as an additional force action on top of AF correlations, which altogether leads to the stabilization of the d-wave symmetry for the $2\mathbf{p}_F$ droplets. Hence the effect of the SU(2) fluctuations will be to select the involution A [Eq. (10)] as the preferential SU(2) partner of d-wave SC.

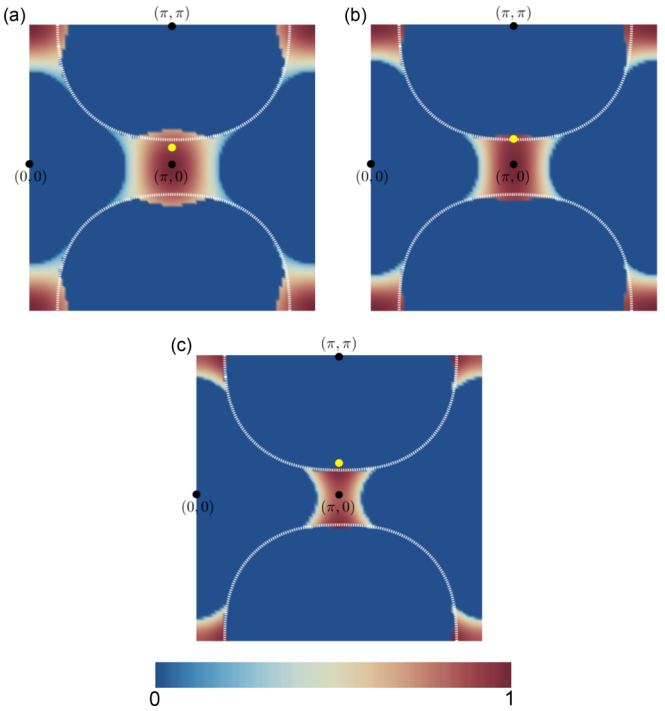

FIG. 14. Density plots of the charge order parameter $|\chi_{k,k'}|$ obtained from a numerical solution of Eq. (102) as a function of the coupling vector $\mathbf{P} = \mathbf{k}' - \mathbf{k}$. Red, white, and blue represents, respectively, high, intermediate, and low values of χ. The white dotted line represents the Fermi surface. We have fixed the k point in (a) the point $(\pi,0)$, (b) the point on the Fermi surface at the zone edge, and (c) a point shifted a little from the Fermi surface (see the yellow point). The interaction is $\bar{\pi}_0 = 0.3$ and the mass $\bar{a}_0 = 5$. The form of the solution only depends on the k point.

The spreading of the wave vectors is typical of the formation of patches in real space, that we have described in a previous paper [164]. The patches have an internal modulation structure very close to the checkerboard observed experimentally. They can be frozen, or fluctuate at a temperature closer to the PG. The detailed study of this intricate dynamics goes beyond the scope of this paper. It relies on the existence of the constraint in the nonlinear σ model, which creates strong effective correlations between the charge and SC modes, and finally a type of mode-mode coupling in the charge sector. This in turn typically leads to phase separation, and entropic effects. In Sec. X A, we give a heuristic picture of the phase diagram in this approach.

3. Solution for $\mathbf{k}' = -\mathbf{k}$

For this type of involution, we do not find any formation of a gap. It is not surprising, since it does not imply any band crossing of the electronic dispersion, as already noticed in Fig. 2(c′). Indeed, the involution that is sending $\mathbf{k} \to -\mathbf{k}$ leaves the electronic dispersion $\xi_{\mathbf{k}}$ invariant.

The parameters in Fig. 16 are $\bar{\pi}_0 = 0.3$, $\bar{J}_1 = 10^{-6}$, $\bar{a}_0 = 5$ in units of the band gap and we take a constant mass $\bar{a}_0$ over the BZ. The dispersion is approximated by a tight-binding

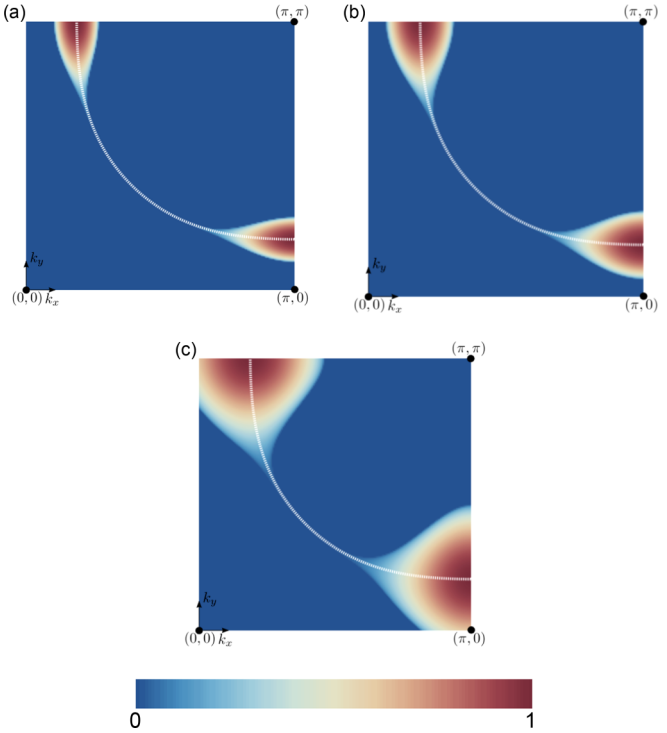

FIG. 15. Density plots of the charge order parameter $|\chi_{k,k'}|$ obtained from a numerical solution of Eq. (102) in the first BZ for the coupling vector $\mathbf{P} = -\mathbf{2k}$ for different interaction strength (a) $\bar{\pi}_0 = 0.01$, (b) 0.03, (c) 0.3 and the mass $\bar{a}_0 = 5$. Red, white, and blue represents high, intermediate, and low values of $|\chi_{k,k'}|$, respectively. The white dotted line represents the Fermi surface. The magnitude as well as the size of the gap increases with the strength of the interaction.

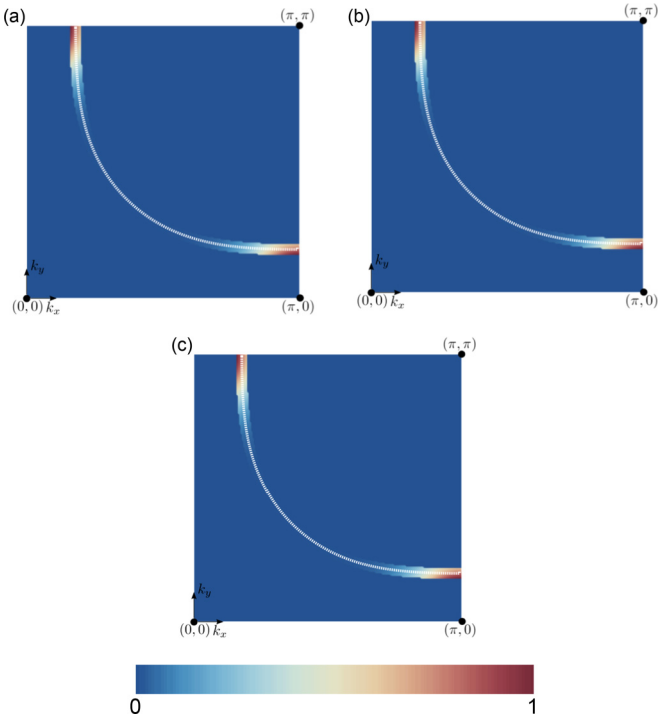

FIG. 16. Density plots of the charge order parameter $|\chi_{k,k'}|$ obtained from a numerical solution of Eq. (102) in the first BZ for the coupling vector $\mathbf{P} = -\mathbf{2k}$ for different interaction strength (a) $\bar{\pi}_0 = 0.03$, (b) 0.3, (c) 3 and the mass $\bar{a}_0 = 5$. Red, white, and blue represents high, intermediate, and low values of $|\chi_{k,k'}|$, respectively. The white dotted line represents the Fermi surface. The magnitude of the peak increases with the interaction contrary to the size of the gap.

dispersion $\xi_{\mathbf{k}}$ with parameter set "tb2" from Ref. [124] and the chemical potential adjusted to account for 10% hole doping. In fact, the shape of the numerical solution of χ turns out to be not very sensitive to the model parameters $\bar{J}_1$ and $\bar{a}_0$.

IX. PAIR DENSITY WAVE (PDW)

In this section, we look at the potential generation of other types of order, and in particular, of the pair density wave (PDW) order from the SU(2) fluctuations.

A. Gap equation

The decoupling of $S^b_{\rm int}$ in Eq. (87) follows the same steps as for Eq. (86) performing the Hubbard-Stratonovich transformation, we get $S^b_{\rm fin}[\psi] = S^b_0[\chi] + S^b_1[\psi,\chi]$, with

$$S^b_0[\chi] = -\sum_{kk'q,\sigma} \pi^{c\,-1}_{k,k',q}\,\Delta^{a\dagger}_{-\sigma,k,k'+Q_0}\,\Delta^{b}_{\sigma,k+Q_0+q,k'+q}, \tag{105}$$

$$S^b_1[\psi,\chi] = \sum_{kk',\sigma}\big[\Delta^{a\dagger}_{-\sigma,k,k'+Q_0}\,\sigma\,\psi_{\mathbf{k}+\mathbf{Q_0}+\mathbf{q},-\sigma}\,\psi_{\mathbf{k}'+\mathbf{q},\sigma} + \sigma\,\psi^{\dagger}_{\mathbf{k},-\sigma}\,\psi^{\dagger}_{\mathbf{k}'+\mathbf{Q_0},-\sigma}\,\Delta^{b}_{\sigma,k+Q_0+q,k'+q}\big]. \tag{106}$$

Herein, $\Delta^{a}_{-\sigma,k,k'+Q_0}$ is the modulated superconducting field whose condensation leads to the PDW state. We follow closely the last section (Sec. VIII C) to derive the corresponding equations for the PDW channel.

Again, the stationarity of the free energy leads to

$$\Delta^{a}_{\sigma,k,k'+Q_0} = \sum_{q} \pi^{c}_{k,k',q}\,\langle\sigma\,\psi_{\mathbf{k}+\mathbf{q},-\sigma}\,\psi_{\mathbf{k}'+\mathbf{Q_0}+\mathbf{q},\sigma}\rangle. \tag{107}$$

As developed in the previous section, we obtain the effective action

$$S^b_0[\psi] + S^b_1[\psi,\chi] = -\sum_{kk'\sigma} \overline{\tilde{\psi}}_{\mathbf{k}\sigma}\,\hat{G}^{-1}_{k,k'}\,\tilde{\psi}_{\mathbf{k}',\sigma} \tag{108}$$

with the four-component fermionic field

$$\tilde{\Psi}_{\mathbf{k},\sigma} = (\psi_{\mathbf{k},-\sigma},\ \psi^{\dagger}_{\mathbf{k}'+\mathbf{Q_0},\sigma},\ \psi_{\mathbf{k}',-\sigma},\ \psi^{\dagger}_{\mathbf{k}+\mathbf{Q_0},\sigma})^{T}, \tag{109}$$

and the conjugation

$$\overline{\tilde{\Psi}} = (\psi^{\dagger}_{\mathbf{k},-\sigma},\ -\psi_{\mathbf{k}'+\mathbf{Q_0},\sigma},\ \psi^{\dagger}_{\mathbf{k}',-\sigma},\ -\psi_{\mathbf{k}+\mathbf{Q_0},\sigma}), \tag{110}$$

and the inverse propagator now writes

$$\hat{G}^{-1}_{k,k'} = \begin{pmatrix} \hat{G}^{b,-1} & \\ & \hat{G}^{a,-1} \end{pmatrix}, \qquad \hat{G}^{a,-1} = \begin{pmatrix} (i\epsilon_n - \xi_{\mathbf{k}}) & -\sigma\,\Delta^{a}_{\sigma,k,k'+Q_0} \\ \sigma\,\Delta^{a\dagger}_{\sigma,k,k'+Q_0} & (-i\epsilon_n - \xi_{\mathbf{k}'+\mathbf{Q_0}}) \end{pmatrix}, \tag{111}$$

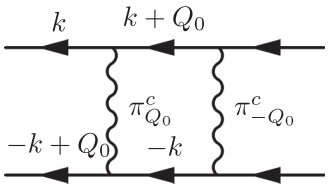

FIG. 17. Infinite ladder series corresponding to the gap equations (116) and (117).

and

$$\hat{G}^{b,-1} = \begin{pmatrix} (i\epsilon_n - \xi_{\mathbf{k}'}) & \sigma\Delta^{b}_{\sigma,k+Q_0,k'} \\ -\sigma\Delta^{b\dagger}_{\sigma,k+Q_0,k'} & (-i\epsilon_n + \xi_{\mathbf{k}+\mathbf{Q_0}}) \end{pmatrix}. \tag{112}$$

The gap equation to study the charge ordering in our system stems directly from the Dyson equation for the fermionic propagators:

$$\hat{G}^{a,-1} = \hat{G}^{-1}_{0,a} - \hat{\Sigma}_a, \tag{113a}$$

$$\text{with} \quad \hat{G}^{-1}_{0,a} = \begin{pmatrix} i\epsilon_n - \xi_{\mathbf{k}} & \\ & -i\epsilon_n - \xi_{\mathbf{k}'+\mathbf{Q_0}} \end{pmatrix}, \tag{113b}$$

$$\text{and} \quad \hat{\Sigma}_a = \begin{pmatrix} & \sigma\Delta^{a}_{-\sigma,k,k'+Q_0} \\ -\sigma\Delta^{a\dagger}_{\sigma,k,k'+Q_0} & \end{pmatrix}, \tag{113c}$$

and

$$\hat{G}^{b,-1} = \hat{G}^{-1}_{0,b} - \hat{\Sigma}_b, \tag{113d}$$

$$\text{with} \quad \hat{G}^{-1}_{0,b} = \begin{pmatrix} i\epsilon_n - \xi_{\mathbf{k}+\mathbf{Q_0}} & \\ & -i\epsilon_n - \xi_{\mathbf{k}'} \end{pmatrix}, \tag{113e}$$

$$\text{and} \quad \hat{\Sigma}_b = \begin{pmatrix} & -\sigma\Delta^{b}_{-\sigma,k+Q_0,k'} \\ \sigma\Delta^{b\dagger}_{\sigma,k+Q_0,k'} & \end{pmatrix}. \tag{113f}$$

$$\hat{G}_{k,k'} = -\langle \mathcal{T}\tilde{\Psi}_k \overline{\tilde{\Psi}}_{k'} \rangle, \tag{114}$$

is obtained by inverting Eq. (111) and one finds

$$\begin{aligned} \left[\hat{G}^{b}_{k,k'}\right]_{12} &= -\sigma \langle \psi_{\mathbf{k}+\mathbf{Q_0},-\sigma} \psi_{\mathbf{k}',-\sigma} \rangle \\ &= -\frac{\Delta^{b}_{-\sigma,k+Q_0,k'}}{(i\epsilon_n - \xi_{\mathbf{k}+\mathbf{Q_0}})(-i\epsilon'_n - \xi_{\mathbf{k}'}) + \left|\Delta^{b}_{-\sigma,k+Q_0,k'}\right|^2}, \end{aligned} \tag{115}$$

and the modulated superconducting field $\Delta^{a}_{-\sigma,k,k'+Q_0}$ finally yields (see Fig. 17):

$$\Delta^{a}_{-\sigma,k,k'+Q_0} = -\sum_q \pi^{c}_{k,k',q} \left[\hat{G}^{b}_{k+q,k'+q}\right]_{12}. \tag{116}$$

The same derivation goes for the field $\Delta^{b}_{\sigma,k,k'+Q_0}$, leading to

$$\Delta^{b}_{\sigma,k+Q_0,k'} = -\sum_q \pi^{c}_{k,k',q} \left[\hat{G}^{a}_{k+q,k'+q}\right]_{12}, \tag{117}$$

with

$$\begin{aligned} \left[\hat{G}^{a}_{k,k'}\right]_{12} &= -\sigma \langle \psi_{\mathbf{k},\sigma} \psi_{\mathbf{k}'+\mathbf{Q_0},\sigma} \rangle \\ &= -\frac{\Delta^{a}_{\sigma,k,k'+Q_0}}{(i\epsilon_n - \xi_{\mathbf{k}})(-i\epsilon'_n - \xi_{\mathbf{k}'+\mathbf{Q_0}}) + \left|\Delta^{a}_{\sigma,k,k'+Q_0}\right|^2}. \end{aligned} \tag{118}$$

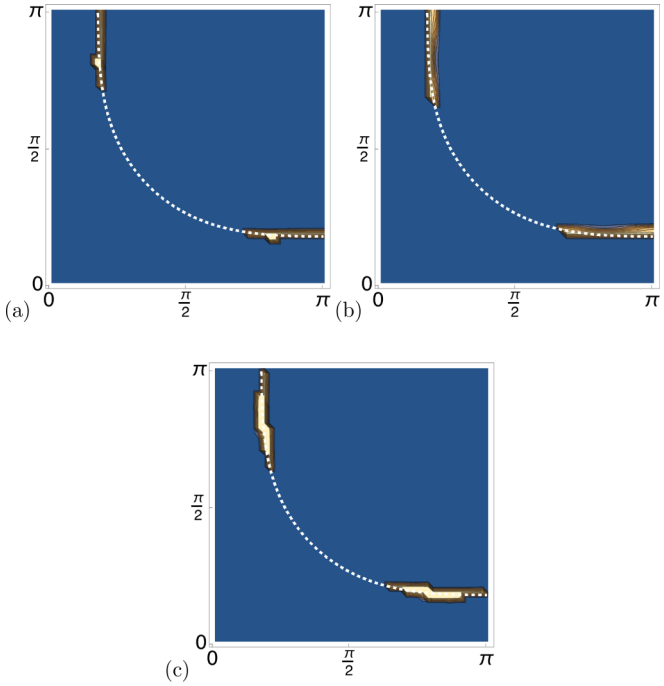

FIG. 18. Density plot of the solution of Eqs. (116) and (117), searching for a finite center of mass pairing around the resulting wave vectors (a) $(Q_0,0)$, (b) $(0,Q_0)$, and (c) (Q_0,Q_0). Vanishing solutions are color-coded in blue, while nonvanishing points are depicted in yellow. We obtain a finite response in the antinodal region. We are not able to distinguish here between wave vectors along the axes and on the diagonal, but on the other hand our result give wave vectors starting with the first frequency $\mathbf{Q_0}$ and not from the second harmonics $2\mathbf{Q_0}$ [87].

B. Numerical solution

The solution of Eqs. (115) and (116) is given in Fig. 18. We observe the formation of a PDW order, or superconducting order with finite resulting momentum. The wave vector obtained from the SU(2) fluctuations directly depends on our starting point wave vector for the charge channel. When we start with a diagonal wave vector $\mathbf{Q}_0$, which led to the effective actions Eqs. (68), (64), and (66), this in turn led to a diagonal wave vector for the PDW instability as seen in Fig. 18(c). However, starting with the two axial wave vectors $\mathbf{Q}_x$ and $\mathbf{Q}_y$ (with $\mathbf{Q}_x \sim 0.3\pi/a$ and $\mathbf{Q}_y \sim 0.3\pi/a$) forming the checkerboard structure observed in experiments, we obtain the formation of a similar PDW instability, but with axial wave vectors, respectively, $\mathbf{Q}_y$ and $\mathbf{Q}_x$, as depicted in Figs. 18(a) and 18(b).

An important point concerns the symmetry of the PDW order generated this way. As was commented previously, since the SU(2) propagator π^c_q is centered around $\mathbf{q} = \mathbf{0}$ in Eq. (117) the SU(2) fluctuations alone do not select any specific symmetry, whether it is s' or d wave. Contrarily to the previous modulations, which were already generated by the AF correlations described in Sec. III, here the PDW order parameter is directly emerging from the SU(2) fluctuations. Hence the symmetry could be either s' or d wave at this stage of the theory. It is possible that the experimental context, like the presence of strong disorder finally selects the s'

symmetry, as recently seen in experiments [77]. Another important point in our study, is modulation wave vector associated with the PDW order is precisely the wave vector of the CDW observed experimentally, and not its second, or higher harmonics. This is in agreement with the findings of the key STM experiment, showing the presence of a very small PDW order with the same wave vector as the charge order [77]. The generation of PDW starting from a CDW instability has been described in detailed in a recent work, using a Ginzburg-Landau formalism [87]. Here we give an alternative way to generate the PDW instability, starting from a formalism which involves the SU(2) fluctuations. Note that the form of the SU(2) fluctuations obtained in Eqs. (68), (64), and (66) remains unchanged, when the starting wave vector is varied.

X. GLOBAL PHASE DIAGRAM FOR CUPRATE SUPERCONDUCTORS

A. The physical lines

1. Generic trends

In order to obtain the temperature-hole doping phase diagram, we developed a minimal model based on Ginzburg-Landau functional. The free energy depends on the SU(2) order parameter $\Delta_{SU(2)}$ and writes

$$F_{SU(2)} = a_{SU(2)}\Delta^2_{SU(2)} + \frac{g_{SU(2)}}{2}\Delta^4_{SU(2)}, \qquad (119)$$

where we assume that $\Delta_{SU(2)}$ is homogeneous and $a_{SU(2)}$ and $g_{SU(2)}$ are energy parameters. Minimizing the free energy (119) as regards to $\Delta_{SU(2)}$ gives the relation $\Delta_{SU(2)} = \sqrt{\frac{a_{SU(2)}}{g_{SU(2)}}}$. We assume that the magnitude of the order parameter at zero temperature is proportional to the critical temperature. The doping dependence of the critical temperature of the SU(2) can be reproduced by parametrizing the energy parameters as $a_{SU(2)} = \bar{a}_{SU(2)}(p^c_{SU(2)} - p)$ and $g_{SU(2)} = 1 + m_{SU(2)}(p - p^c_{SU(2)})$, where $p^c_{SU(2)}$ is the hole doping where the SU(2) is expected to disappear. In our model, the temperature where the SU(2) symmetry disappear is associated with T^*.

In this simple model, the Copper pairing (CP) and preformed excitonic pairing (PEP) energy scales are related by SU(2) symmetry. From a theoretical point of view, it means that both SC and PhP order parameter are constrained as exposed in the relation (4) that writes $\Delta_{SU(2)} = \sqrt{\Delta^2_{CP} + \Delta^2_{PEP}}$, where Δ_{CP} and Δ_{PEP} are the CP and PEP gap scales, respectively. Considering, in a mean-field heuristic picture, a coexisting SC and PhP phase, we can write the free energy as

$$F_1 = a_{CP}\Delta^2_{CP} + \frac{g_{CP}}{2}\Delta^4_{CP} + a_{PEP}\Delta^2_{PEP} + \frac{g_{PEP}}{2}\Delta^4_{PEP}, \qquad (120)$$

where a_{CP}, g_{CP}, a_{PEP}, and g_{PEP} are energy parameters. Taking into account the SU(2) constraint of Eq. (4), we can replace the order parameter in Eq. (120) by the relation $\Delta_{PEP} = \sqrt{\Delta^2_{SU(2)} - \Delta^2_{CP}}$, where $\Delta_{SU(2)}$ has been determined from Eq. (119). Minimizing the free energy as regards to the CP energy scale, one can find the expression of the SC and PhP

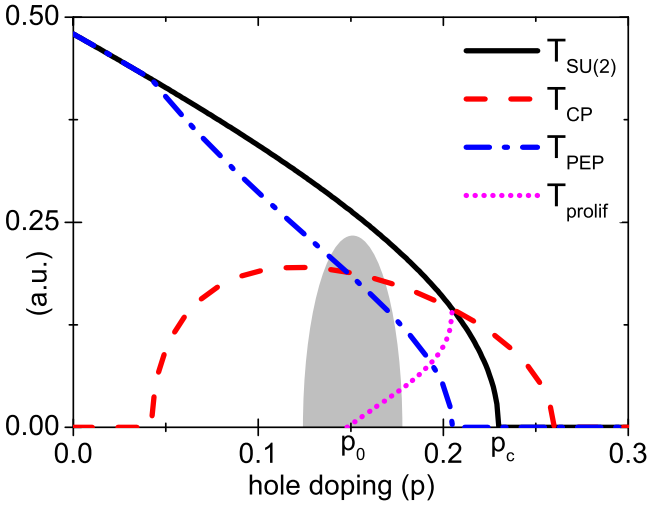

FIG. 19. Temperature-hole (T, p) phase diagram calculated from the simplified Ginzburg-Landau model. The SU(2) order parameter critical temperature (solid line) follows the PG critical temperature T^*. The temperature scale corresponding to Cooper pairing T_{CP} has the form of a domelike in real compounds. The PEP critical temperature (dash-dotted line) decreases with doping. The "excitonic" patches proliferation temperature vanishes in the underdoped regime and increases at doping close to 0.12.

scales as

$$\Delta_{CP} = \sqrt{\frac{a_{CP} - a_{PEP} + g_{PEP}\Delta^2_{SU(2)}}{g_{PEP} + g_{CP}}},$$
$$\Delta_{PEP} = \sqrt{\Delta^2_{SU(2)} - \Delta^2_{CP}}, \qquad (121)$$

where $a_{CP} = l_{CP}(p^c_{CP} - p)$, $a_{PEP} = l_{PEP}(p^c_{PEP} - p)$, $g_{PEP} = M + p$, and $g_{CP} = M + Mp$ with M, L_{PEP}, and l_{SC} are free parameters.

The phase diagram of Fig. 19, can be understood as follows. The black line $T_{SU(2)}$ corresponds to the SU(2)-dome, depicted in Sec. III, Fig. 7. It defines the upper energy scale, above which we lose the SU(2) fluctuations. The temperature T_{CP}(dashed line, red) corresponds to the typical energy for Cooper pairing. The temperature T_{PEP} (dashed-dotted line, blue) is the typical energy associated with the formation of particle-hole pairs. It is proportional to the SU(2) fluctuations, as shown in Secs. IV and VIII. The particle hole pairing strength is driven by the SU(2) propagator for the nonlinear σ model, as visible in Eq. (101). Note that at the point where $T_{CP} = T_{SU(2)}$, $T_{PEP} = 0$ since there is space for fluctuations. As doping decreases, T_{PEP} increases, and crosses T_{CP} in the middle, for a doping $0.010 < p_c < 0.013$. We note that there is a threshold in temperature, above which the patches of excitons start to proliferate. For $p < p_c$, since $T_{PEP} > T_{CP}$ the excitonic patches have a higher binding energy, and entropic effects due to the finite size of the patches, leads to a proliferation temperature very close to zero. Alternatively, for $p > p_c$, since $T_{PEP} < T_{CP}$, there is a competition between Cooper pairing with the tendency to form a global SC state, and formation of excitonic patches. In this case, the competition holds between the two states, and the proliferation temperature T_{prolif}(dotted magenta line) gradually increases up to $T_{SU(2)}$ around optimal doping. A

simple evaluation of the proliferation temperature is given in the next paragraph.

Interestingly, the phase diagram of Fig. 19 singles out an intermediate critical doping $p_c \simeq 0.12$, which differentiates two regions in the underdoped regime. For $p < p_c$, the picture is of a complete fractionalization of the Fermi surface, with at $T = 0$ a SC order around the nodes and the antinodal region fully gapped out by excitonic patches. It is in line with a "two-gap" picture. On the other hand, for $p > p_c$, at $T = 0$ the system in in the SC state, with excitonic patches starting to proliferate as temperature is raised. It is a one gap picture, which becomes fully valid at $p_0 \simeq 0.21$, where the SC state is gapping out the Fermi surface up to the energy $T_{\mathrm{SU(2)}}$.

The doping $p_c \simeq 0.12$ is thus the doping at which the two scales of formation of the excitonic patches and Cooper pairs are equal $T_{\mathrm{CP}} = T_{\mathrm{PEP}}$. It is conceivable that around this doping, the SU(2) symmetry is strong enough to produce phase separation, but the SU(2) fluctuations are frozen enough so that we observe experimentally one (or two) resulting modulation wave vectors around $(Q_0,0)$ and $(0,Q_0)$ extending up to ten lattice sites, and thus experimentally detectable. A real-space picture of this scenario is given in Ref. [164].

a. Proliferation temperature. We give here a simple derivation of the proliferation temperature. We have a competition between Cooper pairing, leading to the formation of a global SC state, and a local state of particle hole excitonic patches, each carrying a specific entropy. Suppose there is n_p excitonic patches and thus $1 - n_p$ Cooper pairs (to simplify the discussion we took a "two-fluid" only model). The global free energy writes

$$F = -(1-n_p)\frac{a_{\mathrm{CP}}^2}{4g} + n_p\left(-\frac{a_{\mathrm{PEP}}^2}{4g} + T\ln n_p\right), \qquad (122)$$

where g is a high-energy coupling constant that we take equal for the two fluids, $-a_{\mathrm{CP}}^2/(4g)$ and $-a_{\mathrm{PEP}}^2/(4g)$ come from the mean-field minimization for each order parameter, coming for example from Eq. (120). We have $a_{\mathrm{CP}} = T - T_{\mathrm{CP}}$ and $a_p = T - T_{\mathrm{PEP}}$. Minimizing Eq. (122) with respect to n_p leads to

$$\ln n_p = -\frac{1}{T}\frac{a_{\mathrm{CP}}^2 - a_{\mathrm{PEP}}^2}{4g}, \qquad (123)$$

which leads to a temperature above which $n_p \simeq 1$, also called proliferation temperature

$$T_{\mathrm{prolif}} = \begin{cases} \frac{a_{\mathrm{CP}}^2 - a_{\mathrm{PEP}}^2}{4g}, & \text{if } |a_{\mathrm{CP}}| > |a_{\mathrm{PEP}}| \\ 0, & \text{elsewhere} \end{cases}.$$

B. Strange metal phase

This part explores the consequences of the RES for the phase diagram of cuprates (see Fig. 20) when this mode becomes critical. There are experimental indications that the electric transport in this system has both 2D and 3D character. We will thus calculate the resistivity ρ in $d = 3$ and $d = 2$, in the absence of a gap and show that it differs from the usual Fermi liquid T^2 scaling with a typical $T/\ln T$ behavior. Therefore we evaluate the bosonic polarization induced by critical χ-modes. Details can be found in Appendix F. At quadratic order in the excitonic fluctuations, we obtain the

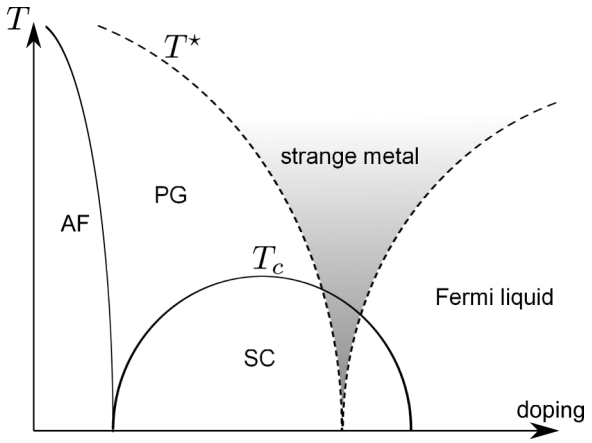

FIG. 20. Schematic phase diagram of cuprate superconductors as a function of hole doping and temperature T where PG is the pseudogap phase, AF is the antiferromagnetic phase, and SC is the superconducting phase. In the grey shaded strange metal phase, the electrical resistivity scales linearly with T.

following effective interaction:

$$S_{\mathrm{crit}}[\psi] = \sum_{kk'qP,\sigma} \Phi_q^{\mathbf{P}}\, \psi^\dagger_{\sigma,\mathbf{k}}\, \psi_{\sigma,\mathbf{k}+\mathbf{P}+\mathbf{q}}\, \psi^\dagger_{-\sigma,\mathbf{k}'}\, \psi_{-\sigma,\mathbf{k}'-\mathbf{P}-\mathbf{q}}, \qquad (124)$$

see Figs. 21(a) and 21(b), with $\Phi_q^{\mathbf{P}} = \langle \chi_{-P-q}\chi_{P+q}\rangle$. The form of above interaction corresponds to a coupling with a collection of bosons [see also Eq. (F1)]. The renormalized bosonic propagator follows from Dyson's equation $[\Phi_{\mathbf{q}}^{\mathbf{P}}(\Omega)]^{-1} = q^2 + m - \Pi_{\mathbf{q}}^{\mathbf{P}}(\Omega)$. Therein, the bare propagator is assumed to have Ornstein-Zernike form. The retarded bosonic polarization $\Pi_{\mathbf{q}}^{\mathbf{P}} = \Pi'_{\mathbf{q}} + i\,\Pi''_{\mathbf{q}}$ in Fig. 21(c), evaluated for $\mathbf{P} = 2\mathbf{p}_{\mathrm{F}}$, yields $\Pi'_{\mathbf{q}}(\Omega) = c[(\Omega + q_\parallel)\ln|\Omega + q_\parallel| - (\Omega - q_\parallel)\ln|\Omega - q_\parallel|]$ and $\Pi''_{\mathbf{q}}(\Omega) = \pi c[(\Omega + q_\parallel)\theta(-\Omega - q_\parallel) + (\Omega - q_\parallel)\theta(\Omega - q_\parallel)]$. With Ω we denote real frequencies and c is a nonuniversal factor depending on the details of the dispersion.

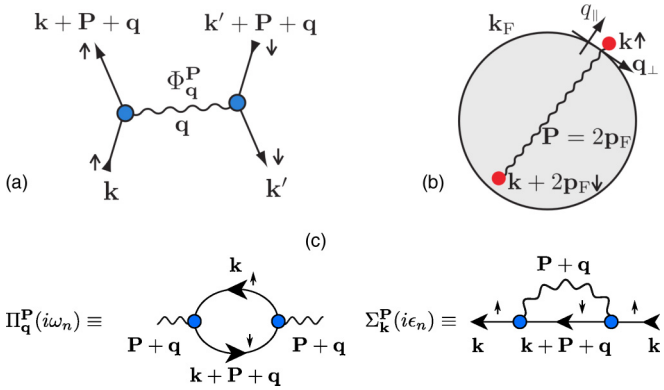

FIG. 21. (a) Graphical representation of the interaction in Eq. (124). The wavy line represents the bosonic propagator $\Phi_{\mathbf{q}}^{\mathbf{P}}$ at criticality for $|\mathbf{q}| \ll |\mathbf{P}|$. (b) RES scattering between two electrons close to the FS at $\mathbf{k}$ and $\mathbf{k} + 2\mathbf{p}_{\mathrm{F}}$ according to Eq. (124). (c) Diagrammatic representation of the one-loop bosonic polarization $\Pi_{\mathbf{q}}$ and the fermionic self-energy $\Sigma_{\mathbf{q}}$ for the RPE mode.

Next, we calculate the electronic self-energy depicted in Fig. 21(c). Here again we refer the reader to Appendix G for details. Note that the self-energy requires a summation over all ordering vectors $\mathbf{P}$. Up to logarithms, each $\mathbf{P}$ wave gives the same contribution. In the quantum critical regime, we have, the scaling behavior $\Pi'_{\mathbf{q}}(\Omega) \sim 2cq_{\parallel} \ln|\Omega|$, and $\Pi''_{\mathbf{q}}(\Omega) \sim \pi c\Omega$. We use this scaling law to evaluate the self-energy of an electron scattering through a single bosonic mode written in Matsubara form as $\Phi_{\mathbf{P}}^{-1}(i\omega_n) = \gamma|\omega_n| - v_{\parallel}q_{\parallel} \ln|\omega_n| + v_{\perp}q_{\perp}^2/2$. The evaluation is performed in $d = 3$, and at the first order in the leading singularity, we obtain $\Sigma(i\epsilon_n) = i\epsilon_n/(4\pi v_{\parallel}v_{\perp} \ln|\epsilon_n|)$. We note that with logarithmic corrections, this form is typical of a marginal Fermi liquid [165] and can account for the properties of the strange metal phase depicted in Fig. 20. In $d = 2$, the self-energy scales like $\Sigma(i\epsilon_n) \sim i\sqrt{|\epsilon_n|}\mathrm{Sgn}(\epsilon_n)$.

We turn now to the discussion of the relaxation time for electron-electron scattering process from a semiclassical Boltzmann treatment. Details are given in Appendix H. The Boltzmann equation for the nonequilibrium electron distribution $f_{\mathbf{k}}$ writes [166,167]

$$\left(\frac{\partial f_{\mathbf{k}}}{\partial t}\right)_{\text{collisions}} = -e\mathbf{E}\cdot\nabla_{\mathbf{k}}f_{\mathbf{k}} = -I_{ei}[f_{\mathbf{k}}] - I_{ee}[f_{\mathbf{k}}], \quad (125)$$

where e is the elementary charge, $\mathbf{E}$ a static electric field and I_{ei}, respectively, I_{ee} are the electron-impurity, respectively, electron-electron collision integrals. The electron-electron collision integral is obtained from Fermi's golden rule,

$$\begin{aligned} I_{ee}[f_{\mathbf{k}}] = &\frac{1}{V}\sum_{\mathbf{q}}\int_{-\infty}^{\infty} d\Omega\, \mathrm{Im}\Phi_{\mathbf{q}}(\Omega)\delta(\epsilon_{\mathbf{k}} - \epsilon_{\mathbf{k}+\mathbf{P}-\mathbf{q}} - \Omega) \\ &\times [f_{\mathbf{k}}(1 - f_{\mathbf{k}+\mathbf{P}-\mathbf{q}})(1 + n_{\mathrm{B}}(\Omega)) \\ &- (1 - f_{\mathbf{k}})f_{\mathbf{k}+\mathbf{P}-\mathbf{q}}n_{\mathrm{B}}(\Omega)], \end{aligned} \quad (126)$$

with $n_{\mathrm{B}}(x) = (\exp(x/T) - 1)^{-1}$ and we drop the contribution from I_{ei}. The relaxation-time approximation amounts to setting $f_{\mathbf{k}} \simeq f_{0,\mathbf{k}} - g_{\mathbf{k}}f_{0,\mathbf{k}}(1 - f_{0,\mathbf{k}})$, where f_0 is the equilibrium distribution and $g_{\mathbf{k}} = \tau e\mathbf{E}\cdot\mathbf{v}_{\mathbf{k}}/T$. In this approximation, Eq. (126) becomes

$$\begin{aligned} I_{ee}[f_{\mathbf{k}}] = &\frac{1}{V}\sum_{\mathbf{q}}\int_{-\infty}^{\infty} d\Omega\, \mathrm{Im}\Phi_{\mathbf{q}}(\Omega)n_{\mathrm{B}}(\Omega)f_{0,\mathbf{k}+\mathbf{P}-\mathbf{q}}(1 - f_{0,\mathbf{k}}) \\ &\times (g_{\mathbf{k}+\mathbf{P}-\mathbf{q}} - g_{\mathbf{k}})\delta(\epsilon_{\mathbf{k}} - \epsilon_{\mathbf{k}+\mathbf{P}-\mathbf{q}} - \Omega). \end{aligned} \quad (127)$$

We see from Eq. (127) that this theory has a nonvanishing imbalance velocity factor, since for $\mathbf{q} = 0$, $(g_{\mathbf{k}+\mathbf{P}} - g_{\mathbf{k}}) \neq 0$. This implies that no additional T dependence arises from the angular part of the integral. To make the connection of the scattering time τ and resistivity ρ, we write the electrical current density as $\mathbf{J} = -2e\langle\mathbf{v}\rangle$ and note its connection to ρ via $\mathbf{J} = \rho^{-1}\mathbf{E}$. For small electric fields, $\rho \sim \tau^{-1}$, and solving the above Boltzmann equation for τ yields $\tau^{-1} \sim T/\ln(T)$, such that $\rho \sim T/\ln(T)$. In $d = 2$, the resistivity scales like $\rho \sim \sqrt{T}$. The scaling forms given here are valid in the antinodal region of the BZ, while the nodal region will provide a Fermi liquidlike T^2 law both in the PG phase and in the strange metal phase. The study of the strong anisotropy of the scattering rates along the Fermi surface, and interplay between the T^2 and anomalous behaviors is the subject of active experimental investigations [168–170] and we will devote a further detailed development of our theory to address the issue.

XI. CONCLUSION

This paper has been devoted to the study of the implications of the nonlinear σ model, which describes the fluctuations of the SU(2) rotation matrix between the d-wave SC state and the d-wave charge order. One important result of this paper is that, when interacting with the conduction electrons, hot regions are created in the Brillouin zone, and in particular a line where the SU(2) fluctuations are massless, which we called an SU(2) line, was found, crossing the Fermi surface at the AF hot spots. The main effect of the SU(2) pairing fluctuations on the charge sector is to tilt the modulation wave vector from the diagonal to the axial wave vectors $(0, Q_0)$ and $(Q_0, 0)$. Secondarily, SU(2) fluctuations affect the SC sector by creating a small PDW instability on top of an already existing d-wave superconducting phase. Lastly, the SU(2) pairing fluctuations lead to the formation of preformed particle-hole pairs, which we have called "excitons," for which a range of $2\mathbf{p}_{\mathrm{F}}$ wave vectors are allowed. The intrinsic constraint of the nonlinear σ model creates some strong mode coupling within the charge sector and thus the creation of excitonic patches, which then proliferate up to the PG temperature T^*. We give a preliminary description of the phase diagram of the cuprates, including a preliminary theory for the anomalous transport properties in the strange metal part of the phase diagram. Implications of the theory for various experimental probes are left for future publications.

The ultimate goal of this theory is to address all possible experimental results, but this goes beyond the scope of this paper. Note that, within the SU(2) scenario, a few experimental issues have already been addressed. The phase diagram as a function of magnetic field and temperature was considered in Ref. [81], the structure of the modulations inside a vortex core in Ref. [83]. A study of the Raman A_{1g} mode was given in Ref. [120], and the gapping out of the Fermi surface in the antinodal region seen in ARPES was described in Ref. [171]. The findings of modulations up to T^* seen, by STM in Bi2212, as well as the resonance of neutron scattering in Hg1201 will be addressed in forthcoming publications [164].

The presence of electron pockets in the AN zone of the first BZ is a very ongoing debate in the cuprate community [172]. The Hall resistivity measurements in YBCO have shown a change in the carrier density n (between the $n = p$ regime at low doping to $n = 1 - p$ regime at high doping) around $p = 0.19$ [173,174]. This change of regime has been associated with the opening of the PG around the hot spot, in the AN zone of the first BZ that should be present at any doping [172]. Our scenario can provide an explanation of the change in the carrier density that will be addressed in a shortcoming work [175]. Therefore the absence of such electron pockets in the AN zone of the first BZ at any doping could be one check of the validity of our scenario.

Moreover, one specific signature of the preformed particle-hole pairs could be the photoluminescence signal. It is well-known in semiconductor physics that excitons exhibit a photoluminescence signal [176]. In our model, the stabilization of such exciton particle-hole pair patches could also lead to such

photoluminescence signal. The exploration and the calculation of such signature is left to later work.

The SU(2) scenario presented here should be applicable for materials where the SC and the CDW states are close in energy. Another condition should be the presence of an interaction that could stabilize such SU(2) fluctuations (like short-range AF correlations). The underdoped cuprate compounds are currently the best candidates wherein these two conditions are present.

ACKNOWLEDGMENTS

We thank Y. Sidis, I. Paul, H. Alloul and Ph. Bourges, for stimulating discussions. This work has received financial support from LabEx PALM (ANR-10-LABX-0039-PALM), ANR project UNESCOS ANR-14-CE05-0007, as well as Grant No. Ph743-12 of the COFECUB. The authors also like to thank the IIP (Natal, Brazil), the Aspen Center for Physics and the Perimeter Institute (Ontario, Canada), where parts of this work were done, for hospitality. This work is supported by the ERC, under Grant agreement AdG-694651-CHAMPAGNE.

APPENDIX A: MEAN-FIELD GAP EQUATIONS: STRONG COUPLING CASE

We give in Fig. 22 the solution of the gap equations (19) and (21) in the strong coupling case, for which we have taken $J = 0.9$ eV. We observe, as the coupling is increased, a pronounced difference between the SC solution and the CDW solutions, in that the SC solution gaps out the entire Fermi surface, whereas the CDW solution remain confined in the antinodal regions of the Brillouin zone.

APPENDIX B: ZONE EDGE HOT LINES

We present in Fig. 23 the evolution of the hot regions for a charge wave vector located at the zone edge. Note that the fractionalization of the Fermi surface is also efficient in that case, with a minimum of the mass (or infinite fluctuations) located at the zone edge.

APPENDIX C: TEST OF VARIOUS ANISOTROPIES

This Appendix gives a thorough study of the effect of the SU(2) hot regions in the response of the charge susceptibility. We look at various types of anisotropy (Figs. 24 and 25) in the size and shape of the hot regions. The main conclusion is that in all cases, the axial response is favored compared to the diagonal one.

The typical form of the Aslamazov-Larkin polarization is shown in Fig. 26,

$$\Pi_{AL}(p,0) = -T \sum_{q} \pi^{s}_{q} \pi^{s}_{p+q} (B_q)^2, \tag{C1}$$

$$\text{with} \quad B_q = \sum_{k} G_k G_{k+p} G_{-k-q}, \tag{C2}$$

with the four variables $k = (\mathbf{k},\varepsilon)$, $q = (\mathbf{q},\omega)$, $G_k^{-1} = i\varepsilon_n - \xi_{\mathbf{k}}$, and $G_{-k}^{-1} = -i\varepsilon_n - \xi_{-\mathbf{k}}$. This contribution typically behaves in the same manner as the vertex corrections. We show it here for completeness for one typical form of the SU(2) hot region.

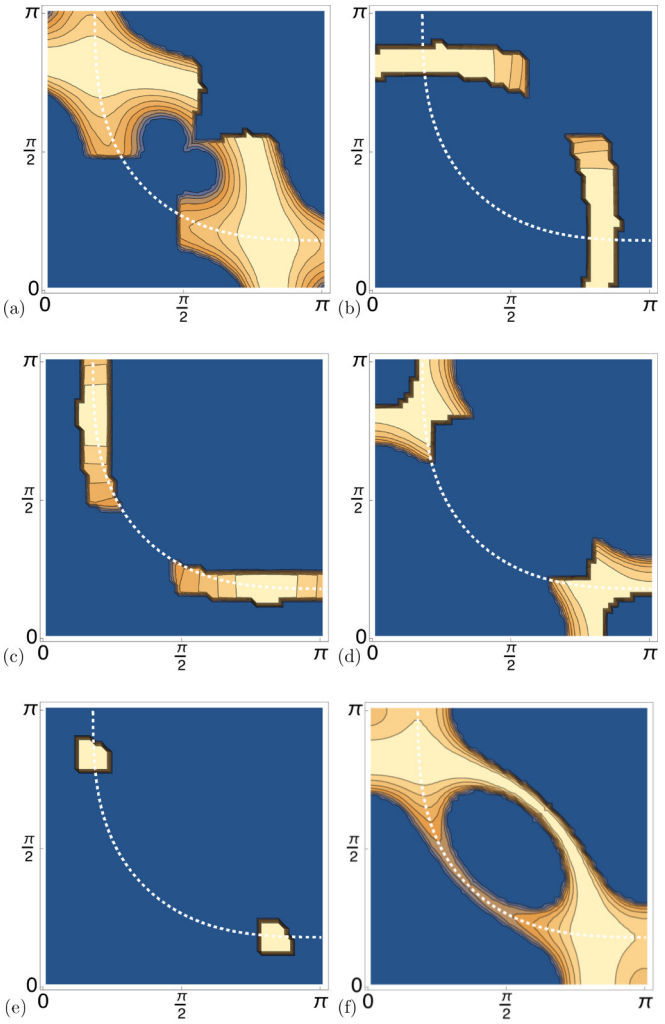

FIG. 22. Solution of the gap equations, in the case of a strong AF coupling, from Eqs. (19) and (21) for various modulation wave vectors with (a) the diagonal wave vector (Q_0, Q_0) linking two hot spots, (b) the axial wave vector $(Q_0,0)$, (c) $(0, Q_0)$, which are observed experimentally, (d) the AF wave vector (π,π), and (e) the null wave vector. The solution of the SC gap equation is given in (f). The calculations are made on the band structure of Bi2212 form Ref. [124] (see details in the text for the band parameters). Vanishing solutions are color-coded in blue while nonvanishing points are depicted in yellow. The calculations are made within the approximation $J_{\bar{\mathbf{q}}} = J\delta(\bar{\mathbf{q}})$, with $J = 0.9$, which restricts the q integration at the vector (π,π). The energy units, if not stated otherwise, are in eV.

APPENDIX D: NEMATICITY AND CHARGE CONSERVATION

1. Cancellation in the Fermi liquid case

We first consider the Fermi liquid case depicted in Figs. 27(a) and 27(b). There is a well-known cancellation between the two diagrams:

$$I_a + 2I_b = 0, \tag{D1}$$

which we reproduce here for completeness. We have

$$I_a = \sum_{k,q} F_q G_k G_{k+p} G_{k+q} G_{k+p+q}, \tag{D2}$$

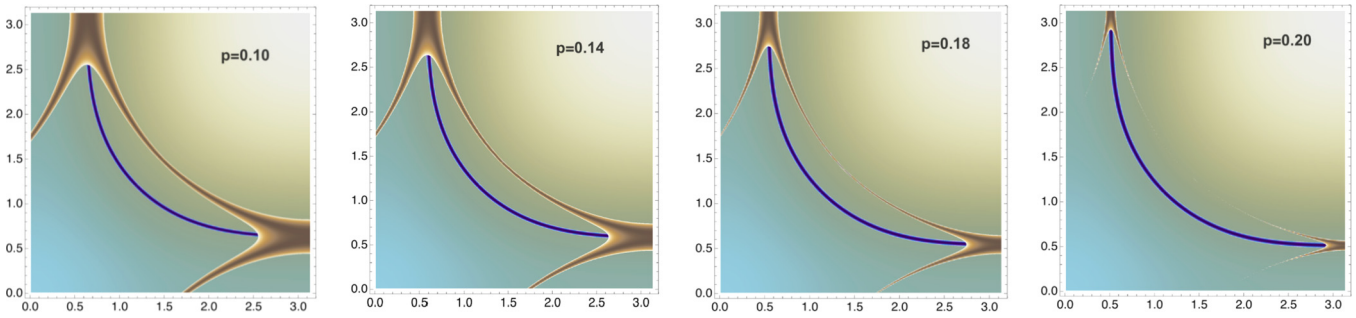

FIG. 23. Evolution of the SU(2) fluctuations as a function of the hole doping. We present two set of curves for the zone edge wave vector $2\mathbf{p}_F$. Note that in this case, the mass has a minimum lying at the ZE. The electron dispersion is modeled in the tight-binding approximation for Bi, Ref. [124] (parameter set tb2).

$$I_b = \sum_{k,q} F_q G_k^2 G_{k+p} G_{k+q}, \tag{D3}$$

where k,q stand for the 4-vector $\mathbf{k},\mathbf{q}$, F_q is the boson line, G_k is the fermionic Green's function, with $G_k^{-1} = i\varepsilon_n + \Sigma(\varepsilon_n) - \xi_{\mathbf{k}}$. We use the decoupling trick

$$G_k G_{k'} = \frac{G_k - G_{k'}}{G_{k'}^{-1} - G_k^{-1}}. \tag{D4}$$

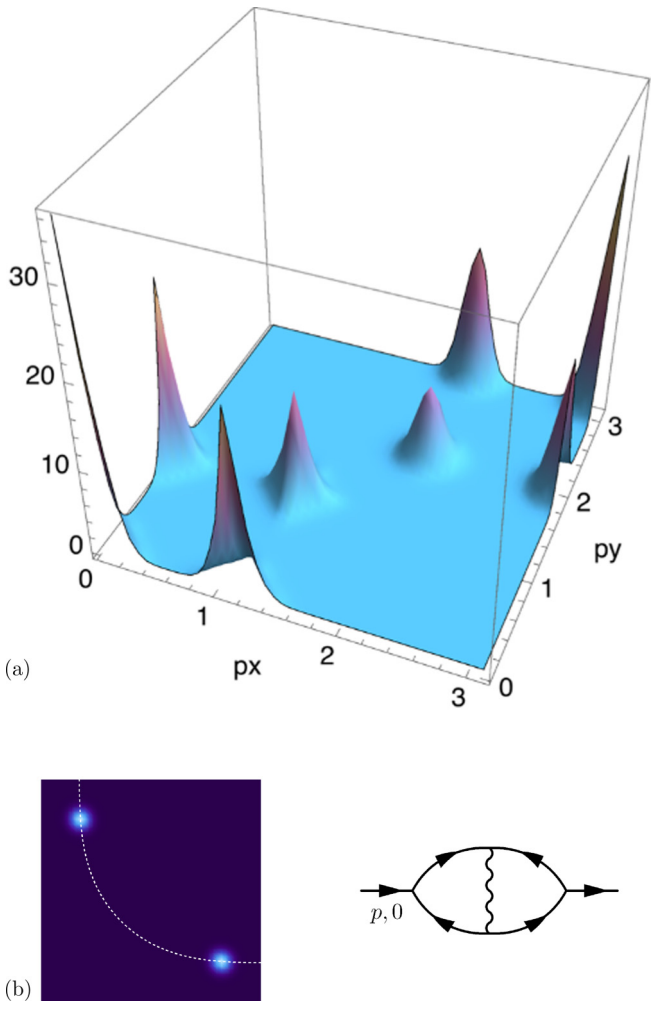

FIG. 24. The real part of the polarization bubble, with one vertex correction, in the static limit. The electron dispersion corresponds to the usual one of Bi2212, Ref. [124]. We show here that for a dispersion centered exclusively at the hot spots (c), the response on the axes $(0, Q_0)$ and $(Q_0, 0)$ has still a stronger amplitude than the response on the diagonal (Q_0, Q_0).

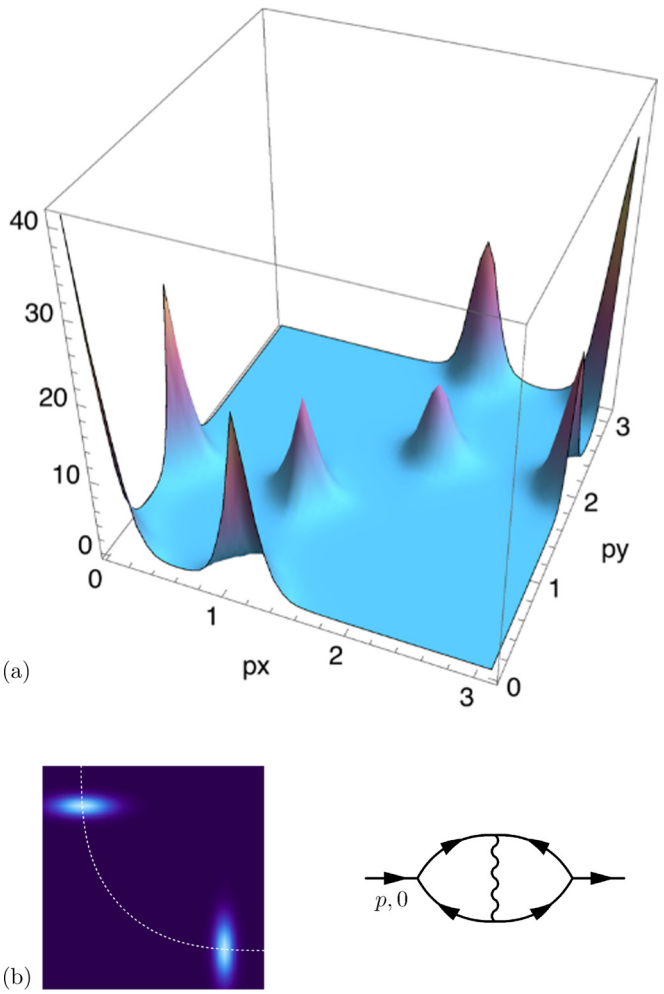

FIG. 25. Real part of the polarization bubble, with one vertex correction, in the static limit. The electron dispersion corresponds to the usual one of Bi2212, Ref. [124]. Same study as in Fig. 25, but for a "flat pancake" shape of the SU(2) fluctuations.

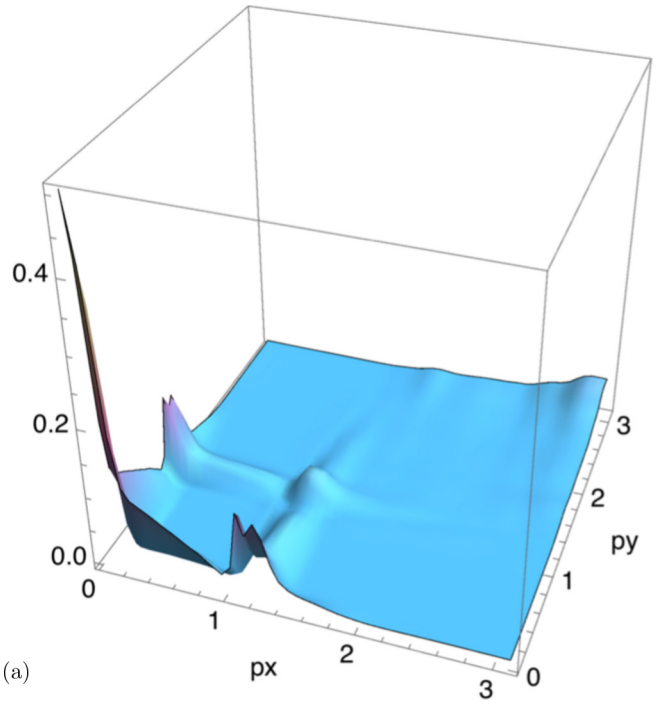

(a)

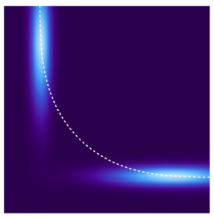

(b)

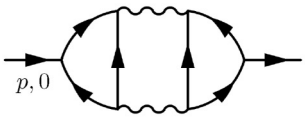

FIG. 26. Real part of the polarization bubble, corresponding to the Aslamozov-Larkin diagrams, in the static limit. The electron dispersion corresponds to the usual one of Bi2212, Ref. [124]. This contribution typically behaves in the same way as the polarization with vertex corrections.

Using Eq. (D4), we have

$$I_a = \sum_{k,q} F_q \left(\frac{G_k G_{k+p} - G_k G_{k+p+q}}{H_q^2} \times \frac{-G_{k+p} G_{k+q} + G_{k+q} G_{k+p+q}}{H_q^2} \right), \tag{D5}$$

$$I_b = \sum_{k,q} F_q \left[\frac{G_k^2 G_{k+q}}{H_q} - G_{k+p} \left(\frac{G_k - G_{k+q}}{H_q^2} \right) \right], \tag{D6}$$

(a)

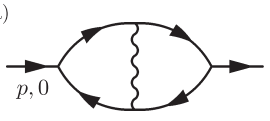

(b)

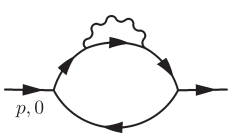

FIG. 27. The standard vertex self-energy cancellation due to charge conservation. The sum of the diagrams $a) + 2b) = 0$.

(a)

(b)

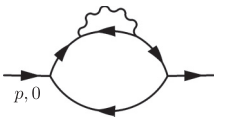

FIG. 28. Vertex corrections and self-energy corrections at the one loop level. We check in the text that there is no cancellation in the case of pairing lines $a) + 2b) \neq 0$.

where $H_q = G_{k+p}^{-1} - G_{k+p+q}^{-1} \simeq -i\omega + \Sigma(\varepsilon_n) - \Sigma(\varepsilon_n + \omega_n) + \mathbf{v}_F \cdot \mathbf{q}$. We observe that terms of the kind $\int_{\mathbf{k}} G_k^n G_{k+p} = 0$ for all integers $n > 1$ because, since the external momentum $p = (\mathbf{p},0)$ carries no frequency, the poles are in the same half-plane, which leads to (in the limit where $p \to 0$)

$$I_a = -2 \sum_q F_q \frac{G_k G_{k+q}}{H_q^2}, \tag{D7}$$

$$I_b = \sum_q F_q \frac{G_k G_{k+q}}{H_q^2}. \tag{D8}$$

This in turn gives the result of Eq. (D1).

2. Absence of cancellation in the case of SC lines

We now apply the same recipes to the diagrams of Fig. 28, and see that the cancelation does not hold in this case. We have

$$I_a = \sum_{k,q} F_q G_k G_{k+p} G_{-k-q} G_{-k-p-q}, \tag{D9}$$

$$I_b = \sum_{k,q} F_q G_k^2 G_{k+p} G_{-k-p}, \tag{D10}$$

with $G_{-k}^{-1} = -i\varepsilon_n + \Sigma(-\varepsilon_n) - \xi_{-\mathbf{k}}$. Using Eq. (D4), this can be cast into

$$I_a = \sum_{k,q} F_q \left(\frac{-G_k G_{k+p} + G_{-k-q} G_{k+p}}{\overline{H}_{k,q}} + \frac{G_k^2 G_{k+p}}{\overline{H}_{k,q}} \right), \tag{D11}$$

$$I_b = \sum_{k,q} F_q \left(\frac{G_k^2 + G_{-k-q}^2 - 2G_k^3}{\overline{H}_{k,q}} \right), \tag{D12}$$

with $\overline{H}_{k,q} = G_{-k-q}^{-1} - G_k^{-1} \simeq -2i\varepsilon_n - i\omega + \Sigma(-\varepsilon_n - \omega_n) - \Sigma(\varepsilon_n) + \mathbf{v}_F \cdot q + 2\xi_{\mathbf{k}}$. To check the noncancellation of diagrams, we can take the difference $dI = I_a + 2I_b$, which gives, in the limit where $p \to 0$,

$$dI = \sum_{k,q} F_q \left(\frac{G_{-k-q}^2 - G_k^2}{\overline{H}_{k,q}} + 2\frac{G_k^3}{\overline{H}_{k,q}} \right). \tag{D13}$$

The first term in Eq. (D13) vanish after a change of variables, and we end up with a nonzero contribution

$$dI = 2 \sum_{k,q} F_q \frac{G_k^2 G_{k+p}}{\overline{H}_{k,q}}. \tag{D14}$$

To fix the ideas, we plot dI in Eq. (D14) in Fig. 29.

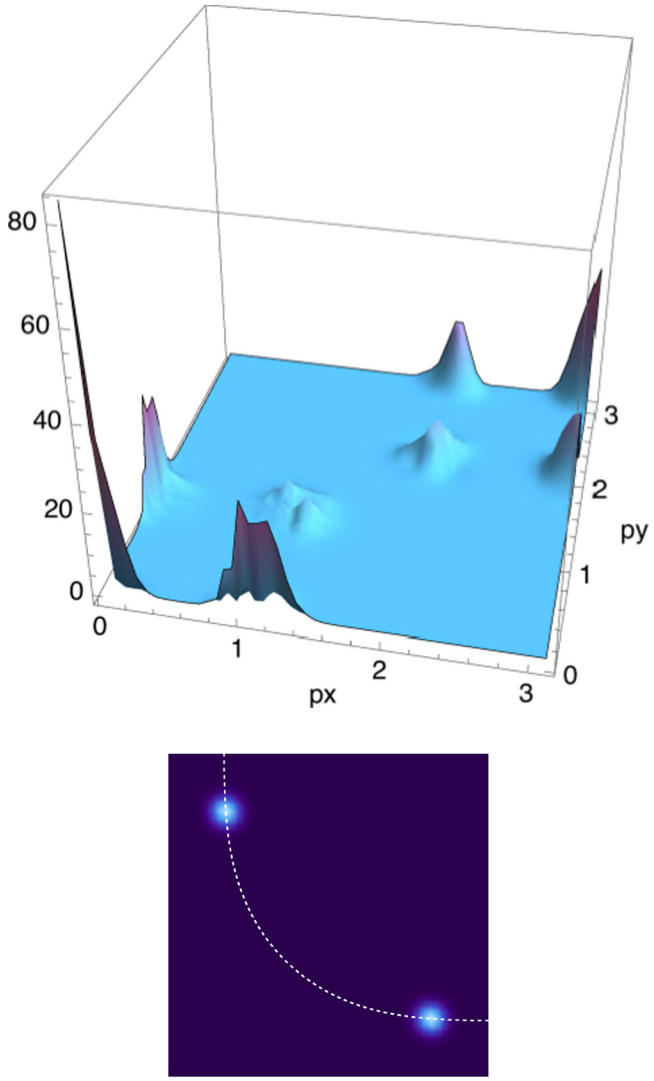

FIG. 29. Plot of dI in Eq. (D14). The electron dispersion corresponds to the usual one of Bi2212, Ref. [124].

APPENDIX E: GAUSSIAN FLUCTUATIONS

We study now the case where the charge order becomes critical for some region of oxygen doping, under the SC dome. Fluctuations of the charge mode are treated at the Gaussian level. The effective action S_1, Eq. (92), which describes the coupling of the fermion to the excitonic patches, can be written as

$$S_1 = \frac{1}{2}\sum_{\sigma,k,p} \chi_{k,k+p}\psi^\dagger_{k,\sigma}\psi_{k+p,\sigma}, \tag{E1}$$

where $p = P + q$ is the fluctuation around the ordering wave vector $\mathbf{P} = 2\mathbf{p}_F$ and $\chi_{k,k+p}$ is the bosonic charge mode with wave vector $\mathbf{P}$. This charge order is peculiar in the sense that χ depends not only on the slow fluctuations around the wave vector $\mathbf{P}$ but as well on the fast momentum $\mathbf{k}$. We account for this dependence through a form factor via the definition

$$\chi_{k,k+p} \equiv \chi_p F_k, \tag{E2}$$

where F_k is a form factor having a finite extension around the nesting point $\mathbf{k}_n$ associated with $\mathbf{P}$. The form of the boson propagator $\Phi_q = \langle \mathcal{T}\chi_{-p}\chi_p\rangle$ is given by

$$\exp[-S_\Phi] = \langle \exp[-S_1]\rangle_\psi = \exp\left[\tfrac{1}{2}\langle S_1^2\rangle_\psi\right]. \tag{E3}$$

Expanding then to the second order in χ we obtain

$$S_\Phi = -\frac{1}{2}\sum_{k,p,\sigma,k',p',\sigma'} \chi_p\chi_{p'}F_kF_{k'}\langle\psi^\dagger_{k,\sigma}\psi_{k+p,\sigma}\psi^\dagger_{k',\sigma'}\psi_{k'+p',\sigma'}\rangle_\psi. \tag{E4}$$

The contraction of indices leads to the conditions $\sigma' = \sigma$, $p' = -p$ and $k' = k + p$. From which we get

$$S_\Phi = \frac{1}{2}\sum_p \chi_{-p}\Phi_p^{-1}\chi_p \tag{E5}$$

$$\text{with} \quad \Phi_p^{-1} = \Phi_{0,p}^{-1} - \Pi_p,$$

$$\Pi_p = -T\sum_{\varepsilon,k,\sigma} F_kF_{k+p}G_kG_{k+p}. \tag{E6}$$

For the evaluation of the bosonic bubble Φ_p, the form factors have been neglected in the evaluation of Π_p. $\Phi_{0,p}^{-1} = \omega^2 + q^2 + m$ is a high-energy contribution of the Ornstein-Zernike type. The resulting scattering of the fermions around the bosonic charge mode writes

$$\exp[-S_{\rm crit}] = \langle \exp[-S_1]\rangle_\chi = \exp\left[\tfrac{1}{2}\langle S_1^2\rangle_\chi\right], \tag{E7}$$

with

$$S_{\rm crit} = -\frac{1}{2}\sum_{k,k',\sigma,\sigma',p,p'} \langle\chi_p\chi_{p'}\rangle_\chi F_kF_{k'}\psi^\dagger_{k,\sigma}\psi_{k+p,\sigma}\psi^\dagger_{k',\sigma'}\psi_{k'+p',\sigma'},$$

$$= -\frac{1}{2}\sum_{k,k',\sigma,\sigma',p} \Phi_pF_kF_{k'}\psi^\dagger_{k,\sigma}\psi_{k+p,\sigma}\psi^\dagger_{k',\sigma'}\psi_{k'-p,\sigma'}. \tag{E8}$$

APPENDIX F: BOSONIC POLARIZATION BUBBLE

The renormalized bosonic propagator follows from Dyson's equation

$$[\Phi_{\mathbf{q}}(\Omega)]^{-1} = q^2 + m - \Pi_{\mathbf{q}}(\Omega). \tag{F1}$$

Therefore we evaluate the bosonic polarization $\Pi_{\mathbf{q}}$ with $\mathbf{P} = 2\mathbf{p}_F$ as depicted in Fig. 4(c) of the main text. The diagram writes

$$\Pi_{\mathbf{q}}(i\omega_m) = -\frac{1}{\beta V}\sum_{\epsilon_n,\mathbf{k}} G(i\epsilon_n + i\omega_m/2,\mathbf{k}+\mathbf{q}/2) \times G(i\epsilon_n - i\omega_m/2,\mathbf{k}+\mathbf{P}-\mathbf{q}/2), \tag{F2}$$

with temperature $T = \beta^{-1}$ and V being the volume of the system. We will evaluate the diagram using bare Green functions of the form

$$G(i\epsilon_n,\mathbf{k})^{-1} = i\epsilon_n - \xi_{\mathbf{k}}, \tag{F3}$$

with $\xi_{\mathbf{k}} = \epsilon_{\mathbf{k}} - \mu$, where $\epsilon_{\mathbf{k}}$ is the fermion dispersion and μ their chemical potential. It is convenient to measure the three-dimensional momentum vector $\mathbf{k} \equiv (k_\parallel, \mathbf{k}_\perp)$ (where $k_\parallel$ is a scalar and $\mathbf{k}_\perp$ is a two-dimensional vector) relative to a point on the Fermi surface. The coordinate system is then chosen such that the two components of $\mathbf{k}_\perp$ are oriented perpendicular to the surface normal vector and the $k_\parallel$ component parallel to it, as depicted in Fig. 4(b) of the main text. The dispersion is then approximated by

$$\xi_{\mathbf{k}} = v_\parallel k_\parallel + v_\perp k_\perp^2/2 \tag{F4}$$

and from the construction follows $\xi_{\mathbf{k}+\mathbf{P}} = \xi_{-\mathbf{k}}$. The momentum transfer $\mathbf{q}$ between the two coupled electrons is quasi-one-dimensional in parallel direction only, so that we calculate $\Pi_{\mathbf{q}}$ for $\mathbf{q} \equiv (q_\parallel, 0)$. Equation (F2) then yields

$$\Pi_{\mathbf{q}}(i\omega_m) = -\frac{1}{\beta V}\sum_{\epsilon_n,\mathbf{k}} \frac{1}{i(\epsilon_n + \omega_m/2) - v_\parallel(k_\parallel + q_\parallel/2) - v_\perp k_\perp^2/2} \times \frac{1}{i(\epsilon_n - \omega_m/2) + v_\parallel(k_\parallel - q_\parallel/2) - v_\perp k_\perp^2/2}, \tag{F5}$$

Evaluating the Matsubara sum at $T = 0$ gives

$$\Pi_{\mathbf{q}}(i\omega_m) = -\frac{1}{v_\parallel v_\perp V} \times \sum_{\mathbf{k}} \frac{\theta(2k_\parallel + q_\parallel + k_\perp^2) - \theta(-2k_\parallel + q_\parallel + k_\perp^2)}{i\omega_m - 2k_\parallel}, \tag{F6}$$

where $\theta(x)$ denotes the Heaviside step function and we have also rescaled the parallel momenta to measure it in units of $v_\parallel$ as well as the perpendicular momenta by $\sqrt{v_\perp}$. We can now perform the analytic continuation to real frequencies Ω by setting $i\omega_m = \Omega + i\delta$ and we write the retarded self-energy as $\Pi_{\mathbf{q}}(\Omega) \equiv \Pi_{\mathbf{q}}(\Omega + i\delta)$ for convenience. In the infinite volume limit and for $\Omega \neq |q_\parallel|$, the polarization yields

$$\Pi_{\mathbf{q}}(\Omega) = -\frac{c}{\pi}\int d\mathbf{k}_\perp \Big[P\int_{-k_\perp^2}^{\Lambda} \frac{dy}{\Omega + q_\parallel - y} - P\int_{-\Lambda}^{k_\perp^2} \frac{dy}{\Omega - q_\parallel - y} - i\pi(\theta(k_\perp^2 + \Omega + q_\parallel) - \theta(k_\perp^2 - \Omega + q_\parallel))\Big], \tag{F7}$$

with $c^{-1} = (4\pi)^2 v_\parallel v_\perp$, P stands for the Cauchy principal value and Λ is an UV cutoff. The special cases for $\Omega = |q_\parallel|$ is not explicated here but can be obtained in the same fashion. After integrating over the parallel component, we get

$$\Pi_{\mathbf{q}}(\Omega) = -\frac{c}{\pi}\int d\mathbf{k}_\perp [\ln|k_\perp^2 + \Omega + q_\parallel| + \ln|k_\perp^2 - \Omega + q_\parallel| - i\pi(\theta(k_\perp^2 + \Omega + q_\parallel) - \theta(k_\perp^2 - \Omega + q_\parallel))], \tag{F8}$$

where some nonuniversal contributions that depend solely on Λ were dropped. The remaining two-dimensional integral over $\mathbf{k}_\perp$ is now easily computed in polar coordinates. Regularizing again the UV sector by a cutoff Λ, we find (up to some pure cutoff contributions)

$$\Pi_{\mathbf{q}}(\Omega) = \Pi'_{\mathbf{q}}(\Omega) + i\Pi''_{\mathbf{q}}(\Omega), \tag{F9a}$$

$$\Pi'_{\mathbf{q}}(\Omega) = c[(\Omega + q_\parallel)\ln|\Omega + q_\parallel| - (\Omega - q_\parallel)\ln|\Omega - q_\parallel|], \tag{F9b}$$

$$\Pi''_{\mathbf{q}}(\Omega) = \pi c[(\Omega + q_\parallel)\theta(-\Omega - q_\parallel) + (\Omega - q_\parallel)\theta(\Omega - q_\parallel)], \tag{F9c}$$

where Π' and Π'' denote the real, respectively, imaginary part of the polarization. In a last step, we invert Dysons equation (F1) to obtain the imaginary part of $\Phi_{\mathbf{q}}$, which is responsible for damping. Because the leading scattering contribution to the resistivity comes from the low momentum and frequency transfer of the critical bosonic mode, one can drop the entire $\Phi_{0,\mathbf{q}}^{-1}(\Omega)$ term compared to $\Pi_{\mathbf{q}}$. One obtains

$$\mathrm{Im}\Phi_{\mathbf{q}}(\Omega) \simeq \frac{\Pi''_{\mathbf{q}}(\Omega)}{(\Pi'_{\mathbf{q}}(\Omega))^2 + (\Pi''_{\mathbf{q}}(\Omega))^2} \tag{F10}$$

and we can write $\mathrm{Im}\Phi_{\mathbf{q}}$ in compact form as

$$\mathrm{Im}\Phi_{\mathbf{q}}(\Omega) = \frac{1}{\pi c} b_{\mathbf{q}}(\Omega) \tag{F11}$$

with

$$b_{\mathbf{q}}(\Omega) = \frac{s\theta(-s) + t\theta(t)}{\pi^{-2}[s\ln|s| - t\ln|t|]^2 + [s\theta(-s) + t\theta(t)]^2} \tag{F12}$$

where $s = \Omega + q_\parallel$ and $t = \Omega - q_\parallel$.

The study of this paper corresponds to the regime $q_\parallel \ll \Omega$. Reporting this approximation in Eqs. (F9), we get

$$\Pi'_{\mathbf{q}}(\Omega) \simeq 2cq_\parallel \ln|\Omega|, \tag{F13a}$$

$$\Pi''_{\mathbf{q}}(\Omega) = \pi c\Omega. \tag{F13b}$$

APPENDIX G: FERMIONIC SELF-ENERGY

The fermionic self-energy is

$$\Sigma_{\mathbf{k}}(i\epsilon_n) = -\frac{1}{\beta V}\sum_{\omega_m,\mathbf{q}} \Phi_{\mathbf{q}}(i\omega_m) G(i\epsilon_n + i\omega_m, \mathbf{k} + \mathbf{q}), \tag{G1}$$

with the fermionic and bosonic Green functions

$$(G(i\epsilon_n, \mathbf{k}))^{-1} = i\epsilon_n - v_\parallel k_\parallel - v_\perp k_\perp^2/2, \tag{G2a}$$

$$\Phi_{\mathbf{q}}^{-1}(i\omega_m) = \gamma|\omega|_m - v_\parallel q_\parallel \ln|\overline{\omega}_m| + v_\perp q_\perp^2/2, \tag{G2b}$$

where the form of the bosonic Green's function is taken from Eqs. (F13a) and (F13b).

The notation $\overline{\omega}_n = \omega_n/\Lambda$ where Λ is an UV cutoff. To simplify the calculation, we will not calculate the full above self-energy, but the truncated one:

$$\Delta\Sigma(i\epsilon_n) = \Sigma_{\mathbf{k}=0}(i\epsilon_n) - \Sigma_{\mathbf{k}=0}(0). \tag{G3}$$

With the above formulas, the truncated self-energy is written as

$$\Delta\Sigma(i\epsilon_n) = -\frac{1}{\beta V}\sum_{\omega_m,\mathbf{q}} \frac{1}{\gamma\omega_m^2 - v_\parallel q_\parallel + v_\perp q_\perp^2/2} \times \left(\frac{1}{i\epsilon_n + i\omega_m - v_\parallel q_\parallel - v_\perp q_\perp^2/2} - \frac{1}{i\omega_m - v_\parallel q_\parallel - v_\perp q_\perp^2/2}\right), \tag{G4}$$

and the sums are evaluated in infinite volume and vanishing temperature limit. Rescaling the variables according to $v_\parallel q_\parallel = x$ and $v_\perp q_\perp^2/2 = y$, the self-energy follows as

$$\Delta\Sigma(i\epsilon_n) = c_2 T \sum_{\omega_n} I_\omega, \tag{G5}$$

with

$$I_\omega = \int_{-\infty}^{\infty} dx \int_0^\infty dy \frac{1}{\gamma|\omega_n| - x\ln\overline{\omega}_n + y} \times \frac{i\epsilon_n}{(i\epsilon_n + i\omega_n - x - y)(i\omega_n - x - y)} \tag{G6}$$

and $c_2^{-1} = 4\pi^2 v_\parallel v_\perp$. We first perform the integration in x, performed in the complex plane. Two types of poles are present, the cones coming from the fermionic Green's functions on the right, and the ones coming from the boson propagator.

1. Poles from the Fermionic Green's function

The contribution of the poles from the fermionic Green's function are taken at $x_0 = i\omega_n - y$ and give a contribution

$$I_1 = \int_0^\infty dy \frac{2i\pi\,\mathrm{Sgn}(\epsilon_n)\theta[|\epsilon_n| - |\omega_n|]}{\gamma|\omega_n| + y - x_0\ln\overline{\omega}_n}. \tag{G7}$$

We keep the term proportional to $\ln\overline{\omega}_n$ in the denominator and get

$$I_1 = \int_0^\infty dy \frac{2i\pi\,\mathrm{Sgn}(\epsilon_n)\theta[|\epsilon_n| - |\omega_n|]}{(-i\omega_n + y)\ln\overline{\omega}_n} = \frac{2i\pi\,\mathrm{Sgn}(\epsilon_n)\theta[|\epsilon_n| - |\omega_n|]}{\ln\overline{\omega}_n}\ln\left(\frac{\Lambda}{-i\omega_n}\right). \tag{G8}$$

Reporting in (G5) and symmetrizing with respect to ω_n leads to

$$\Delta\Sigma(i\epsilon_n) = c_2 T \sum_{\omega_n>0} i\pi\,\mathrm{Sgn}(\epsilon_n)\theta[|\epsilon_n| - |\omega_n|], = c_2 i\pi\epsilon_n. \tag{G9}$$

Note that the logarithmic singularity has been lost here, up to the UV cutoff. This self-energy will not produce a significant shortening of the electron lifetime.

2. Poles from the boson propagator

The contribution from the boson propagator is taken at $x_0 = (\gamma|\omega_n| + y)/\ln|\omega_n|$ and is written as

$$I_2 = \int_0^\Lambda dy \frac{-i\pi}{\ln|\omega_n|}\frac{i\epsilon_n}{(i\epsilon_n + i\omega_n - x_0 - y)(i\omega_n - x_0 - y)}. \tag{G10}$$

Taking only the term not proportional to $1/\ln|\omega_n|$, we get

$$I_2 = \int_0^\Lambda dy \frac{-i\pi}{\ln|\omega_n|}\frac{i\epsilon_n}{(i\epsilon_n + i\omega_n - y)(i\omega_n - y)}. \tag{G11}$$

The integration over y is done exactly and leads to

$$I_2 = \frac{-i\pi}{\ln|\omega_n|}\ln\left|\frac{\overline{\omega}_n}{\overline{\epsilon}_n + \overline{\omega}_n}\right|. \tag{G12}$$

The form (G12) is nonvanishing only in the limit $|\omega_n| \leqslant |\epsilon_n|$. Expanding in this limit, we get

$$I_2 = \frac{i\pi}{\ln|\omega_n|}\ln|\overline{\epsilon}_n|, \tag{G13}$$

and reporting in Eq. (G5), we obtain

$$\Delta\Sigma(i\epsilon_n) = c_2 T \sum_{|\omega_n|\leqslant|\epsilon_n|} i\pi\frac{\ln|\overline{\epsilon}_n|}{\ln|\omega_n|}, = c_2 i\pi li(\overline{\epsilon_n})\ln|\overline{\epsilon_n}|, \tag{G14}$$

where the function logarithmic integral $li(x)$ is defined by

$$li(x) = \int_0^x \frac{dt}{\ln t}.$$

Expanding by part and considering the regime where $x \ll 1$, we get

$$li(x) = \frac{x}{\ln x} + \frac{x}{(\ln x)^2} + \mathcal{O}\left[\frac{x}{(\ln x)^3}\right]. \tag{G15}$$

The second term in Eq. (G15) provides the desired singularity, and we obtain

$$\Delta\Sigma(i\epsilon_n) \simeq c_2\frac{i\pi\epsilon_n}{\ln|\epsilon_n|}, \tag{G16}$$

which, up to a logarithm, is the form for the electron self-energy in the strange metal phase.

APPENDIX H: BOLTZMANN TREATMENT

1. Relaxation time from the Boltzmann equation

The Boltzmann equation for the nonequilibrium electron distribution $f_\mathbf{k}$ is written as [166,167,177]

$$\left(\frac{\partial f_\mathbf{k}}{\partial t}\right)_{\text{collisions}} = -e\mathbf{E}\cdot\nabla_\mathbf{k} f_\mathbf{k} = -I_{ei}[f_\mathbf{k}] - I_{ee}[f_\mathbf{k}], \tag{H1}$$

where e is the elementary charge, $\mathbf{E}$ a static electric field which is supposed to be small and I_{ei}, respectively, I_{ee} are the electron-impurity, respectively, electron-electron collision integrals. We make the approximation to consider only electron-electron scattering such that $I_{ei} = 0$. The equilibrium distribution of noninteracting fermions at temperature T is

$f_{0,\mathbf{k}} = (\exp(\beta\xi_{\mathbf{k}}) + 1)^{-1}$. The distributions are normalized such that

$$\int \frac{d\mathbf{k}}{(2\pi)^3} f_{\mathbf{k}} = \int \frac{d\mathbf{k}}{(2\pi)^3} f_{0,\mathbf{k}} = 2n_0, \tag{H2}$$

for $T \to 0$ and with $n_0 = k_F^3/(3\pi^2)$. For small electric field $\mathbf{E}$, one can develop $f_{\mathbf{k}}$ around the equilibrium distribution $f_{0,\mathbf{k}}$ and the so-called relaxation-time approximation amounts to express the collision integral by $I_{ee}[f_{\mathbf{k}}] = (f_{\mathbf{k}} - f_{0,\mathbf{k}})/\tau$, where τ is the relaxation time. Plugging this ansatz in the kinetic equation (H1), we find

$$\begin{aligned} f_{\mathbf{k}} &\simeq f_{0,\mathbf{k}} + \tau e\mathbf{E}\cdot\nabla_{\mathbf{k}} f_{\mathbf{k}} \simeq f_{0,\mathbf{k}} + \tau e\mathbf{E}\cdot\mathbf{v}_{\mathbf{k}}\frac{\partial f_{0,\mathbf{k}}}{\partial\epsilon_{\mathbf{k}}} \\ &= f_{0,\mathbf{k}} - g_{\mathbf{k}} f_{0,\mathbf{k}}(1 - f_{0,\mathbf{k}}), \end{aligned} \tag{H3}$$

with $g_{\mathbf{k}} = \beta\tau e\mathbf{E}\cdot\mathbf{v}_{\mathbf{k}}$. Note that the standard approximations, to replaced $f_{\mathbf{k}}$ on the right-hand-side again by $f_{0,\mathbf{k}}$, neglecting the momentum dependence of τ and the dispersion relation for free fermions $\epsilon_{\mathbf{k}} = k^2/(2m)$ now solve the Boltzmann equation (H1) within relaxation-time approximation and for small electric field.

The electron-electron collision integral is evaluated using Fermi's golden rule which yields

$$\begin{aligned} I_{ee}[f_{\mathbf{k}}] = \frac{1}{V}\sum_{\mathbf{q}}\int_{-\infty}^{\infty} d\Omega\, \mathrm{Im}\Phi_{\mathbf{q}}(\Omega)\delta(\epsilon_{\mathbf{k}} - \epsilon_{\mathbf{k}+\mathbf{P}-\mathbf{q}} - \Omega) \\ \times [f_{\mathbf{k}}\big(1 - f_{\mathbf{k}+\mathbf{P}-\mathbf{q}}\big)(1 + n_{\mathrm{B}}(\Omega)) \\ - (1 - f_{\mathbf{k}}) f_{\mathbf{k}+\mathbf{P}-\mathbf{q}} n_{\mathrm{B}}(\Omega)]. \end{aligned} \tag{H4}$$

Here, $n_{\mathrm{B}}(\Omega) = (\exp(\beta\Omega) - 1)^{-1}$ is the Bose function. Using the fact that $\mathrm{Im}\Phi_{\mathbf{q}}(-\Omega) = -\mathrm{Im}\Phi_{\mathbf{q}}(\Omega)$, we can rewrite the above integral as

$$\begin{aligned} I_{ee}[f_{\mathbf{k}}] = \frac{1}{V}\sum_{\mathbf{q}}\int_{-\infty}^{\infty} d\Omega\, \mathrm{Im}\Phi_{\mathbf{q}}(\Omega) n_{\mathrm{B}}(\Omega) \\ \times [f_{\mathbf{k}}(1 - f_{\mathbf{k}+\mathbf{P}-\mathbf{q}})\delta(\epsilon_{\mathbf{k}+\mathbf{P}-\mathbf{q}} - \epsilon_{\mathbf{k}} - \Omega) \\ - f_{\mathbf{k}+\mathbf{P}-\mathbf{q}}(1 - f_{\mathbf{k}})\delta(\epsilon_{\mathbf{k}} - \epsilon_{\mathbf{k}+\mathbf{P}-\mathbf{q}} - \Omega)]. \end{aligned} \tag{H5}$$

From Eq. (H3) and since by definition $I_{ee}[f_{0,\mathbf{k}}] = 0$ for the equilibrium distribution $f_{0,\mathbf{k}}$, we can rewrite the collision integral as

$$\begin{aligned} I_{ee}[f_{\mathbf{k}}] = \frac{1}{V}\sum_{\mathbf{q}}\int_{-\infty}^{\infty} d\Omega\, \mathrm{Im}\Phi_{\mathbf{q}}(\Omega) n_{\mathrm{B}}(\Omega) \\ \times f_{0,\mathbf{k}+\mathbf{P}-\mathbf{q}}(1 - f_{0,\mathbf{k}})(g_{\mathbf{k}+\mathbf{P}-\mathbf{q}} - g_{\mathbf{k}}) \\ \times \delta(\epsilon_{\mathbf{k}} - \epsilon_{\mathbf{k}+\mathbf{P}-\mathbf{q}} - \Omega), \end{aligned} \tag{H6}$$

where contributions $\sim E^2$ have been dropped. We see from Eq. (H6) that this theory has a nonvanishing imbalance velocity factor, since for $\mathbf{q} = 0$, $(g_{\mathbf{k}+\mathbf{P}} - g_{\mathbf{k}}) \neq 0$. The nonvanishing velocity imbalance factor provides that no additional T dependence arises from the angular part of the integral.

Setting $\mathbf{v}_{\mathbf{k}} = -\mathbf{v}_{\mathbf{k}+\mathbf{P}} \simeq \mathbf{k}_{\mathrm{F}}/m \equiv \mathbf{v}_{\mathrm{F}}$ such that the relaxation time approximation simplifies to

$$g_{\mathbf{k}} \simeq \beta\tau e\mathbf{E}\cdot\mathbf{v}_{\mathrm{F}}, \tag{H7a}$$

$$g_{\mathbf{k}'-\mathbf{q}} \simeq -\beta\tau e\mathbf{E}\cdot\mathbf{v}_{\mathrm{F}}, \tag{H7b}$$

we further multiply the collision integral with $\mathbf{v}_{\mathbf{k}}\cdot\mathbf{e}$ where $\mathbf{e}$ is a unit vector in the direction of $\mathbf{E}$ and sum over $\mathbf{k}$. We find

$$\frac{1}{V}\sum_{\mathbf{k}}(\mathbf{v}_{\mathbf{k}}\cdot\mathbf{e}) I_{ee}[f_{\mathbf{k}}] = -2\beta\tau e\mathbf{v}_{\mathrm{F}}\cdot\mathbf{E}\,\tilde{I} \tag{H8}$$

and

$$\begin{aligned} \tilde{I} = \frac{1}{V^2}\sum_{\mathbf{k},\mathbf{q}}(\mathbf{v}_{\mathbf{k}}\cdot\mathbf{e})\int_{-\infty}^{\infty} d\Omega\, \mathrm{Im}\Phi_{\mathbf{q}}(\Omega) n_{\mathrm{B}}(\Omega) \\ \times [f_{0,\mathbf{k}+\mathbf{P}-\mathbf{q}/2}(1 - f_{0,\mathbf{k}+\mathbf{q}/2}) \\ \times \delta(\epsilon_{\mathbf{k}+\mathbf{q}/2} - \epsilon_{\mathbf{k}+\mathbf{P}-\mathbf{q}/2} - \Omega)]. \end{aligned} \tag{H9}$$

If we approximate $\mathbf{v}_{\mathbf{k}} \approx v_F$, such that $\tilde{I} = v_{\mathrm{F}} I$ with

$$\begin{aligned} I = \frac{1}{V^2}\sum_{\mathbf{k},\mathbf{q}}\int_{-\infty}^{\infty} d\Omega\, \mathrm{Im}\Phi_{\mathbf{q}}(\Omega) n_{\mathrm{B}}(\Omega) \\ \times [f_{0,\mathbf{k}+\mathbf{P}-\mathbf{q}/2}(1 - f_{0,\mathbf{k}+\mathbf{q}/2})\delta(\epsilon_{\mathbf{k}+\mathbf{q}/2} - \epsilon_{\mathbf{k}+\mathbf{P}-\mathbf{q}/2} - \Omega)]. \end{aligned} \tag{H10}$$

For convenience, the electric field was oriented in the direction of $\mathbf{k}_{\mathrm{F}}$ and we have symmetrize the last expression in $\mathbf{q}$.

The left-hand side of the Boltzmann equation (H1) yields

$$-e\mathbf{E}\cdot\nabla_{\mathbf{k}} f_{\mathbf{k}} = -e\mathbf{E}\cdot\mathbf{v}_{\mathbf{k}}\frac{\partial f_{0,\mathbf{k}}}{\partial\epsilon_{\mathbf{k}}}, \tag{H11}$$

where again the relaxation-time approximation Eq. (H3) was used and we developed for small electric field $\mathbf{E}$. From the definition of the equilibrium distribution f_0, we find for zero temperature

$$\frac{\partial f_{0,\mathbf{k}}}{\partial\epsilon_{\mathbf{k}}} = -\delta(\xi_{\mathbf{k}}). \tag{H12}$$

Moreover, let us define the density of states for free fermions, which yields in $d = 3$ and for vanishing temperature

$$\nu(\epsilon) = \frac{1}{V}\sum_{\mathbf{k}}\delta(\epsilon - \epsilon_{\mathbf{k}}) = \frac{m}{2\pi^2}(2m\epsilon)^{1/2}. \tag{H13}$$

We then have

$$\begin{aligned} \frac{1}{V}\sum_{\mathbf{k}}\frac{\partial f_{0,\mathbf{k}}}{\partial\xi_{\mathbf{k}}} &= -\frac{1}{V}\sum_{\mathbf{k}}\delta(\epsilon_{\mathbf{k}} - \epsilon_{\mathrm{F}}) \\ &= -\frac{1}{V}\sum_{\mathbf{k}}\delta(\epsilon_{\mathbf{k}} - \epsilon_{\mathrm{F}})\int_{-\infty}^{\infty} d\epsilon\,\delta(\epsilon - \epsilon_{\mathbf{k}}) \\ &= -\int_{-\infty}^{\infty} d\epsilon\,\delta(\epsilon - \epsilon_{\mathrm{F}})\nu(\epsilon) = -\rho_0, \end{aligned} \tag{H14}$$

with $\rho_0 = \nu(\epsilon_{\mathrm{F}}) = v_{\mathrm{F}}/(2\pi^2)$ and with $\epsilon_{\mathrm{F}} = k_{\mathrm{F}}^2/(2m)$.

It is again advantageous to multiply Eq. (H11) by $\mathbf{v}_{\mathbf{k}}$ and to sum over $\mathbf{k}$. With the identity $\sum_{\mathbf{k}}(\mathbf{E}\cdot\mathbf{v}_{\mathbf{k}})\mathbf{v}_{\mathbf{k}} = \mathbf{E}/3\sum_{\mathbf{k}} v_{\mathbf{k}}^2$ and

the help of Eqs. (H12) and (H14), we find

$$\frac{1}{V}\sum_{\mathbf{k}} \mathbf{v}_{\mathbf{k}}(\mathbf{E}\cdot\mathbf{v}_{\mathbf{k}})\frac{\partial f_{0,\mathbf{k}}}{\partial \epsilon_{\mathbf{k}}} = -\frac{\rho_0 v_{\mathrm{F}}^2 \mathbf{E}}{3}. \tag{H15}$$

Multiplying above equation by $\mathbf{E}$ and together with Eq. (H8), we can solve the Boltzmann equation for the relaxation time

$$\tau^{-1} = 6\beta I/\rho_0. \tag{H16}$$

2. Connection between resistivity and relaxation time

The electrical current density is [177]

$$\mathbf{J} = -2e\langle \mathbf{v}\rangle = -2e\frac{1}{V}\sum_{\mathbf{k}} f_{\mathbf{k}}\mathbf{v}_{k}, \tag{H17}$$

where the factor 2 accounts for the spin. Inserting Eqs. (H3) in Eq. (H17), the average with the equilibrium distribution $f_{0,\mathbf{k}}$ vanishes and with Eqs. (H12) and (H15), one finds

$$\mathbf{J} = -\frac{2\tau e^2}{V}\sum_{\mathbf{k}} \mathbf{v}_{\mathbf{k}}(\mathbf{E}\cdot\mathbf{v}_{\mathbf{k}})\frac{\partial f_{0,\mathbf{k}}}{\partial \epsilon_{\mathbf{k}}} = \frac{2\tau\rho_0 e^2 v_{\mathrm{F}}^2 \mathbf{E}}{3}. \tag{H18}$$

The conductivity σ is defined as $\mathbf{J} = \sigma\mathbf{E}$, such that the resistivity $\rho = \sigma^{-1}$ follows from the above equation as

$$\rho = 3/\left(2\rho_0 e^2 v_{\mathrm{F}}^2 \tau\right). \tag{H19}$$

Combining Eqs. (H16) and (H19), the resistivity is

$$\rho = \left(\frac{3}{e\rho_0 v_{\mathrm{F}}}\right)^2 \beta I. \tag{H20}$$

The last step is to calculate the integral in Eq. (H10) with $\mathrm{Im}F_{\mathbf{q}}$ that we derived previously in Appendix F.

3. Evaluation of the collision integral

To evaluate the integral I in Eq. (H10), we obtain from the dispersion relation, Eq. (F4),

$$\xi_{\mathbf{k}+\mathbf{q}/2} = v_{\parallel}(k_{\parallel} + q_{\parallel}/2) + v_{\perp}k_{\perp}^2/2, \tag{H21a}$$

$$\xi_{\mathbf{k}+\mathbf{P}-\mathbf{q}/2} = -v_{\parallel}(k_{\parallel} - q_{\parallel}/2) + v_{\perp}k_{\perp}^2/2, \tag{H21b}$$

such that

$$I = \frac{1}{V^2}\sum_{\mathbf{k},\mathbf{q}}\int_{-\infty}^{\infty} d\Omega\, \mathrm{Im}\Phi_{\mathbf{q}}(\Omega) n_{\mathrm{B}}(\Omega) \times [f_{0,\mathbf{k}+\mathbf{P}-\mathbf{q}/2}(1 - f_{0,\mathbf{k}+\mathbf{q}/2})\delta(2v_{\parallel}k_{\parallel} - \Omega)]. \tag{H22}$$

Now the integration over Ω is trivially performed and we take the infinite volume limit $V \to \infty$. This amounts to replace

$$\frac{1}{V}\sum_{\mathbf{k}} \to \int \frac{d\mathbf{k}}{(2\pi)^3} \equiv \frac{1}{(2\pi)^3}\int_{-\infty}^{\infty} dk_{\parallel}\int d\mathbf{k}_{\perp}, \tag{H23a}$$

$$\frac{1}{V}\sum_{\mathbf{q}} \to \frac{1}{2\pi}\int_{-\infty}^{\infty} dq_{\parallel}, \tag{H23b}$$

which yields

$$I = \frac{1}{(2\pi)^4}\int_{-\infty}^{\infty} dk_{\parallel}\int d\mathbf{k}_{\perp}\int_{-\infty}^{\infty} dq_{\parallel}\, \mathrm{Im}\Phi_{\mathbf{q}}(2v_{\parallel}k_{\parallel}) \times n_{\mathrm{B}}(2v_{\parallel}k_{\parallel})[f_{0,\mathbf{k}+\mathbf{P}-\mathbf{q}/2}(1 - f_{0,\mathbf{k}+\mathbf{q}/2})]. \tag{H24}$$

For small temperatures, we further approximate

$$f_{0,\mathbf{k}} \to \theta(-\xi_{\mathbf{k}}) = 1 - \theta(\xi_{\mathbf{k}}), \tag{H25}$$

and we rescale the variables as

$$2v_{\parallel}k_{\parallel} = x, \quad v_{\perp}k_{\perp}^2 = y, \quad v_{\parallel}q_{\parallel} = q, \tag{H26}$$

in order to obtain

$$I = c_1\int_{-\infty}^{\infty} dx\int_{0}^{\infty} dy\int_{-\infty}^{\infty} dq\, \mathrm{Im}\Phi_q(x) n_{\mathrm{B}}(x) \times \theta(x + y + q)\theta(x - y - q), \tag{H27}$$

with $c_1 = (4(2\pi)^3 v_{\parallel}^2 v_{\perp})^{-1}$. The integral over y yields

$$\int_0^{\infty} dy\theta(x + y + q)\theta(x - y - q) = (x - q)\theta(x + q)\theta(x - q) + 2x\theta(x)\theta(x - q)\theta(-x - q). \tag{H28}$$

Substituting this integral in the above equation (H27) gives $I = I_1 + I_2$, with

$$I_1 = c_1\int_0^{\infty} dx\int_{-x}^{x} dq\,(x - q)\,\mathrm{Im}\Phi_q(x) n_{\mathrm{B}}(x) \tag{H29}$$

and

$$I_2 = c_1\int_0^{\infty} dx\int_{-\infty}^{-x} dq\, 2x\,\mathrm{Im}\Phi_q(x) n_{\mathrm{B}}(x). \tag{H30}$$

To extract the temperature scaling from I, we first rescaling the variables as $\beta x = \tilde{x}$ and $\beta q = \tilde{q}$. With Eq. (F11) the integrals in Eqs. (H29) and (H30) can be written as $I_{1/2} = (2\pi^2 v_{\parallel}\beta^2)^{-1}\tilde{I}_{1/2}$, where

$$\tilde{I}_1 = \int_0^{\infty} d\tilde{x}\int_{-\tilde{x}}^{\tilde{x}} d\tilde{q}\,\frac{1}{e^{\tilde{x}} - 1} \times \frac{\tilde{t}^2}{\pi^{-2}[\tilde{s}\ln\tilde{s} - \tilde{t}\ln\tilde{t} + 2\tilde{q}\ln T]^2 + \tilde{t}^2} \tag{H31}$$

and

$$\tilde{I}_2 = \int_0^{\infty} d\tilde{x}\int_{\tilde{x}}^{\infty} d\tilde{q}\,\frac{1}{e^{\tilde{x}} - 1} \times \frac{4\tilde{x}^2}{\pi^{-2}[\tilde{s}\ln\tilde{s} - \tilde{t}\ln(-\tilde{t}) + 2\tilde{q}\ln T]^2 + 4\tilde{x}^2}. \tag{H32}$$

We have also used $c_1/c = 1/(2\pi v_{\parallel})$, which follows from above definitions and defined $\tilde{s} = \tilde{x} + \tilde{q}$ and $\tilde{t} = \tilde{x} - \tilde{q}$. Both integrands in Eqs. (H31) and (H32) are strictly positive within the integral bounds such that the resistivity, which follows from Eq. (H20) as

$$\rho = \frac{T}{2v_{\parallel}}\left(\frac{3}{\pi e\rho_0 v_{\mathrm{F}}}\right)^2 \tilde{I}, \tag{H33}$$

is positive and physically meaningful. In the last step, we will evaluate $\tilde{I}$ in the absence and then in the presence of logarithmic corrections.

First, we will evaluate $\tilde{I}_{1/2}$ in Eqs. (H31) and (H32) without logarithmic corrections, that is we set all logarithms to one and neglect the explicit $\ln T$ term. One finds

$$\tilde{I}_1 \simeq \int_0^\infty d\tilde{x} \int_{-\tilde{x}}^{\tilde{x}} d\tilde{q}\, \frac{1}{e^{\tilde{x}}-1} = 2\int_0^\infty d\tilde{x}\, \frac{\tilde{x}}{e^{\tilde{x}}-1} = \frac{\pi^2}{3} \tag{H34}$$

and

$$\tilde{I}_2 \simeq \int_0^\infty d\tilde{x}\, \frac{\tilde{x}^2}{e^{\tilde{x}}-1} \int_{\tilde{x}}^\infty d\tilde{q} \frac{1}{(\tilde{q}/\pi)^2+\tilde{x}^2} = \frac{\pi^3 \arctan\pi}{6}, \tag{H35}$$

and we have also neglected the $(2\tilde{q}/\pi)^2$ term in the denominator of $\tilde{I}_1$ of Eq. (H31) to perform the integration. From Eq. (H33), the resistivity follows as

$$\rho = \frac{3(1+(\pi \arctan\pi)/2)T}{2v_\parallel (e\rho_0 v_F)^2}, \tag{H36}$$

such that $\rho \sim T$.

Second, we evaluate $\tilde{I}_{1/2}$ in Eqs. (H31) and (H32) including logarithmic corrections. Since $\tilde{q} < \tilde{x}$ in $\tilde{I}_1$, we set $\tilde{x} - \tilde{q} \simeq \tilde{x}$. One finds from Eq. (H31)

$$\tilde{I}_1 \simeq \int_0^\infty d\tilde{x} \int_{-\tilde{x}}^{\tilde{x}} d\tilde{q}\, \frac{1}{e^{\tilde{x}}-1} \frac{\tilde{x}^2}{(2\tilde{q}/\pi)^2[\ln\tilde{x}+\ln T]^2+\tilde{x}^2}. \tag{H37}$$

The above $\tilde{q}$ integral has the typical scale

$$\tilde{q}_{\rm typ} = -\frac{\pi\tilde{x}}{2(\ln\tilde{x}+\ln T)}, \tag{H38}$$

such that the main contribution to the integral comes from the $|\tilde{q}| \leqslant \tilde{q}_{\rm typ}$ sector, while the tail $\tilde{x} \geqslant |\tilde{q}| > \tilde{q}_{\rm typ}$ is only subleading. We have chosen the sign such that $\tilde{q}_{\rm typ}$ is positive for $\tilde{x} < 1$ and $T < 1$. Neglecting the contribution from the tails, we obtain

$$\begin{aligned}\tilde{I}_1 &\simeq \int_0^\infty d\tilde{x} \frac{1}{e^{\tilde{x}}-1} \int_{-\infty}^\infty d\tilde{q}\, \frac{1}{1+(\tilde{q}/\tilde{q}_{\rm typ})^2} \\ &= -\frac{\pi^2}{2}\int_0^\infty d\tilde{x} \frac{\tilde{x}}{e^{\tilde{x}}-1} \frac{1}{\ln\tilde{x}+\ln T}.\end{aligned} \tag{H39}$$

We split the remaining integral in two contributions $\tilde{I}_1 \simeq \tilde{I}_{\gg T} + \tilde{I}_{\gg\tilde{x}}$, such that the first one $\tilde{I}_{\gg T}$ captures the limit $1 > \tilde{x} \gg T$ while the second one $\tilde{I}_{\gg\tilde{x}}$ the $1 > T \gg \tilde{x}$ limit.

For the $1 > \tilde{x} \gg T$ limit,

$$\begin{aligned}\tilde{I}_{\gg T} &\simeq -\frac{\pi^2}{2\ln T}\int_T^\infty d\tilde{x} \frac{\tilde{x}}{e^{\tilde{x}}-1} \\ &\simeq -\frac{\pi^2}{2\ln T}\int_T^1 d\tilde{x} = -\frac{\pi^2}{2}\frac{1}{\ln T} + \mathcal{O}(T/\ln T).\end{aligned} \tag{H40}$$

The $1 > T \gg \tilde{x}$ limit gives

$$\begin{aligned}\tilde{I}_{\gg\tilde{x}} &\simeq -\frac{\pi^2}{2}\int_0^T d\tilde{x} \frac{\tilde{x}}{e^{\tilde{x}}-1}\frac{1}{\ln\tilde{x}} \\ &\simeq -\frac{\pi^2}{2}\int_0^T \frac{d\tilde{x}}{\ln\tilde{x}} \propto -\frac{T}{\ln T}.\end{aligned} \tag{H41}$$

Next, we evaluate $\tilde{I}_2$ in Eq. (H32) including logarithmic corrections. Since $\tilde{q} > \tilde{x}$, we set $\tilde{q} \pm \tilde{x} \simeq \tilde{q}$ in the logarithms. One finds from Eq. (H32)

$$\tilde{I}_2 \simeq \int_0^\infty d\tilde{x} \int_{\tilde{x}}^\infty d\tilde{q}\, \frac{1}{e^{\tilde{x}}-1} \frac{\tilde{x}^2}{(\tilde{q}/\pi)^2[\ln\tilde{q}+\ln T]^2+\tilde{x}^2}. \tag{H42}$$

Again, we split the integral in two contributions $\tilde{I}_2 \simeq \tilde{I}_{\gg T} + \tilde{I}_{\gg\tilde{x}}$, such that the first one $\tilde{I}_{\gg T}$ captures the limit $\tilde{x} \gg T$ while the second one $\tilde{I}_{\gg\tilde{x}}$ the $T \gg \tilde{x}$ limit and in both cases $T \ll 1$. For the $\tilde{x} \gg T$ limit,

$$\begin{aligned}\tilde{I}_{\gg T} &\simeq \int_T^\infty d\tilde{x} \int_{\tilde{x}}^\infty d\tilde{q}\, \frac{\tilde{x}^2}{e^{\tilde{x}}-1} \frac{1}{(\tilde{q}\ln T/\pi)^2+\tilde{x}^2} \\ &\simeq -\frac{\pi^2}{2\ln T}\int_T^\infty d\tilde{x}\, \frac{\tilde{x}}{e^{\tilde{x}}-1} \simeq -\frac{\pi^2}{2}\frac{1}{\ln T} + \mathcal{O}(T/\ln T),\end{aligned} \tag{H43}$$

similar to Eq. (H40) and for $T \gg \tilde{x}$, one obtains

$$\begin{aligned}\tilde{I}_{\gg\tilde{x}} &\simeq \int_0^T d\tilde{x} \int_{\tilde{x}}^\infty d\tilde{q}\, \frac{\tilde{x}^2}{e^{\tilde{x}}-1} \frac{1}{(\tilde{q}\ln T/\pi)^2+\tilde{x}^2} \\ &\simeq -\frac{\pi^2}{2\ln T}\int_0^T d\tilde{x} = -\frac{\pi^2}{2}\frac{T}{\ln T}.\end{aligned} \tag{H44}$$

The total integral is therefore

$$\tilde{I}_1 = -\frac{\pi^2}{\ln T} + \mathcal{O}(T/\ln T), \tag{H45}$$

such that the resistivity with Eq. (H33) yields

$$\rho = -\frac{1}{2v_\parallel}\left(\frac{3}{e\rho_0 v_F}\right)^2 \frac{T}{\ln T} + \mathcal{O}(T^2/\ln T). \tag{H46}$$

Because T is small, the second contribution is subdominant and the resistivity scales like $\rho \sim T/|\ln T|$, with a logarithmic correction compared to Eq. (H36).

[1] H. Alloul, T. Ohno, and P. Mendels, Phys. Rev. Lett. **63**, 1700 (1989).

[2] W. W. Warren, R. E. Walstedt, G. F. Brennert, R. J. Cava, R. Tycko, R. F. Bell, and G. Dabbagh, Phys. Rev. Lett. **62**, 1193 (1989).

[3] M. R. Norman and C. Pépin, Rep. Prog. Phys. **66**, 1547 (2003).

[4] E. W. Carlson, S. A. Kivelson, D. Orgad, and V. J. Emery, *Concepts in High Temperature Superconductivity* (Springer Berlin Heidelberg, Berlin, Heidelberg, 2004).

[5] P. A. Lee, N. Nagaosa, and X.-G. Wen, Rev. Mod. Phys. **78**, 17 (2006).

[6] K. Le Hur and T. M. Rice, Ann. Phys. **324**, 1452 (2009).

[7] T. M. Rice, K.-Y. Yang, and F. C. Zhang, Rep. Prog. Phys. **75**, 016502 (2012).
[8] M. R. Norman and C. Proust, New J. Phys. **16**, 045004 (2014).
[9] B. Keimer, S. A. Kivelson, M. R. Norman, S. Uchida, and J. Zaanen, Nature (London) **518**, 179 (2015).
[10] J. P. Carbotte, T. Timusk, and J. Hwang, Rep. Prog. Phys. **74**, 066501 (2011).
[11] M. Eschrig, Adv. Phys. **55**, 47 (2006).
[12] E. Fradkin, S. A. Kivelson, and J. M. Tranquada, Rev. Mod. Phys. **87**, 457 (2015).
[13] J. C. Campuzano, M. R. Norman, H. Ding, M. Randeria, T. Yokoya, T. Takeuchi, T. Takahashi, T. Mochiku, K. Kadowaki, P. Guptasarma, and D. G. Hinks, Nature (London) **392**, 157 (1998).
[14] J. C. Campuzano, H. Ding, M. R. Norman, H. M. Fretwell, M. Randeria, A. Kaminski, J. Mesot, T. Takeuchi, T. Sato, T. Yokoya, T. Takahashi, T. Mochiku, K. Kadowaki, P. Guptasarma, D. G. Hinks, Z. Konstantinovic, Z. Z. Li, and H. Raffy, Phys. Rev. Lett. **83**, 3709 (1999).
[15] I. M. Vishik, M. Hashimoto, R.-H. He, W.-S. Lee, F. Schmitt, D. Lu, R. G. Moore, C. Zhang, W. Meevasana, T. Sasagawa, S. Uchida, K. Fujita, S. Ishida, M. Ishikado, Y. Yoshida, H. Eisaki, Z. Hussain, T. P. Devereaux, and Z.-X. Shen, Proc. Natl. Acad. Sci. USA **109**, 18332 (2012).
[16] I. M. Vishik, N. Barišić, M. K. Chan, Y. Li, D. D. Xia, G. Yu, X. Zhao, W. S. Lee, W. Meevasana, T. P. Devereaux, M. Greven, and Z.-X. Shen, Phys. Rev. B **89**, 195141 (2014).
[17] K. M. Shen, F. Ronning, D. H. Lu, F. Baumberger, N. J. C. Ingle, W. S. Lee, W. Meevasana, Y. Kohsaka, M. Azuma, M. Takano, H. Takagi, and Z.-X. Shen, Science **307**, 901 (2005).
[18] A. Kaminski, S. Rosenkranz, H. M. Fretwell, J. C. Campuzano, Z. Li, H. Raffy, W. G. Cullen, H. You, C. G. Olson, and C. M. Varma, Nature (London) **416**, 610 (2002).
[19] P. W. Anderson, Science **235**, 1196 (1987).
[20] G. Kotliar and J. Liu, Phys. Rev. B **38**, 5142 (1988).
[21] G. Kotliar, Phys. Rev. B **37**, 3664 (1988).
[22] P. A. Lee, N. Nagaosa, T.-K. Ng, and X.-G. Wen, Phys. Rev. B **57**, 6003 (1998).
[23] A. Georges, G. Kotliar, W. Krauth, and M. J. Rozenberg, Rev. Mod. Phys. **68**, 13 (1996).
[24] E. Gull, O. Parcollet, and A. J. Millis, Phys. Rev. Lett. **110**, 216405 (2013).
[25] G. Sordi, P. Sémon, K. Haule, and A.-M. S. Tremblay, Phys. Rev. Lett. **108**, 216401 (2012).
[26] G. Sordi, P. Sémon, K. Haule, and A. M. S. Tremblay, Sci. Rep. **2**, 547 (2012).
[27] E. Gull and A. J. Millis, Phys. Rev. B **90**, 041110 (2014).
[28] N. Nagaosa and P. A. Lee, Phys. Rev. Lett. **64**, 2450 (1990).
[29] N. Nagaosa and P. A. Lee, Phys. Rev. B **45**, 966 (1992).
[30] A. Ferraz and E. Kochetov, Europhys. Lett. **109**, 37003 (2015).
[31] M. Franz and Z. Tešanović, Phys. Rev. Lett. **87**, 257003 (2001).
[32] Z. Tešanović, O. Vafek, and M. Franz, Phys. Rev. B **65**, 180511 (2002).
[33] C. Castellani, C. Di Castro, and W. Metzner, Phys. Rev. Lett. **72**, 316 (1994).
[34] A. M. Tsvelik and A. V. Chubukov, Phys. Rev. Lett. **98**, 237001 (2007).
[35] A. V. Chubukov and A. M. Tsvelik, Phys. Rev. B **76**, 100509 (2007).
[36] K.-Y. Yang, T. M. Rice, and F.-C. Zhang, Phys. Rev. B **73**, 174501 (2006).
[37] V. Barzykin and D. Pines, Phys. Rev. B **52**, 13585 (1995).
[38] A. Abanov, A. V. Chubukov, and J. Schmalian, Adv. Phys. **52**, 119 (2003).
[39] F. Onufrieva and P. Pfeuty, Phys. Rev. B **61**, 799 (2000).
[40] F. Onufrieva and P. Pfeuty, Phys. Rev. B **65**, 054515 (2002).
[41] A. Chubukov, D. Pines, and J. Schmalian, *J 2003 The Physics of Conventional and Unconventional Superconductors*, edited by K.H. Bennemann and J. B. Ketterson (Springer, Berlin, 2003), Vol. 1.
[42] S. Sachdev, *Quantum Phase Transitions* (Cambridge University Press, New York, 1998).
[43] S. Sur and S.-S. Lee, Phys. Rev. B **90**, 045121 (2014).
[44] S. Sur and S.-S. Lee, Phys. Rev. B **91**, 125136 (2015).
[45] Y. Schattner, M. H. Gerlach, S. Trebst, and E. Berg, Phys. Rev. Lett. **117**, 097002 (2016).
[46] M. H. Gerlach, Y. Schattner, E. Berg, and S. Trebst, Phys. Rev. B **95**, 035124 (2017)
[47] S. Lederer, Y. Schattner, E. Berg, and S. A. Kivelson, Phys. Rev. Lett. **114**, 097001 (2015).
[48] X. Wang, Y. Schattner, E. Berg, and R. M. Fernandes, arXiv:1609.09568v1.
[49] A. Perali, C. Castellani, C. Di Castro, and M. Grilli, Phys. Rev. B **54**, 16216 (1996).
[50] V. J. Emery and S. A. Kivelson, Nature (London) **374**, 434 (1995).
[51] M. R. Norman, A. Kanigel, M. Randeria, U. Chatterjee, and J. C. Campuzano, Phys. Rev. B **76**, 174501 (2007).
[52] S. Banerjee, T. V. Ramakrishnan, and C. Dasgupta, Phys. Rev. B **83**, 024510 (2011).
[53] S. Banerjee, T. V. Ramakrishnan, and C. Dasgupta, Phys. Rev. B **84**, 144525 (2011).
[54] M. R. Norman, M. Randeria, H. Ding, and J. C. Campuzano, Phys. Rev. B **52**, 615 (1995).
[55] M. Franz and A. J. Millis, Phys. Rev. B **58**, 14572 (1998).
[56] A. P. Kampf and A. A. Katanin, Phys. Rev. B **67**, 125104 (2003).
[57] J. Zaanen and O. Gunnarsson, Phys. Rev. B **40**, 7391 (1989).
[58] J. Zaanen, J. Phys. Chem. Solids **59**, 1769 (1998).
[59] K. Machida, Physica C: Superconductivity **158**, 192 (1989).
[60] M. Kato, K. Machida, H. Nakanishi, and M. Fujita, J. Phys. Soc. Jpn. **59**, 1047 (1990).
[61] V. J. Emery, S. A. Kivelson, and J. M. Tranquada, Proc. Natl. Acad. Sci. USA **96**, 8814 (1999).
[62] S. A. Kivelson, E. Fradkin, and V. J. Emery, Nature (London) **393**, 550 (1998).
[63] S. A. Kivelson, D.-H. Lee, E. Fradkin, and V. Oganesyan, Phys. Rev. B **66**, 144516 (2002).
[64] S. A. Kivelson, I. P. Bindloss, E. Fradkin, V. Oganesyan, J. M. Tranquada, A. Kapitulnik, and C. Howald, Rev. Mod. Phys. **75**, 1201 (2003).
[65] D. Chakraborty and A. Ghosal, New J. Phys. **16**, 103018 (2014).
[66] J. Corson, R. Mallozzi, J. Orenstein, and J. N. Eckstein, Nature (London) **398**, 221 (1999).
[67] H. Alloul, F. Rullier-Albenque, B. Vignolle, D. Colson, and A. Forget, Europhys. Lett. **91**, 37005 (2010).
[68] L. Benfatto, C. Castellani, and T. Giamarchi, Phys. Rev. Lett. **98**, 117008 (2007).

[69] L. Benfatto, S. Caprara, and C. D. Castro, Eur. Phys. J. B **17**, 95 (2000).

[70] M. A. Metlitski and S. Sachdev, Phys. Rev. B **82**, 075128 (2010).

[71] L. E. Hayward, D. G. Hawthorn, R. G. Melko, and S. Sachdev, Science **343**, 1336 (2014).

[72] K. B. Efetov, H. Meier, and C. Pépin, Nat. Phys. **9**, 442 (2013).

[73] T. Kloss, X. Montiel, and C. Pépin, Phys. Rev. B **91**, 205124 (2015).

[74] T. Kloss, X. Montiel, V. S. de Carvalho, H. Freire, and C. Pépin, Rep. Prog. Phys. **79**, 084507 (2016).

[75] D. Chowdhury and S. Sachdev, Phys. Rev. B **90**, 134516 (2014).

[76] D. Chowdhury and S. Sachdev, in *Quantum Criticality in Condensed Matter: Phenomena, Materials and Ideas in Theory and Experiment: 50th Karpacz Winter School of Theors*, edited by J. Jedrzejewski (World Scientific, 2015), pp. 1–43.

[77] M. H. Hamidian, S. D. Edkins, S. H. Joo, A. Kostin, H. Eisaki, S. Uchida, M. J. Lawler, E.-A. Kim, A. P. Mackenzie, K. Fujita, J. Lee, and J. C. Séamus Davis, Nature (London) **532**, 343 (2016).

[78] A. Allais, J. Bauer, and S. Sachdev, Phys. Rev. B **90**, 155114 (2014).

[79] W. A. Atkinson, A. P. Kampf, and S. Bulut, New J. Phys. **17**, 013025 (2015).

[80] W. A. Atkinson and A. P. Kampf, Phys. Rev. B **91**, 104509 (2015).

[81] H. Meier, M. Einenkel, C. Pépin, and K. B. Efetov, Phys. Rev. B **88**, 020506 (2013).

[82] H. Meier, C. Pépin, M. Einenkel, and K. B. Efetov, Phys. Rev. B **89**, 195115 (2014).

[83] M. Einenkel, H. Meier, C. Pépin, and K. B. Efetov, Phys. Rev. B **90**, 054511 (2014).

[84] D. F. Agterberg, D. S. Melchert, and M. K. Kashyap, Phys. Rev. B **91**, 054502 (2015).

[85] Y. Wang and A. Chubukov, Phys. Rev. B **90**, 035149 (2014).

[86] Y. Wang, D. F. Agterberg, and A. Chubukov, Phys. Rev. B **91**, 115103 (2015).

[87] Y. Wang, D. F. Agterberg, and A. Chubukov, Phys. Rev. Lett. **114**, 197001 (2015).

[88] Y. Wang and A. Chubukov, Phys. Rev. B **91**, 195113 (2015).

[89] C. Pépin, V. S. de Carvalho, T. Kloss, and X. Montiel, Phys. Rev. B **90**, 195207 (2014).

[90] H. Freire, V. S. de Carvalho, and C. Pépin, Phys. Rev. B **92**, 045132 (2015).

[91] S. Caprara, M. Grilli, C. Di Castro, and G. Seibold, J. Supercond. Nov. Magn. **30**, 25 (2017).

[92] S. Caprara, C. Di Castro, G. Seibold, and M. Grilli, arXiv:1604.07852v1.

[93] J. E. Hoffman, E. W. Hudson, K. M. Lang, V. Madhavan, H. Eisaki, S. Uchida, and J. C. Davis, Science **295**, 466 (2002).

[94] K. Fujita, C. K. Kim, I. Lee, J. Lee, M. Hamidian, I. A. Firmo, S. Mukhopadhyay, H. Eisaki, S. Uchida, M. J. Lawler, E. A. Kim, and J. C. Davis, Science **344**, 612 (2014).

[95] M. Vershinin, Science **303**, 1995 (2004).

[96] E. H. da Silva Neto, P. Aynajian, A. Frano, R. Comin, E. Schierle, E. Weschke, A. Gyenis, J. Wen, J. Schneeloch, Z. Xu, S. Ono, G. Gu, M. Le Tacon, and A. Yazdani, Science **343**, 393 (2014).

[97] Y. He, Y. Yin, M. Zech, A. Soumyanarayanan, M. M. Yee, T. Williams, M. C. Boyer, K. Chatterjee, W. D. Wise, I. Zeljkovic, T. Kondo, T. Takeuchi, H. Ikuta, P. Mistark, R. S. Markiewicz, A. Bansil, S. Sachdev, E. W. Hudson, and J. E. Hoffman, Science **344**, 608 (2014).

[98] W. D. Wise, M. C. Boyer, K. Chatterjee, T. Kondo, T. Takeuchi, H. Ikuta, Y. Wang, and E. W. Hudson, Nat. Phys. **4**, 696 (2008).

[99] N. Doiron-Leyraud, C. Proust, D. LeBoeuf, J. Levallois, J.-B. Bonnemaison, R. Liang, D. A. Bonn, W. N. Hardy, and L. Taillefer, Nature (London) **447**, 565 (2007).

[100] D. LeBoeuf, N. Doiron-Leyraud, J. Levallois, R. Daou, J. B. Bonnemaison, N. E. Hussey, L. Balicas, B. J. Ramshaw, R. Liang, D. A. Bonn, W. N. Hardy, S. Adachi, C. Proust, and L. Taillefer, Nature (London) **450**, 533 (2007).

[101] T. Wu, H. Mayaffre, S. Krämer, M. Horvatic, C. Berthier, W. N. Hardy, R. Liang, D. A. Bonn, and M.-H. Julien, Nature (London) **477**, 191 (2011).

[102] T. Wu, H. Mayaffre, S. Krämer, M. Horvatić, C. Berthier, P. L. Kuhns, A. P. Reyes, R. Liang, W. N. Hardy, D. A. Bonn, and M.-H. Julien, Nat. Commun. **4**, 2113 (2013).

[103] T. Wu, H. Mayaffre, S. Krämer, M. Horvatić, C. Berthier, W. N. Hardy, R. Liang, D. A. Bonn, and M.-H. Julien, Nat. Commun. **6**, 6438 (2015).

[104] J. Chang, E. Blackburn, O. Ivashko, A. T. Holmes, N. B. Christensen, M. Huecker, R. Liang, D. A. Bonn, W. N. Hardy, U. Ruett, M. V. Zimmermann, E. M. Forgan, and S. M. Hayden, Nat. Commun. **7**, 11494 (2016).

[105] J. Chang, E. Blackburn, A. T. Holmes, N. B. Christensen, J. Larsen, J. Mesot, R. Liang, D. A. Bonn, W. N. Hardy, A. Watenphul, M. v. Zimmermann, E. M. Forgan, and S. M. Hayden, Nat. Phys. **8**, 871 (2012).

[106] E. Blackburn, J. Chang, M. Hücker, A. T. Holmes, N. B. Christensen, R. Liang, D. A. Bonn, W. N. Hardy, U. Rütt, O. Gutowski, M. V. Zimmermann, E. M. Forgan, and S. M. Hayden, Phys. Rev. Lett. **110**, 137004 (2013).

[107] G. Ghiringhelli, M. Le Tacon, M. Minola, S. Blanco-Canosa, C. Mazzoli, N. B. Brookes, G. M. De Luca, A. Frano, D. G. Hawthorn, F. He, T. Loew, M. M. Sala, D. C. Peets, M. Salluzzo, E. Schierle, R. Sutarto, G. A. Sawatzky, E. Weschke, B. Keimer, and L. Braicovich, Science **337**, 821 (2012).

[108] M. Le Tacon, G. Ghiringhelli, J. Chaloupka, M. M. Sala, V. Hinkov, M. W. Haverkort, M. Minola, M. Bakr, K. J. Zhou, S. Blanco-Canosa, C. Monney, Y. T. Song, G. L. Sun, C. T. Lin, G. M. De Luca, M. Salluzzo, G. Khaliullin, T. Schmitt, L. Braicovich, and B. Keimer, Nat. Phys. **7**, 725 (2011).

[109] S. Blanco-Canosa, A. Frano, T. Loew, Y. Lu, J. Porras, G. Ghiringhelli, M. Minola, C. Mazzoli, L. Braicovich, E. Schierle, E. Weschke, M. Le Tacon, and B. Keimer, Phys. Rev. Lett. **110**, 187001 (2013).

[110] S. Blanco-Canosa, A. Frano, E. Schierle, J. Porras, T. Loew, M. Minola, M. Bluschke, E. Weschke, B. Keimer, and M. Le Tacon, Phys. Rev. B **90**, 054513 (2014).

[111] S. Gerber, H. Jang, H. Nojiri, S. Matsuzawa, H. Yasumura, D. A. Bonn, R. Liang, W. N. Hardy, Z. Islam, A. Mehta, S. Song, M. Sikorski, D. Stefanescu, Y. Feng, S. A. Kivelson, T. P. Devereaux, Z.-X. Shen, C. C. Kao, W. S. Lee, D. Zhu, and J. S. Lee, Science **350**, 949 (2015).

[112] S. E. Sebastian, N. Harrison, M. M. Altarawneh, C. H. Mielke, R. Liang, D. A. Bonn, and G. G. Lonzarich, Proc. Natl. Acad. Sci. USA **107**, 6175 (2010).
[113] D. LeBoeuf, S. Kramer, W. N. Hardy, R. Liang, D. A. Bonn, and C. Proust, Nat. Phys. **9**, 79 (2013).
[114] Y. Gallais, A. Sacuto, and D. Colson, Physica C **408–410**, 785 (2004).
[115] S. Blanc, Y. Gallais, A. Sacuto, M. Cazayous, M. A. Méasson, G. D. Gu, J. S. Wen, and Z. J. Xu, Phys. Rev. B **80**, 140502 (2009).
[116] S. Blanc, Y. Gallais, M. Cazayous, M. A. Méasson, A. Sacuto, A. Georges, J. S. Wen, Z. J. Xu, G. D. Gu, and D. Colson, Phys. Rev. B **82**, 144516 (2010).
[117] A. Sacuto, Y. Gallais, M. Cazayous, M.-A. Méasson, G. D. Gu, and D. Colson, Rep. Prog. Phys. **76**, 022502 (2013).
[118] S. Benhabib, Y. Gallais, M. Cazayous, M.-A. Méasson, R. D. Zhong, J. Schneeloch, A. Forget, G. D. Gu, D. Colson, and A. Sacuto, Phys. Rev. B **92**, 134502 (2015).
[119] Y. Gallais, A. Sacuto, P. Bourges, Y. Sidis, A. Forget, and D. Colson, Phys. Rev. Lett. **88**, 177401 (2002).
[120] X. Montiel, T. Kloss, C. Pépin, S. Benhabib, Y. Gallais, and A. Sacuto, Phys. Rev. B **93**, 024515 (2016).
[121] A. V. Chubukov, T. P. Devereaux, and M. V. Klein, Phys. Rev. B **73**, 094512 (2006).
[122] M. Eschrig and M. R. Norman, Phys. Rev. Lett. **85**, 3261 (2000).
[123] A. V. Chubukov, B. Jankó, and O. Tchernyshyov, Phys. Rev. B **63**, 180507 (2001).
[124] M. R. Norman, Phys. Rev. B **75**, 184514 (2007).
[125] O. Tchernyshyov, M. R. Norman, and A. V. Chubukov, Phys. Rev. B **63**, 144507 (2001).
[126] J. Rossat-Mignod, L. Regnault, C. Vettier, P. Bourges, P. Burlet, J. Bossy, J. Henry, and G. Lapertot, Physica C **185–189**, 86 (1991).
[127] H. He, Y. Sidis, P. Bourges, G. D. Gu, A. Ivanov, N. Koshizuka, B. Liang, C. T. Lin, L. P. Regnault, E. Schoenherr, and B. Keimer, Phys. Rev. Lett. **86**, 1610 (2001).
[128] V. Hinkov, P. Bourges, S. Pailhès, Y. Sidis, A. Ivanov, C. D. Frost, T. G. Perring, C. T. Lin, D. P. Chen, and B. Keimer, Nat. Phys. **3**, 780 (2007).
[129] V. Hinkov, S. Pailhes, P. Bourges, Y. Sidis, A. Ivanov, A. Kulakov, C. T. Lin, D. P. Chen, C. Bernhard, and B. Keimer, Nature (London) **430**, 650 (2004).
[130] M. K. Chan, C. J. Dorow, L. Mangin-Thro, Y. Tang, Y. Ge, M. J. Veit, G. Yu, X. Zhao, A. D. Christianson, J. T. Park, Y. Sidis, P. Steffens, D. L. Abernathy, P. Bourges, and M. Greven, Nat. Commun. **7**, 10819 (2016).
[131] M. K. Chan, Y. Tang, C. J. Dorow, J. Jeong, L. Mangin-Thro, M. J. Veit, Y. Ge, D. L. Abernathy, Y. Sidis, P. Bourges, and M. Greven, Phys. Rev. Lett. **117**, 277002 (2016).
[132] P. Bourges, B. Keimer, S. Pailhès, L. Regnault, Y. Sidis, and C. Ulrich, Physica C **424**, 45 (2005).
[133] P. Bourges and Y. Sidis, C. R. Phys. **12**, 461 (2011).
[134] B. Fauqué, Y. Sidis, V. Hinkov, S. Pailhès, C. T. Lin, X. Chaud, and P. Bourges, Phys. Rev. Lett. **96**, 197001 (2006).
[135] O. Cyr-Choinière, G. Grissonnanche, S. Badoux, J. Day, D. A. Bonn, W. N. Hardy, R. Liang, N. Doiron-Leyraud, and L. Taillefer, Phys. Rev. B **92**, 224502 (2015).
[136] C. M. Varma, Phys. Rev. B **73**, 155113 (2006).
[137] V. Aji, Y. He, and C. M. Varma, Phys. Rev. B **87**, 174518 (2013).
[138] V. Aji and C. M. Varma, Phys. Rev. B **75**, 224511 (2007).
[139] L. Nie, G. Tarjus, and S. A. Kivelson, Proc. Natl. Acad. Sci. USA **111**, 7980 (2014).
[140] L. Nie, Lauren E. Hayward Sierens, R. G. Melko, S. Sachdev, and S. A. Kivelson, Phys. Rev. B **92**, 174505 (2015).
[141] K. Lee, S. A. Kivelson, and E.-A. Kim, Phys. Rev. B **94**, 014204 (2016).
[142] V. S. de Carvalho, T. Kloss, X. Montiel, H. Freire, and C. Pépin, Phys. Rev. B **92**, 075123 (2015).
[143] V. S. de Carvalho and H. Freire, Ann. Phys. **348**, 32 (2014).
[144] J. Schmalian and P. G. Wolynes, Phys. Rev. Lett. **85**, 836 (2000).
[145] H. Terletska and V. Dobrosavljević, Phys. Rev. Lett. **106**, 186402 (2011).
[146] R. Micnas, J. Ranninger, and S. Robaszkiewicz, Rev. Mod. Phys. **62**, 113 (1990).
[147] X. Montiel, T. Kloss, and C. Pépin, arXiv:1510.03038.
[148] S. Q. Shen and X. C. Xie, J. of Phys. Cond. Mat. **8**, 4805 (1996).
[149] E. Demler and S.-C. Zhang, Phys. Rev. Lett. **75**, 4126 (1995).
[150] S. C. Zhang, Science **275**, 1089 (1997).
[151] S. C. Zhang, J. P. Hu, E. Arrigoni, W. Hanke, and A. Auerbach, Phys. Rev. B **60**, 13070 (1999).
[152] E. Demler, W. Hanke, and S.-C. Zhang, Rev. Mod. Phys. **76**, 909 (2004).
[153] E. Demler, A. J. Berlinsky, C. Kallin, G. B. Arnold, and M. R. Beasley, Phys. Rev. Lett. **80**, 2917 (1998).
[154] B. C. den Hertog, A. J. Berlinsky, and C. Kallin, Phys. Rev. B **59**, R11645 (1999).
[155] C. N. Yang, Phys. Rev. Lett. **63**, 2144 (1989).
[156] C. N. Yang and S. C. Zhang, Mod. Phys. Lett. B **04**, 759 (1990).
[157] C. Nayak, Phys. Rev. B **62**, R6135 (2000).
[158] H.-Y. Kee, H. Doh, and T. Grzesiak, J. Phys. Condens. Matter **20**, 255248 (2008).
[159] F. C. Zhang and T. M. Rice, Phys. Rev. B **37**, 3759 (1988).
[160] M. J. Lawler, K. Fujita, J. Lee, A. Schmidt, Y. Kohsaka, C. K. Kim, H. Eisaki, S. Uchida, J. C. Davis, J. P. Sethna, and E.-A. Kim, Nature (London) **466**, 347 (2010).
[161] A. Mesaros, K. Fujita, H. Eisaki, S. Uchida, and J. C. Davis, Science **333**, 426 (2011).
[162] L. P. Gor'kov and A. V. Sokol, JETP Lett. **46**, 420 (1987).
[163] L. P. Gor'kov and A. V. Sokol, Physica C: Superconductivity **159**, 329 (1989).
[164] X. Montiel, T. Kloss, and C. Pepin (unpublished).
[165] C. M. Varma, P. B. Littlewood, S. Schmitt-Rink, E. Abrahams, and A. E. Ruckenstein, Phys. Rev. Lett. **63**, 1996 (1989).
[166] A. A. Abrikosov, *Fundamentals of the Theory of Metals* (North-Holland, Amsterdam, 1988).
[167] I. Paul, C. Pépin, and M. R. Norman, Phys. Rev. Lett. **110**, 066402 (2013).
[168] N. E. Hussey, R. A. Cooper, X. Xu, Y. Wang, I. Mouzopoulou, B. Vignolle, and C. Proust, Philos. Trans. R. Soc. A-Math. Phys. Eng. Sci. **369**, 1626 (2011).

[169] R. A. Cooper, Y. Wang, B. Vignolle, O. J. Lipscombe, S. M. Hayden, Y. Tanabe, T. Adachi, Y. Koike, M. Nohara, H. Takagi, C. Proust, and N. E. Hussey, Science **323**, 603 (2009).
[170] N. Barišić, M. K. Chan, M. J. Veit, C. J. Dorow, Y. Ge, Y. Tang, W. Tabis, G. Yu, X. Zhao, and M. Greven, arXiv:1507.07885.
[171] X. Montiel, T. Kloss, and C. Pépin, Europhys. Lett. **115**, 57001 (2016).
[172] C. Collignon, S. Badoux, S. A. A. Afshar, B. Michon, F. Laliberte, O. Cyr-Choiniere, J.-S. Zhou, S. Licciardello, S. Wiedmann, N. Doiron-Leyraud, and L. Taillefer, arXiv:1607.05693.
[173] L. Taillefer, S. Badoux, and G. Grissonnanche, Nature (London) **531**, 210 (2016).
[174] J. G. Storey, Europhys. Lett. **113**, 27003 (2016).
[175] C. Morice and C. Pépin (unpublished).
[176] C. F. Klingshirn, *Semiconductor Optics* (Springer, Berlin Heidelberg, 2012).
[177] G. D. Mahan, *Many-Particle Physics* (Kluwer Academics, New York, 2000).